MASTERARBEIT / MASTER’S THESIS

Titel der Masterarbeit / Title of the Master‘s Thesis

„A COMPARISON OF VOLUME-, TEMPERATURE- AND FRESHWATER TRANSPORTS THROUGH ARCTIC GATE-WAYS: OCEAN REANALYSIS vs. IN-SITU OBSERVATIONS“

verfasst von / submitted by

Sebastian Stichelberger, BSc.

angestrebter akademischer Grad / in partial fulfilment of the requirements for the degree of

Master of Science (MSc.)

Wien, 2017 / Vienna 2017

Studienkennzahl lt. Studienblatt / degree programme code as it appears on the student record sheet:	A 066 614
Studienrichtung lt. Studienblatt / degree programme as it appears on the student record sheet:	Meteorologie
Betreut von / Supervisor:	Ao. Univ.-Prof. Mag. Dr. Leopold Haimberger

„. . . Dazu kommt noch, daß derjenige, welcher das Wetter vorhersagen soll, wenn er es mit Zuneigung und gewissenhaft tuht, kein ruhiges Leben mehr hat und große Gefahr läuft durch Nervenleiden wahnsinnig zu werden.“ (C. H. D. Buijs Ballot, 1847)

i. Abstract

The Arctic Ocean is unique in many ways, not only due to its geographic location, but also due to the land masses surrounding it. The aim of this master´s thesis is to determine the transport of volume, heat and freshwater through the Arctic Gateways (Davis Strait, Fram Strait, Barents Sea Opening and Bering Strait) out of different ocean reanalyses (Centro Euro-Mediterraneo sui Cambiamenti Climatici Global Ocean Reanalysis System (C-GLORSv5) & European Centre for Medium Range Weather Forecasts Ocean Reanalysis System (ORAS5)) and subsequently compare them to observation-based data from the Arctic Ocean Gateway array (ARCGATE). This comparison makes it possible to assess the quality of the ocean reanalyses in the Arctic domain. The knowledge about this quality is particularly interesting in connection with the determination of coupled energy, mass and freshwater budgets for the Arctic, among others from reanalysis data. Reliable ocean reanalyses are therefore essential for a good database.

The evaluation of the results of this work does not allow a clear statement about the performance of ocean reanalysis. Generally, the reanalyses reflect adequately the regimes in the gateways and agree well with observations. However, if the gateways are treated separately, there are still major differences. The reasons for these differences could be localized in the course of this work and partly explained.

ii. Zusammenfassung

Der Arktische Ozean ist in vielerlei Hinsicht einzigartig. Das trifft nicht nur auf seine geografische Lage, sondern auch auf die Landmassen die ihn umgeben zu. Ziel dieser Masterarbeit ist die Flüsse von Volumen, Wärme und Süßwasser durch die arktischen Wasserstraßen (Davis Straße, Fram Straße, Barents Sea Opening und Bering Straße) mit Hilfe von Ozean Reanalysen zu bestimmen und mit beobachtungsbasierten Daten zu vergleichen. Durch diesen Vergleich ist es möglich, die Güte der Ozean Reanalysen im Bereich der Arktis zu erfassen. Das Wissen über diese Güte ist vor allem im Zusammenhang mit der Bestimmung gekoppelter Energie-, Massen-, und Süßwasserhaushalte für die Arktis interessant, unter anderem aus Reanalysedaten. Verlässliche Ozean Reanalysen sind daher für eine gute Datengrundlage unerlässlich.

Die Auswertung der Ergebnisse dieser Arbeit lässt allerdings keine klare Aussage über die Performance der Ozean Reanalysen zu. Im Großen und Ganzen können sowohl C-GLORSv5, als auch ORAS5 die Flüsse durch die Wasserstraßen adäquat wiedergeben. Betrachtet man die Wasserstraßen allerdings separat, so fallen doch größere Unterschiede auf. Die Ursachen für diese Unterschiede konnten im Zuge diese Arbeit lokalisiert und zum Teil auch begründet werden.

iii. Acronyms

ADCP = Acoustic Doppler Current Profiler
ARCGATE = Arctic Ocean Gateway
ASOF = Arctic-Subarctic Ocean Fluxes
AUV = Autonomous Underwater Vehicle
AVISO = Archiving, Validation and Interpretation of Satellite Oceanographic data
AWI = Alfred Wegener Institute
AW = Atlantic Waters
BIC = Baffin Island Current
BSO = Barents Sea Opening
CAA = Canadian Arctic Archipelago
C-GLORS = CMCC Global Ocean Reanalysis System
CMCC = Centro Euro-Mediterraneo sui Cambiamenti Climatici
CORE = Coordinated Ocean-Ice Reference Experiment
CTD = Conductivity Temperature and Depth
DAMOCLES = Developing Arctic Modelling and Observing Capabilities for Long-term Studies
DEWLINE = Distant Early Warning Line
ECMWF = European Centre for Medium Range Weather Forecasts
EGC = East Greenland Current
ERA-Interim = ECMWF Interim reanalysis project
FFT = Fast Fourier Transform
GDAC = Global Data Assembly Centre
IABP = International Arctic Buoy Program
IGY = International Geophysical Year
IMGW = Institute for Meteorology and Geophysics Vienne
IPY = International Polar Year
LIM2 = Louvain-La-Neuve sea ice Model
NAS = National Academy of Science
NASA = National Aeronautics and Space Administration
NCAR = National Centre for Atmospheric Research
NCL = NCAR Command Language
NEMO = Nucleus for European Modelling of the Ocean
NOAA = National Oceanic and Atmospheric Administration
NSF = National Science Foundation
NSIDC = National Snow and Ice Data Centre
OHC = Ocean Heat Content
ORAP = Ocean Reanalysis Prototype
ORAS = Ocean Reanalysis System
PSU = Practical Salinity Unit

SCICEX = Scientific Ice Expeditions
STDDEV = Standard deviation
SLA = Sea Level Altitude
SSH = Sea Surface Hight
Sv = Sverdrup
TW = Terawatt
VEINS = Variability of Exchanges in Northern Seas
WGC = West Greenland Current
WGS = West Greenland Slope
WSC = West Spitsbergen Current
XBT = Expendable Bathythermographs
3DVAR = 3-D Variational (Data Assimilation)

iv. Contents

1. Introduction

The Climate of the earth is changing, especially in recent decades the impacts of these changes have become more obvious and dramatic. This is particularly true for the Arctic region. In the following chapter a quick review over the history of the Arctic, the Arctic Ocean itself and the state of scientific knowledge about energy transports into and out of the Arctic will be given. At the end of this chapter the research question will be formulated.

1.1. Historical Background

The following section is mainly based on Serreze and Barry (2014) and some other sources cited in the text.
The region north of the Polar Circle has been of major interest for mankind for several centuries. For sure, the midnight sun, Aurora Borealis or the mighty glaciers must have been fascinating for the first visitors of the Arctic and even today they are impressive. Nevertheless, it was the ambition of European traders to find a faster way to China that instigated the exploration of the Arctic (Serreze & Barry, 2014). In the 16th century, miscellaneous routes were discussed, for example the Northwest Passage or the Northeast Passage. The Northwest Passage starts at Davis Strait, continues northward through the Canadian Arctic Archipelago and along the Alaskan coast. On the east side of the Arctic Ocean, the Northeast Passage connects the Northern Seas. Beginning at Norwegian Sea and White Sea, it takes course through Kara, Laptev and East Siberian Sea finally ending in Chukchi Sea (Serreze & Barry, 2014) (Fig.1).

In the following centuries, many adventurers from different countries (Britain, Netherlands, Norway, Russia or Denmark) tried to travel along these routes though the Arctic ice, but they all failed or did not find/arrive at their target. Although many crews and ships were lost, these expeditions had a major contribution to the exploration of the Arctic (Serreze & Barry, 2014) and therefore several features in the Arctic are named after the expedition leaders. The most prominent are for example Hudson Bay, Baffin Bay and Baffin Island or the Bering and Davis Straits.
In the 19th century as well as in more recent times the Arctic gained importance again as it was discovered, that large parts of the Arctic were rich in mineral resources. Gold and diamonds or other important materials like copper or nickel attracted thousands of people (Alaska Gold rush), in the 20th century it was the discovery of large oil and gas fields in Alaska. Nowadays, with about ten percent of the world's oil and a quarter of its natural gas coming from the Arctic, this region plays a major role in the world’s energy supply. Since the natural resources are not equally distributed over the

area, the Russian Arctic accounts for nearly 80 percent of this oil and most of the gas. Furthermore, recent studies presume large and undiscovered petroleum fields within the Arctic Circle. (Russian Geographical Society (RGS), 2017)

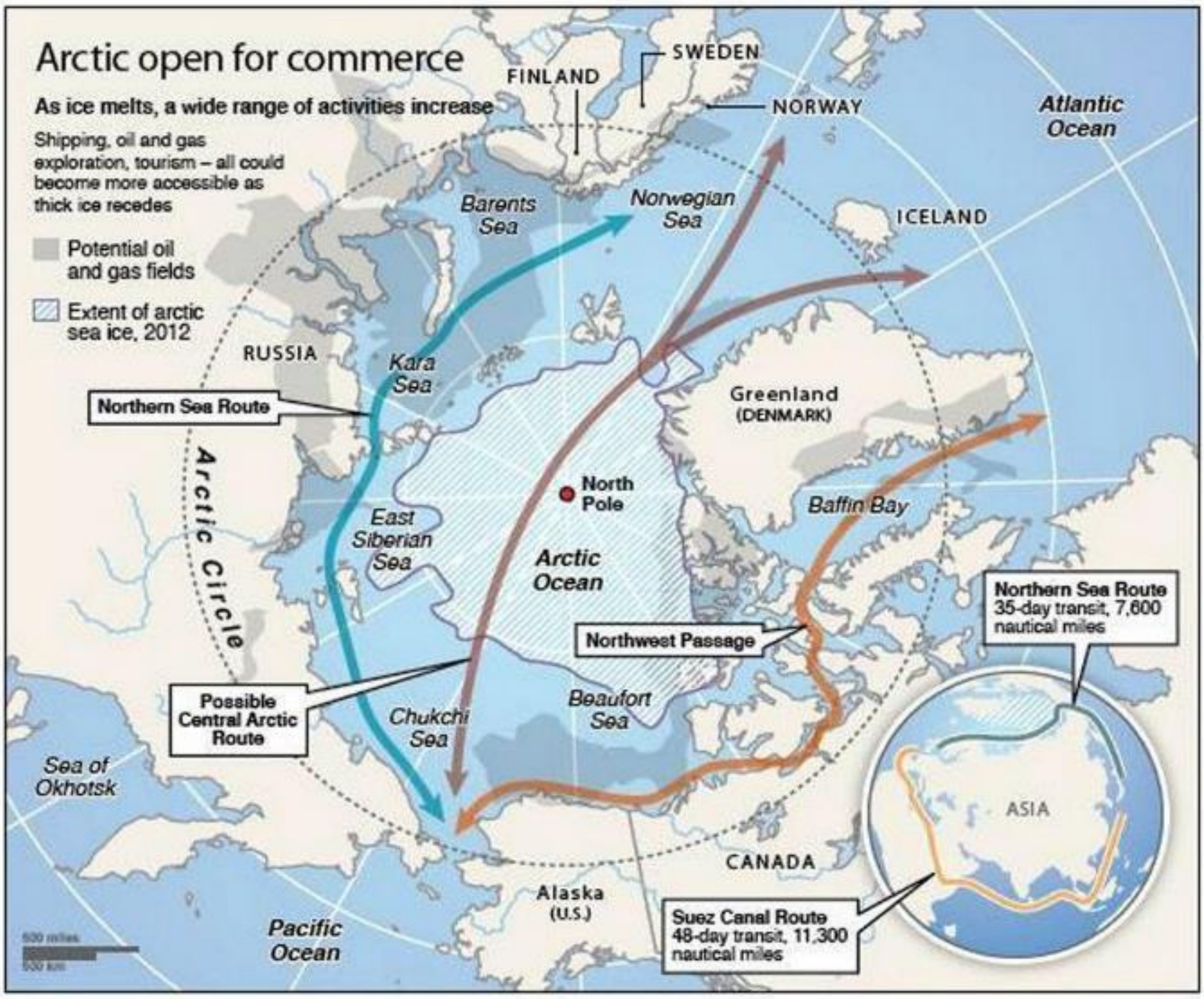

Figure 1: Map of the Arctic region. The brown arrow shows the route of the Northwest Passage, while the blue one shows the Northeast Passage (Northern Seas Route). The dark brown arrow in the middle shows the direct way through the Arctic.
Source: https://eurasiangeopolitics.com/arctic-maps/

1.1.1. Historical Observations

The first meteorological and oceanographic observations in the Arctic region coincide with the expeditions that took place there, as it was routine to collect this data for the ships logbook. Regular reports of the most important atmospheric and oceanic variables started in the 1850s in most countries (Serreze & Barry, 2014).

The Arctic gained more and more interest by scientists and so Karl Weyprecht suggested coordinated expeditions to the Polar region. Weyprecht died in 1881, but nevertheless, one year later the first International Polar Year (IPY) 1882-1883 was announced. During this year, the first internationally coordinated expeditions to the Arctic were undertaken. Another achievement of this year was the installation of

twelve observational stations, which provide data of surface air temperature and sea level pressure in daily resolution (Wood & Overland, 2016).
In the early 20th century, an increasing number of big vessels frequented the passage through the North Atlantic, transporting passengers or freight. By doing so, icebergs became a more important issue. This was especially true after the sinking of the Titanic caused by an iceberg and therefore the International Ice Patrol Service was founded. This organization documents the number and movement of icebergs; hence provided additional and very useful oceanic information. The U.S. Coast Guard collected further important knowledge about the oceanographic and sea ice conditions in the Davis Strait and the Labrador Sea between 1928 and 1935 (Smith, Soule, & Mosby, 1937).
During the years 1932 and 1933 a second IPY was conducted. At this time, 94 Arctic meteorological stations were in use. Unfortunately, the Second World War hampered much of the collected data to be published or analysed in detail although there were plans to archive the data at the Danish Meteorological Institute.

1.1.2. Modern Observations

The Second World War marks a turning point in Arctic Sciences. Several countries had noticed the strategic importance of the Arctic Region, primarily the U.S.A and the Soviet Union, and therefore installed many weather stations to get a deeper understanding of the Arctic's climate and weather. During the following years, both parties launched several programs, the U.S. Distant Early Warning Line (DEWLINE) or the Soviet's North Pole drifting station program. Since scientific exchange and communication between these two countries was limited, it was decided to hold an International Geophysical Year (IGY). As an expansion of the International Polar Year, the IGY was held in the years 1957 and 1958 and marks a major breakthrough in scientific interchange between East and West, which has been disturbed because of the Cold War. It encompassed eleven Earth sciences, amongst others meteorology, oceanography and seismology (NAS, 2005). Also, the first satellites were launched at this time and therefore the IGY marks the beginning of global observations from space.
In the 1970s it was the yearning of finding cheap oil and gas in the Arctic that supported further studies of the near-shore marine environment what lead to an improved knowledge of near-shore conditions of the ocean, its sea ice and the climate in shore regions. At this time, the U.S. nuclear submarine *Nautilus* carried out the first deep-sea sonar measurements of the Arctic Ocean. Even though this cruise was part of the Cold War game, it can be seen as a catalyst for further submarine expeditions to the Arctic, peaking in the Submarine Arctic Science Program (SCICEX). The SCICEX started in the mid-1990s and was a collaboration of the U.S. Navy with several research agencies and marine research community. (Serreze & Barry, 2014)

The next major step-stone in Arctic Sciences was the launch of the Arctic Ocean Buoy Program by the University of Washington in 1979. This program and its successor the International Arctic Buoy Program (IABP) collected data on surface air pressure and temperature as well as sea ice drift in the central Arctic. The data from these measurements was for the first time transmitted to the Global Telecommunication System. Together with measurements from submarines and newer technologies like drifter buoys and arrays of moored upward looking sensors, these programs represent a major source of Oceanographic data. (Serreze & Barry, 2014)

Another - still growing - data source are satellites. Beginning with the first passive microwave sensors on NASA satellites in 1973, this technology has become more and more important in recent years. Nowadays, parameters like sea surface height (SSH), sea level anomalies (SLA) or sea ice thickness as well as its velocity are directly observed by or derived from various satellite instruments. Examples are NASA's ICESat and ICESat-2 or ESA's CryoSAT-2. (Serreze & Barry, 2014)

According to Beszczynska-Mo¨ller et al (2011), observational arrays are essential for quantifying fluxes of volume, freshwater and heat into and out of the Arctic. The longest records are available for Bering Strait, starting in 1990. However, until 2004 only the U.S. part of the Strait was monitored continuously, afterwards new moorings on the Russian side enabled a permanent and complete observation of the Bering Strait. In the course of the third International Polar Year (2007-2009), the U.S. National Science Foundation (NSF) has deployed a new high-resolution mooring array in the Strait (Beszczynska-Mo¨ller et al., 2011).

For monitoring the Atlantic inflow sections east of Greenland, the VEINS Project (Variability of Exchanges in Northern Seas 1997-2000) was a precursor. Although it was a regional project, it was soon followed by the international pan-Arctic ASOF study (Arctic-Subarctic Ocean Fluxes, 2003– 2006) and the DAMOCLES project (Developing Arctic Modelling and Observing Capabilities for Long- term Environment Studies, 2006–2010). Transports through Davis Strait, to the west of Greenland, are measured as part of the NSF Freshwater Initiative since 2004. Longer records are available for the channels of the Canadian Arctic Archipelago (CAA) with records back to 1998. (Beszczynska-Mo¨ller et al., 2011)

1.2. The Arctic Ocean

More than two thirds of the earth's surface is covered by oceanic waters – the World Ocean. In total, this Ocean has a volume of about $1{,}335 \cdot 10^6$ cubic kilometres of water and therefore incorporates the major part of the Earth's hydrosphere (Eakins & Sharman, 2010). The World Ocean can be divided into five smaller Oceans, namely the Pacific Ocean, the Atlantic Ocean, the Indian Ocean, the Southern Ocean and the Arctic Ocean (UN, 2016). Compared to the others, the Arctic Ocean is the smallest and shallowest of the five major Oceans. With a surface area covering about $12 \cdot 10^6$

square kilometres and a total volume of about $17 \cdot 10^6$ cubic kilometres, the Arctic Ocean accounts for 3% to the total oceanic surface area but only 1.3% to the total volume (Tomczak & Godfrey, 2003).

The Arctic Ocean is almost completely surrounded by landmasses (Eurasia and North America) and is therefore often called Arctic Mediterranean Sea. By definition, a mediterranean sea has only marginal exchange with the major ocean basins and a primarily thermohaline circulation (Tomczak & Godfrey, 2003). Figure 2 shows the topography of the Arctic Sea and clarifies its mediterranean character. The Arctic Sea can be further subdivided into the Greenland, Iceland, Norwegian and North Polar Sea. The last one includes the Chukchi, East Siberian, Laptev, Kara, Barents, and White Seas on the Siberian coast line and the Lincoln and Beaufort Seas on the Greenland-Canadian-Alaskan shelf (International Hydrographic Organization, 1953) (see Fig. 2).

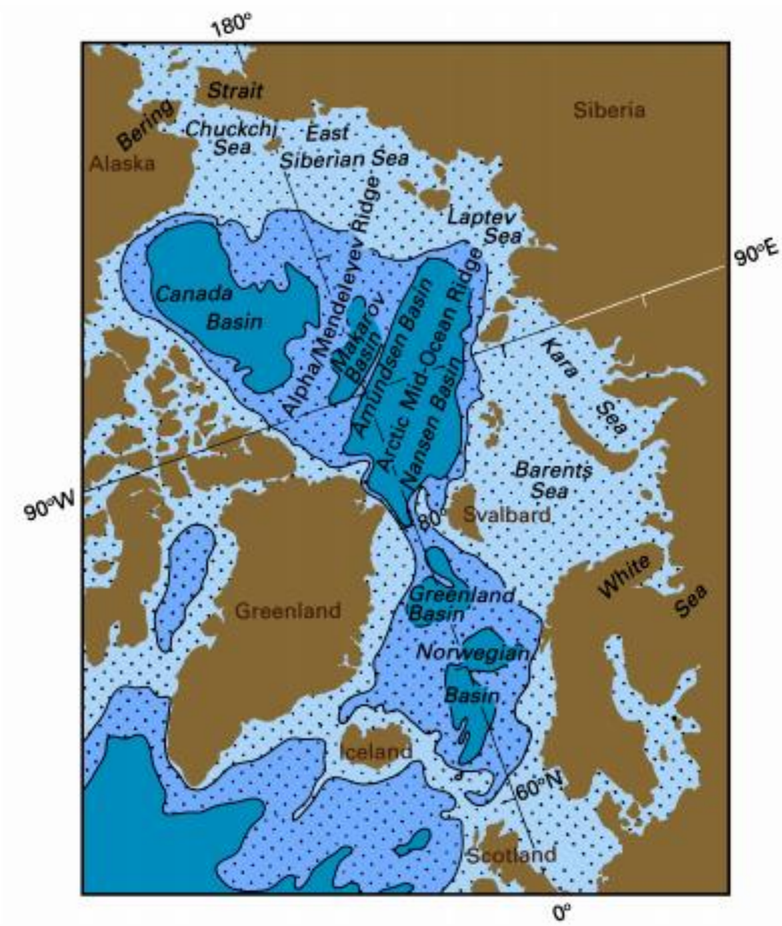

Figure 2: Geography and bottom topography of the Arctic Ocean. The 1000, 3000, and 5000 metre isobaths are shown and the regions are coloured (light to dark blue). Regions less than 3000 m deep are additionally dotted (Tomczak & Godfrey, 2003).

According to Tomczak & Godfrey (2003), the Arctic Ocean is also the shallowest of the five major Oceans. This is contributed to the large shelf areas in the Arctic Ocean, which are usually of minor depth. The average water depth in the shelf regions varies between 10 and 40 metres in the Laptev Sea, 20 to 60 metres in the Chukchi and East Siberian Sea and 100 to 350 metres in the Kara and Barents Sea. By covering almost 70% of the surface area of the entire Arctic Ocean, the shelf on the American and

Canadian side of the Ocean is about 50 to 90 kilometres wide, while it can reach over 800 kilometres along the Siberian coastline. (Tomczak & Godfrey, 2003)

Nevertheless, the North Polar Sea itself contains some deeper parts too. It is divided into a series of ridges (Alpha and Mendeleyev Ridge system, Lomonossov Ridge, Arctic Mid-Ocean Ridge) and basins (Canadian Basin, Makarov Basin, Nansen Basin and Amundsen Basin). The average depth of the basins is between 3600 and 3800 metres in the Canadian Basin and between 4300 and 4500 metres in the Amundsen Basin, whereas the depth of the separating ridges is between 850 metres at the Lomonossov Ridge and 2500 metres at the Arctic Mid-Ocean Ridge, which is sometimes referred to as the Nansen Ridge. (Tomczak & Godfrey, 2003)

Another specific characteristic of the Arctic Sea is the on average very low salinity (NSIDC, 2017). The main reasons for this extraordinarily low salt concentration in the Arctic Ocean are strong fresh water inflow from rivers in the shelf regions, a low evaporation rate and limited exchange with the surrounding oceanic deep waters. (Tomczak & Godfrey, 2003)

1.2.1. Arctic Ocean Gateways

The Arctic Ocean, or Arctic Mediterranean Sea, has several connections to the World Ocean. However, the transports of volume, heat and freshwater through these connections are highly variable and each strait modifies the state of the Arctic Ocean in a different way. Major connections to the Atlantic Ocean are for example through Fram Strait - between East Greenland and Svalbard - and through the Barents Sea Opening (BSO) between Svalbard and the Norwegian coastline. Another connection to the Atlantic is Davis Strait - between West Greenland and the Canadian Archipelago - although in some publications minor openings through the Canadian Archipelago, mainly through Nares Strait and Smith Sound are considered more important (Melling et al., 2008; Serreze et al., 2006).

Bering Strait represents the connection to the Pacific Ocean. Among the four major gateways used in this thesis (Bering Strait, BSO, Davis Strait and Fram Strait), the Bering Strait is the narrowest opening and with maximum depths around 40 metres also the shallowest (Worldatlas, 2017). The currents through the Bering Strait have only little consequence for the Arctic circulation patterns, but major importance for the freshwater cycle (Tomczak & Godfrey, 2003).

In the following section, mainly based on Beszczynska-Möller et al. (2011) and other authors cited, these four gateways will be described in more detail.

1.2.2. Bering Strait

The Bering Strait connects the Pacific and the Arctic Ocean and is with a width of about 90 kilometres the narrowest of the four major gateways. Furthermore, it is divided by the Diomede Islands and the International Dateline into two approximately 45 kilometres wide channels (Fig. 3). In each of the channels an important current can be found, the Alaskan Coastal Current and the Siberian Coastal Current. While the Alaskan Coastal Current and its contribution to the total Bering Strait throughflow is already properly understood, the impact of the current on the Russian side of the Strait is mostly unquantified (Woodgate et al., 2004).

Figure 3: Map of the location of the Bering Strait. The horizontal dashed line represents the Arctic Circle, while the dashed and bent vertical line represents the International Date Line.
Source: http://www.worldatlas.com/aatlas/infopage/bering.htm

Collecting observational data in the Bering Strait is, due to its shallowness and the high risk of damage due to ice, not easy. Nevertheless, since 1990, moorings in the centre of the channels provide continuous data of the flow about 40 metres below the surface (Woodgate et al., 2006). A sophisticated observational array, consisting of eight moorings, is available since 2007. These moorings include upper-layer sensors to quantify the three-dimensional structure of the flow (Woodgate, 2008). Although the annual mean volume flow is weak compared to the other gateways, the Bering Strait is highly important for nutrients and freshwater in the Arctic Ocean. Approximately one third of the Arctic's freshwater is supplied through this strait (Serreze et al., 2006). This freshwater supply plays also a major role in the upper-ocean stratification. The less salty water of the Pacific is floating above the saline Atlantic waters and therefore prevents the water from mixing. For heat transport, respectively, the Bering strait is important, especially in the summer months and can lead to significant sea-ice melt (Woodgate et al., 2010). Interannual variability of Bering Strait heat flux is large due to the variability in volume transport and temperature (Woodgate et al., 2010). Although it is much smaller than the other gateways, during summer the heat import through the Pacific is in magnitude nearly comparable to Davis or Fram strait (compare figures in Section 3.2).

According to Woodgate et al. (2004), there are two different mechanisms for volume transport in Bering Strait. The first mechanism is the sea surface pressure gradient between the Pacific and Arctic Ocean, what causes northward motion, hence inflow. The second, and partially opposing mechanism, are atmospheric pressure differences and local winds. These winds result in a southwest- or westward flow on average, thus driving Bering Strait outflow. Because of the shallowness of the Bering Strait, this second mechanism plays an important role and neglecting this influence can lead to an overestimation of volume imports by about 20% when inferring transports from this proxy (Woodgate et al., 2004; Woodgate et al., 2010). The estimates for total volume and heat transports through Bering Strait vary between 0.6 and 1.0 ± 0.1 *Sv* (1 *Sv* = 10^6 m^3/s) and 10 - 20 *TW* (Woodgate et al., 2010).

1.2.3. Barents Sea Opening

Figure 4: Map of the location of the Barents Sea and the Barents Sea Opening.
Source: http://www.worldatlas.com/aatlas/infopage/barentssea.htm

The Barents Sea Opening (BSO) is an approximately 600 kilometres wide Ocean passage between Spitsbergen and the North Cape (Fig. 4). With a maximum depth of about 450 metres, it is the major source of warm and saline Atlantic water (AW) for the Barents Sea. On the other hand, it is also a sink for cold and fresh water, leaving the Arctic Ocean near Bear Island. This issue was already discovered by Helland-Hansen and Nansen in the early 20th century and improvements in the estimates of the heat fluxes have been made in recent years (Smedsrud et al., 2013). Estimates for heat flux are approximately 70 ± 5 *TW* (Smedsrud et al., 2010), and clarify why the Barents Sea is nearly ice free all year around. Due to the lack of ice, large parts of the imported heat is lost to the atmosphere through latent, sensible and longwave radiation (Smedsrud et al., 2010).

Regarding volume transports, the estimates for volume import into the Arctic Ocean through the BSO are the largest among all gateways. The average inflow is about 3.2 *Sv*, but with very large interannual variability (Smedsrud et al., 2010). Additionally, approximately one third of this inflow is recirculated in the Barents Sea and leaves it around Bear Island about 2°C colder (Skagseth, 2008), which leads to an net inflow of 2 *Sv* (Smedsrud et al., 2010).

1.2.4. Davis Strait

Figure 5: Map of Greenland and the North Atlantic. Davis Strait is located between Greenland and Baffin Island. On the East side of Greenland also Denmark Strait is shown between Greenland and Iceland.
Source:
http://www.worldatlas.com/aatlas/infopage/destrait.htm

The Davis Strait, approximately 360 kilometres wide and 650 metres deep, is situated between Baffin Island, Canada and Greenland and connects the northern most part of the Labrador Sea with Baffin Bay (see Fig. 5). From the north, the narrow channels of the Canadian Arctic Archipelago (CAA), connect the Arctic Ocean with the Baffin Bay. About half of the total freshwater export of the Arctic Ocean (Beszczynska-Möller et al., 2011) flows through CAA and further south along Baffin Island as the cold and fresh Baffin Island Current (BIC) (Tang et al., 2004). This outflow is partially compensated by an inflow of fresh water masses above the West Greenland shelf (West Greenland Current (WGC)). Additionally, warm and salty water masses enter Davis Strait through the West Greenland Slope Current (Beszczynska-Möller et al., 2011). In the northern Baffin Bay, these inflowing waters turn west and join the outflowing waters of the Baffin Island Current (Tang et al., 2004). By looking at the Ice conditions in Baffin Bay, this flow regime becomes even clearer. Heavy ice movement can be found on the western shore, whereas on the eastern shore open waters are dominant (Finlayson, 2006). Because of the complex flow patterns in the Davis Strait, the observational data has to have a good spatial resolution to resolve its small-scale eddies, in order to calculate the transports through the strait correctly (Beszczynska-Möller et al., 2011).

Early estimates of volume and freshwater transports obtained by Tang et al. (2004) yield -3.3 to -2.6 (± 1.2) *Sv* for volume and -120 to -92 (± 34) *mSv* for freshwater. Newer studies, using an improved data coverage obtain similar values (volume transports -2.3 ± 0.7 *Sv*, freshwater -116 ± 41 *mSv* (Curry et al., 2011)). Regarding heat transports, Curry et al. (2011), receive values around 20 ± 9 *TW*, which is about a quarter of BSO heat fluxes.

1.2.5. Fram Strait

The last of the four major gateways is Fram Strait. Located between Greenland and Svalbard, it is more than 600 kilometres wide and with a maximum depth around 2600 metres in the centre of the strait it is the only deep water connection between the Arctic and the Atlantic Ocean (fig. 6). The exchange of deep waters in Fram Strait occurs in either direction and is essential for the oxygen and freshwater supply of the Arctic Ocean. (von Appen, Schauer, Somavilla, Bauerfeind, & Beszczynska-Möller, 2015).

Figure 6: Map of the Greenland Sea. Fram Strait is located between East Greenland and the West coast of Svalbard (NOR) and marks the northern boundary of the Greenland Sea.
Source:
http://www.worldatlas.com/aatlas/infopage/greenlandsea.htm

Two major currents, the West Spitsbergen Current (WSC) and the East Greenland Current (EGC), emboss Fram Strait. While the West Spitsbergen Current on the eastern side of the strait transports warm and salty water from the North Atlantic into the Arctic, the East Greenland Current conveys cold and relatively fresh water out of the Arctic. Since the Fram Strait is downwind of the Transpolar Drift, it also plays a major role in sea ice export. About half of the Arctic's freshwater export to the Atlantic Ocean occurs through Fram Strait, sea-ice and liquid water in equal parts (Serreze et al., 2006). The net freshwater transport through the strait accounts together with Davis Strait´s freshwater export, for about 80% of the Arctic's total freshwater export (Serreze et al., 2006).

Two opposing currents, the West Spitsbergen Current (WSC) and the East Greenland Current (EGC), mainly drive the volume transport through Fram Strait. The volume import through the WSC has been estimated with 6.6 ± 0.4 *Sv* in average by Beszczynska-Möller et al. (2012) for the period 1997 – 2010, while for the opposing EGC, the estimates are - 8.7 ± 2.5 *Sv* (avg. 2002 - 2009), obtained by de Steur et al. (2014). Regarding the heat flux through Fram Strait, Schauer & Beszczynska-Möller (2009) estimated it to be 36 ± 6 *TW*, again for a 1997 – 2009 period.

1.3. Arctic Energy Budget Considerations

Polar regions are an integral part of the global climate system. Outgoing longwave radiation in the Polar Regions outweighs absorbed solar radiation, i.e. they act as "heat sinks" of the planet. This negative imbalance is opposite to the imbalance in the tropics. The negative imbalance is strongest during winter months on the Northern Hemisphere when there is hardly any solar radiation in the Arctic. To balance this differential radiative heating, strong poleward transports of energy occur in the atmosphere as well as in the ocean. Through these transports large amounts of heat are transferred to the North. In other words, these transports warm the Arctic and cool the Equatorial Region. (Serreze & Barry, 2014)
Comparing the zonally averaged magnitude of atmospheric and oceanic heat transports, the atmospheric part is, except from lower latitudes, significantly larger than the heat transport through the ocean (Trenberth & Caron, 2001). To understand and quantify the energy fluxes entering the Arctic, energy budget considerations are very useful. For the Arctic, three components are fundamental: the atmosphere, the ocean and sea ice. Although for each of these components a separate equation can be defined, the energy budgets are coupled (Serreze & Barry, 2014). In fact, the three components are interacting with each other and a simplified model can be illustrated as followed:
In ice-free conditions the atmosphere gains energy from the ocean through surface net energy fluxes. If there is ice, then the atmosphere receives or loses energy through the ice-atmosphere interface. If there is ice on the ocean, an additional energy exchange at the ocean -ice interface takes place.

A schematic graphic of these exchanges is shown in figure 7. Following Haimberger (2015) and Serreze & Barry (2014), the simplified energy budget equations for the atmosphere, ocean and sea ice can be defined as:

$$\frac{\partial A_E}{\partial t} = -\nabla \cdot F_A + Rad_{TOA} - F_S \qquad Eq.1$$

$$\frac{\partial O_E}{\partial t} = -\nabla \cdot F_O + F_{IB} \cdot f_{ice} + F_S(1 - f_{ice}) \qquad Eq.2$$

$$\frac{\partial I_E}{\partial t} = -\nabla \cdot F_I - F_{IB} \cdot f_{ice} + F_S \cdot f_{ice} \qquad Eq.3$$

In the equations 1-3 the suffix "A, O, I" represent the atmosphere, the ocean and ice.
To ease the interpretation of *Eq.1 – Eq.3* all vertical fluxes are defined to be positive

downward. The first term on the right-hand side of each equation is the contribution of the horizontal convergence, the last term describes the net flux of energy through the surface to the atmosphere (positive in upward direction), where f_{ice} is the fraction of ice in the ocean surface. The interaction between the floating sea ice and the underlying ocean is represented by the second term on the right side in Eq.1 and Eq.2 (Haimberger, 2015).

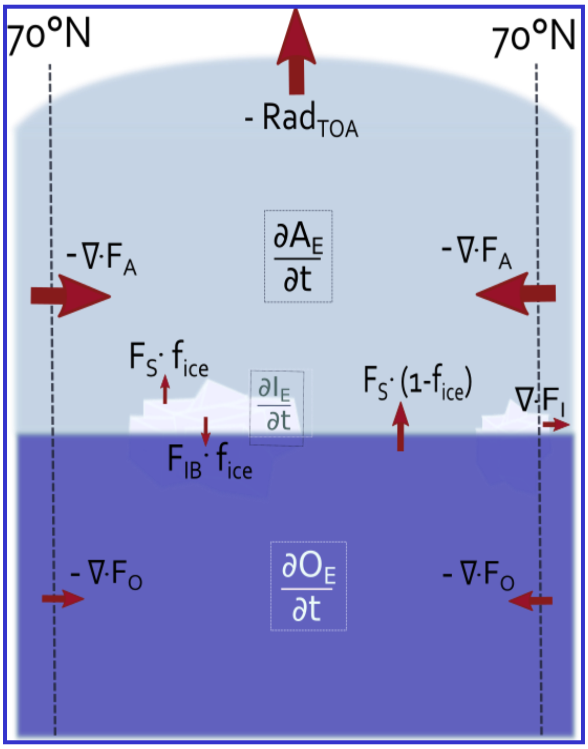

Figure 7: Arctic energy budgets. The figure is showing atmospheric, oceanic and sea ice energy budgets using equations from Haimberger (2015). (adapted from Fig. 3.5 in Serreze and Barry (2014, p.71)).

From the above equations, it is easy to see, that the rate of change of atmospheric energy stored in a column is governed by the sum of three terms (Eq. 1). The first term -$\nabla \cdot F_A$ represents the horizontal convergence of moist static plus kinetic energy flux within the atmosphere (Serreze & Barry, 2014). The second term in this equation represents the net radiative energy input at the top of the atmosphere (TOA). Rad_{TOA} is defined as incoming shortwave minus outgoing longwave radiation (during winter this term is negative). The last term is the contribution of vertical energy transfer through the bottom of the column. For the atmospheric column a positive F_S means energy is leaving the column, while negative F_S indicates energy gain. (Haimberger, 2015; Serreze & Barry, 2014)

To get a deeper understanding of Eq. 1, different formulations from Trenberth (1997) and Mayer & Haimberger (2012), can be combined, yielding:

$$\frac{\partial A_E}{\partial t} = -\frac{1}{g}\int_0^{p_S} [\nabla \cdot (c_p T + k + Lq + \Phi) v_2] dp + Rad_{TOA} - F_S \qquad Eq.4$$

This equation can be written even more detailed for energy budget evaluations (see Mayer et al. (2017)), but for the scope of this thesis *Eq. 4* is sufficient. In this equation, g represents the gravitational acceleration, p is the pressure (p_s = surface pressure), T is the temperature, c_p is the specific heat at constant pressure, L is the latent heat of vaporization, q is the specific humidity, Φ is the geopotential and v_2 is the horizontal wind vector (u, v). In this representation, one can see, that the -$\nabla \cdot \boldsymbol{F_A}$-term consists of four parts. The first part represents enthalpy or sensible heat (c_pT), followed by the kinetic energy (k), the latent heat (Lq) and the potential energy (Φ), all in Joules per kilogram. With v_2 being the horizontal wind, equation 2 can be inter-

preted as follows: If more energy is transported into the column than being transported out of it, the energy within this column increases. Another interpretation might be: If air temperature, moisture content or kinetic energy in this column rises, the atmospheric energy increases. (Serreze & Barry, 2014)
These considerations can of course be expanded over the whole Arctic, meaning that instead of a single air column, the volume of the air over the Arctic can be used. By doing so, equation 4 changes slightly too (see Mayer et al., 2016)):

$$\frac{1}{g}\frac{\partial A_E}{\partial t}\iiint_{ArcVol} dV_p =$$
$$= -\frac{1}{g}\oint\!\!\oint_{ArcBound}\left(c_p + k + Lq + \Phi\right) v dx dp + \iint_{B_A} F_S \, dA + \iint_{T_A} Rad_{TOA} \, dA \qquad Eq.5$$

With *ArcVol* being the Volume of the Atmosphere above the Arctic, surrounded by *ArcBound* as vertical boundary, B_A the bottom of the atmosphere and T_A the top of the atmosphere.
Similar considerations can be made for the ocean component as well. Recalling Eq.2 from above, it states that the tendency in ocean energy storage is depending on the convergence of oceanic energy transport (first term), the transfer of energy to the atmospheric column through the ice-free boundary ($F_S(1 - f_{ice})$) and the exchange with the sea ice itself. Neglecting the sea ice, the oceanic heat storage tendency can be written according to Schauer & Beszczynska-Möller (2009) as:

$$\frac{\partial}{\partial t}\iiint_{ArcVol(O)} (T - T_{ref})\rho c_w dV =$$
$$= -\oint\!\!\oint_{ArcBound(O)} (T - T_{ref})\rho c_w v dx dz - \iint_{B_O} F_S(1 - f_{ice}) dA \qquad Eq.6$$

Respectively with slight modifications:

$$\frac{\partial}{\partial t}\iiint_{ArcVol(O)} (T - T_{ref})\rho c_w dV =$$
$$= -\oint\!\!\oint_{ArcBound(O)+B_O} (T - T_{ref})\rho c_w v dA \qquad Eq.7$$

The left-hand side of this equation represents the change in ocean heat content (OHC). It only depends on one single term on the right side of the equation, meaning, if the ring integral is different from zero, there is a change in OHC. Holding ρ constant and using the product rule, one can rewrite Eq.7 as:

$$\frac{\partial}{\partial t} \iiint\limits_{ArcVol(O)} (T - T_{ref})\rho c_w dV =$$

$$= (T - T_{ref}) \oiint\limits_{ArcBound(O)+B_A} v dA - \oiint\limits_{ArcBound(O)+B_A} \frac{\partial(T - T_{ref})}{\partial x \partial y} \cdot \left(\oiint\limits_{ArcBound(O)+B_A} v dA \right) dA \quad Eq.8$$

With the help of Eq. 8, the role of the reference temperature can be seen a bit clearer. If the velocity perpendicular to the boundaries is zero, then, obviously, no change in OHC occurs regardless of the choice of the reference temperature. If v is different from zero, things change completely. The last term on the right-hand side of Eq. 8 remains independent of the choice of reference temperature. This is due to the fact, that the gradient stays the same for every reference temperature. In contrast, it is clear to see, that for the first term on the right-hand side T_{ref} is important. Summing up, if the net flux does not disappear ($v \neq 0$), the heat flux through the boundaries of a Volume is controlled by the volume flux imbalance and the choice of the reference temperature.

Therefore, it is important to use the same T_{ref} when comparing absolute values of heat fluxes for different locations or cross sections (Schauer & Beszczynska-Möller, 2009) and to avoid unrealistically large mass imbalances (Tsubouchi et al., 2012).

1.4. Seasonal variability in Arctic's energy budgets

Throughout the year, the individual terms of the above equations vary significantly. For understanding this seasonal cycle, monthly values of the energy budget terms have to be evaluated. The following passage is a summary of Serreze & Barry (2014, p. 76-84) and an earlier work from Serreze et al. (2007).

When considering the atmospheric part of the coupled Arctic energy budget, the energy storage depends on three terms (see Eq.1). Starting with the second term on the right-hand side, net radiation, the thoughts are very simple. This term represents the net external energy input to the Arctic through radiation. The largest energy fluxes can be found in summer, while during winter the energy imbalance between incoming shortwave radiation and from the emitted longwave radiation is strongly negative. If the energy input decreases, the zonal mean temperature gradient between Polar Regions and Mid-latitudes increases, and therefore the first term in Eq.1 becomes more important. That means, that the atmosphere tries to compensate for the loss of energy by an increased meridional heat transport to the North ($-\nabla \cdot \boldsymbol{F_A}$). The second compensating effect is the surface flux. This flux becomes negative if the atmosphere is cooler than the underlying surface.

During the summer months, the situation is different. Since the net radiation flux is only slightly negative (positive in June and July) at that time of the year, the energy gradient between high and mid latitudes and therefore the horizontal energy convergence decreases. At the same time the surface flux gets positive, meaning the atmosphere is warming the surface. Since large parts of the Arctic's surface consist of oceanic waters, here the interaction between the individual energy budgets comes into play. Turning now to the left side of the equation, one can see, that the energy storage in the atmosphere is weak, but strongly linked to the net solar radiation. The storage rate is highest in spring, when energy input through the sun increases rapidly and becomes negative in fall when solar radiation decreases again. At this point it is worth noting, that the energy budget for the individual months, obtained by Serreze et al. (2007) from ERA-40 Reanalysis and CERES satellite data, is not closed (see residual in table 1). The values for each month can be seen in table 1, adapted from Serreze et al. (2007). (Serreze & Barry, 2014)

Table 1: Monthly and annual mean values for the components of the Arctic's energy budget equation for the atmospheric part (Eq.1). All values are in W/m².
Source: Serreze & Barry (2014) after Serreze et al. (2007), slightly modified.

MONTH	$\frac{\partial A_E}{\partial t}$	Rad_{TOA}	$-\nabla \cdot \boldsymbol{F_A}$	F_S	*Res.*
January	-2	-175	108	56	-9
February	5	-171	112	51	-13
March	12	-143	110	40	-5
April	25	-88	92	17	-4
May	21	-27	66	-18	0
June	18	23	89	-70	24
July	1	11	94	-85	19
August	-17	-66	98	-39	10
September	-27	-145	106	17	5
October	-22	-183	114	53	6
November	-11	-184	105	55	-13
December	-3	-178	111	58	-6
Mean	0	-110	110	11	-1

The former paragraph outlined the seasonal cycle for atmospheric energy storage. Because the energy budgets for atmosphere, ocean and ice are coupled, in the next step, the oceanic energy storage (Eq.2) on monthly scale is outlined. According to Trenberth & Caron (2001) the meridional energy transport through the ocean is much smaller than through the atmosphere. In other words, when considering the annual cycle, the horizontal convergence term in the Arctic Ocean is of less importance for the energy storage in the ocean throughout the year. The net surface fluxes are the largest contribution to the change of OHC. These fluxes are downward during summer, when the ocean gains energy from the overlying atmosphere, and upward in winter, when the opposite happens. The energy gain from ice is strongest in the melting season (summer), whereas the loss of latent energy because of freezing processes is largest in fall and winter. (Serreze & Barry, 2014)

1.5. Research Question/Motivation

Measurements of oceanic variables such as velocity, temperature and salinity are often temporally or spatially limited. Albeit the data coverage is improving in the last years (GDAC, 2000), there are still some regions of very sparse data, for example the Arctic Ocean. Another problem of observational data is the consistency of these measurements. A variety of instruments were used over the years and adding their individual time series together to a consecutive time series can lead to significant errors (Aguilar et al., 2003). Additionally, some time series have gaps and others are too short to be used. To fill this gap of information, reanalysis products can be used. In contrast to observational data, ocean reanalysis products provide dynamically consistent three-dimensional and consecutive time series and fields of ocean variables (Storto et al., 2016). These fields can be very useful for many different diagnostics, for example for the investigation of transports of freshwater and energy across the Arctic (Storto et al., 2016).

Understanding and quantifying oceanic heat-, volume- and freshwater fluxes is important to understand the response of the Arctic to climate change. Nevertheless, many studies only quantify components of these fluxes by measurements and their attempts to integrate these results over the whole Arctic fail for different reasons (T. Tsubouchi et al., 2012).

Recently, new estimates of volume-, temperature and freshwater transports into the Arctic Ocean through the four major gateways (Davis-, Fram-, and Bering Strait and the Barents Sea Opening) have become available through the ARCGATE project ("Maximizing the potential of the Arctic Ocean Gateway array ") (AWI, 2017). These new and largely independent flux estimates provide a perfect dataset for the validation of reanalysis products. This is especially true for heat- and freshwater fluxes, since most of the other temperature- and salinity observations available are usually assimilated in the reanalysis (Masina et al., 2011).

The aim of this thesis is to compare the ARCGATE dataset to data of the Centro Euro-Mediterraneo sui Cambiamenti Climatici Global Ocean Reanalysis System (CMCC) "C-GLORS, Version 5" (Storto et al., 2016) and the latest ECMWF Ocean Reanalysis System "ORAS5", to validate their performance. To quantify the influence of a higher vertical resolution and the assimilation of observations, a more recent version of CMCC's ocean reanalysis, namely "C-GLORS Version 7" is used, however only for a limited time period. By doing so, this thesis represents an extension of earlier work by Pietschnig et al. (2017).

2. Data and Methods

In the next section, a brief summary of the used data and the methods applied will be given. In addition to the observational data, some instruments will be described.

2.1. C-GLORS (version 5)

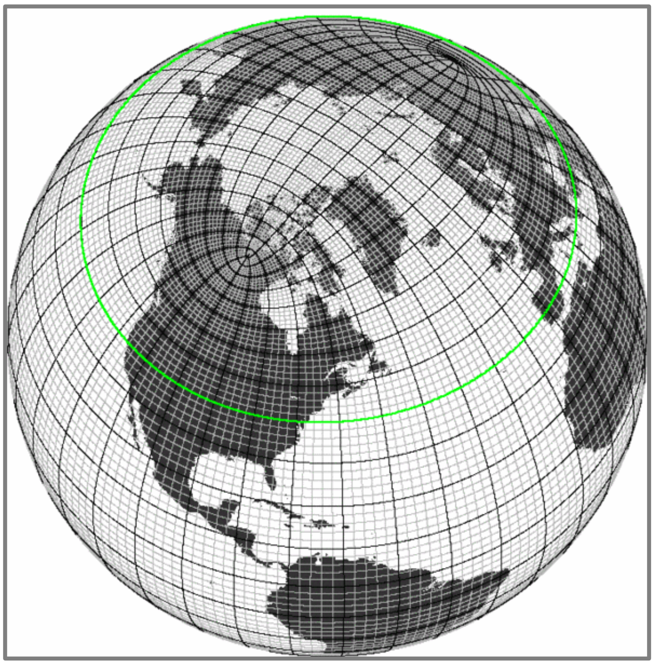

Figure 8: Tripolar grid from ORCA model configurations. The green line represents the latitude of transition between a regular grid with two poles and this tripolar grid.
Source:
http://www.geomar.de/en/research/fb1/fb1-tm/ocean-models/

For this thesis, two different versions of the CMCC Global Ocean Reanalysis System (C-GLORS) were used, version 5 and the later to be described version 7. Both versions are based on the NEMO ocean model (v3.2) in ORCA025 configuration with a horizontal resolution of ¼° (Storto et al., 2016). Because of the meridian convergence, this resolution results in a grid spacing from approximately 10 kilometres in the Arctic, while on the equator it would be 30 kilometres. The NEMO ocean model is equipped with a tripolar grid, to avoid singularities in the computations due to the convergence of gridlines in higher latitudes (Dawson & Gerritsen, 2013). With the implementation of a tripolar grid, the Northern Hemisphere has two poles, both on landmasses, not disturbing the computation of ocean fluxes. This grid enables the creation of a curvilinear, orthogonal ocean mesh for the Northern Hemisphere, while south of 20°N the grid is comparable to a regular, spherical grid (Madec, 2017). Despite its unaccustomed shape, no loss of continuity along the mesh lines or the scale factors is present (Madec, 2017). An example of this tripolar grid is shown in Figure 8. With the above prescribed tripolar grid, the C-GLORS v5 mesh consists of 1442 zonal grid points, 1021 meridional grid points and 50 vertical levels. However, the vertical levels are not equally spaced, having the narrowest grid spacing in the upper layers (Storto et al., 2016).

To account for sea ice, the implemented version of the NEMO ocean model is coupled with the Louvain-La-Neuve sea ice model in version 2 (LIM2) (Storto et al., 2016). Observations of oceanic variables like temperature or salinity from XBT (expendable

bathythermographs); CTDs (Conductivity-Temperature-Depth-Sensors), Argo floats, etc. are assimilated. The so-called EN3v2a and EN4 datasets, provided by the U.K. Met Office, are collections of these data (a detailed description of the instruments follows in section 2.4). In addition, satellite derived data for sea level anomalies (SLA) from the AVISO dataset are included (Storto et al., 2016a). Atmospheric forcings from ECMWF's ERA-Interim reanalysis (Dee et al., 2011) are implemented using CORE bulk formulas (Storto et al., 2016; Large & Yeager, 2009). The assimilation itself works with a three-dimensional variational assimilation scheme (3DVAR).
To improve computational performance, the NEMO model uses a special staggered grid, adapted from Arakawa C grid (Madec, 2016). Using a staggered grid means, that the computation of individual variables can be on different grids, all shifted by a half grid cell (Collins et al., 2013).

2.2. C-GLORS (version 7)

Recently, a newer version of CMCC's Global Ocean Reanalysis System has been released, named C-GLORSv7. Compared to the earlier version 5, it comes with some improvements. One of the main improvements is the increased vertical resolution, with now 75 vertical levels in total compared to 50 levels in Version 5. Also, the horizontal resolution changes slightly. While in the older v5 1021 meridional grid points are available, the new grid has 29 more points "attached" south of the old grid to allow an extension in the Antarctic region. Since this new grid points do not affect the Arctic region, the resolution in this area is the same as in v5. Further improvements are due to the update of the NEMO ocean model (v3.6) and a change in the formulation of the sea surface height. The time period covered in v7 (1993-2016) is shorter than in v5 (1980-2015), but both cover the period of interest (2004-2010).
In addition to the full v7 run, this latest version of C-GLORS also includes monthly data from the control run. For the control run, the data-assimilation and surface nudging are switched off. Therefore, the influence of data assimilation can be assessed from the difference of full and control run.

2.3. ORA-S5

For further comparison, the soon to be published ECMWF Ocean reanalysis ORAS5 is included in this thesis. Since detailed information about the model configuration is not available yet, the description of the model is based on a technical memorandum about ORAP5 (Zuo & Mogensen, 2014) a prototype of the upcoming ORAS5. ECMWF ocean reanalysis uses the NEMO ocean model (v3.4) in the ORCA025.L75 configura-

tion again, meaning it has a tripolar grid with a resolution of ¼° and 75 vertical levels. The horizontal resolution in high latitudes varies between less than 5 kilometres on the CAA and 17 kilometres around Bering Sea. Again, the vertical levels are not equally spaced, increasing from 1 metre spacing at the surface to several hundred metres in the deep ocean.
Concerning the influences of sea ice, ORAS5 uses the dynamic-thermodynamic sea ice model LIM2, with a coupling to the ocean model every three time-steps. The model uses in-situ observations of oceanic variables like temperature and salinity through the EN4 dataset and satellite observations of SLA through the AVISO dataset. Sea surface temperature and sea ice concentration are taken from several sources throughout the 1993 to 2012 period. Atmospheric forcings are included from ECMWF's ERA-Interim reanalysis (Dee et al., 2011). All Observations and forcings are assimilated by NEMOVAR in a 3DVAR mode (Zuo & Mogensen, 2014).

2.4. ARCGATE

In the year 2015 a new research project by the Alfred Wegener Institute (AWI) was launched with the goal to efficiently use the Arctic Gateway array. This project is called ARCGATE and follows a new, pan-Arctic approach to calculate transports of oceanic quantities such as volume, heat and freshwater for a 2004-2010 period (AWI, 2017).
The description of this dataset is therefore mainly based on AWI (2017) and Tsubouchi et al. (2012, 2017). Due to its special geometry, the Arctic Ocean can be treated as a single box, bounded by landmasses and hydrographic lines. In these hydrographic lines – the Arctic Gateways – arrays of moored instruments were installed for the measurement of variables like velocity, temperature and salinity. From these in-situ observations, the above-mentioned oceanic fluxes are calculated. Nevertheless, the box is not fully closed, since smaller gateways in the Canadian Arctic Archipelago are not directly included in the model. To account for this gap, estimated transports from a six-week measurement campaign in early 1972 are added to the uncertainty of the fluxes. The bottom of the model box is the seabed, where no exchange is possible. The upper boundary of the box, the sea surface or the upper part of floating sea ice, is, in contrast to the bottom, designed to allow for exchanges between sea and the overlying atmosphere. These exchanges can be for example freshwater fluxes like precipitation, evaporation and runoff or heat transfer from the ocean to the atmosphere or vice-a-versa (Tsubouchi et al., 2012). Furthermore, it is important to note, that no storage of volume or freshwater is permitted in this box, meaning volume and freshwater are conserved (Tsubouchi et al., 2012).

The Arctic Gateway array consists of 138 moored instruments, distributed to 41 mooring sites, providing observations of the oceanic variables temperature, salinity and velocity. As it can be seen in Figures 9 & 10, despite this high number of observations, there are locations with poor data coverage - for example Bjørnøya Bank between Svalbard and Bear Island. Generally, in shallow waters the data coverage is less dense than in deep water, due to problems with sea ice.

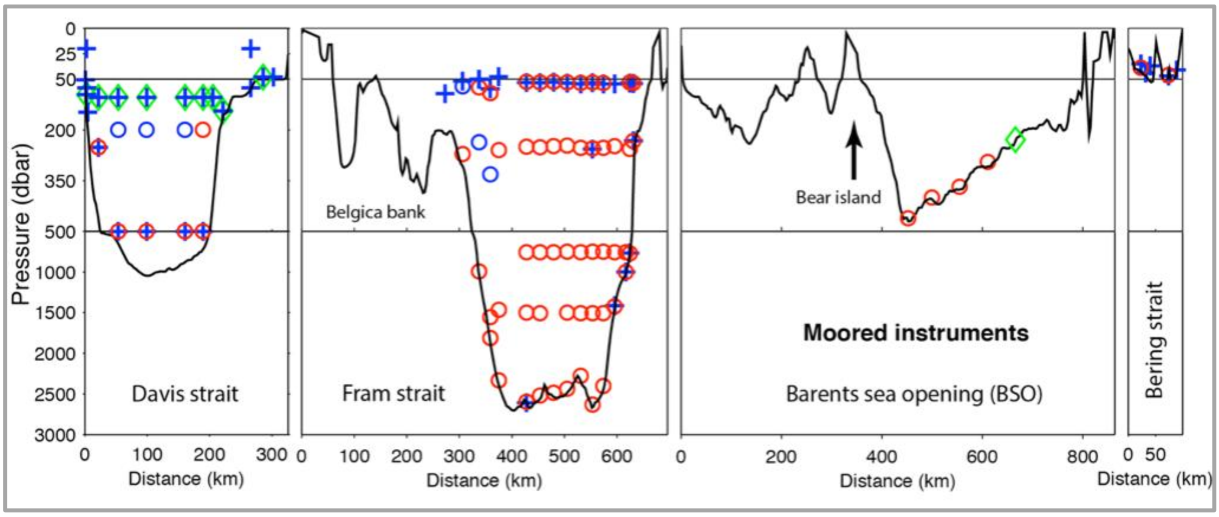

Figure 9: Location of 138 instruments at 41 mooring sites in the Arctic Gateways. Blue crosses are temperature and salinity measurements by SeaBird microCATs. Blue circles are Aanderaa single point current meters, also measuring salinity. Red circles are current meters without salinity measurements. The green diamonds indicate ADCP (acoustic Doppler Current Profiler) measurements for velocity profiles. This figure is taken from Tsubouchi et al. (2017)

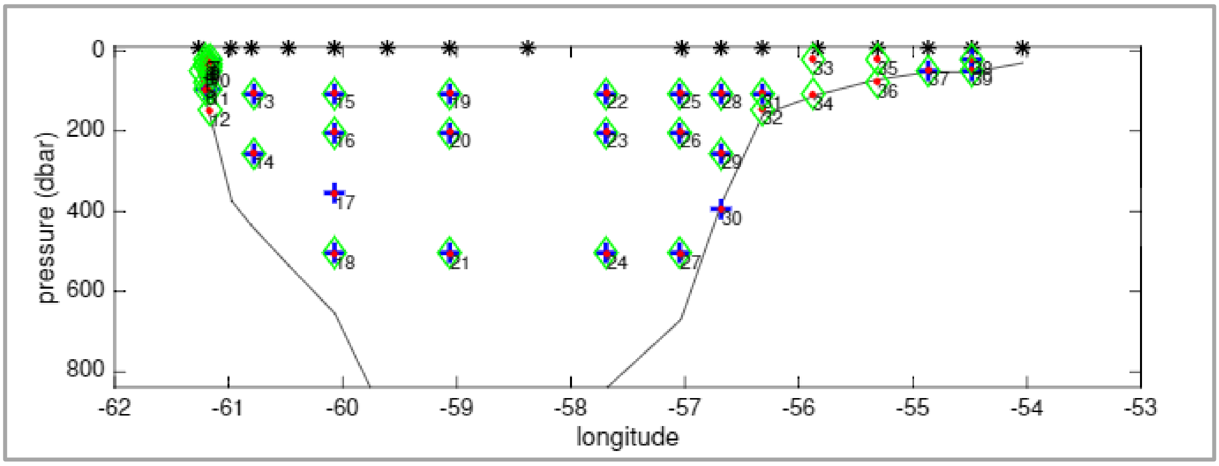

Figure 10: Location of the instruments in Davis Strait. Blue crosses are temperature and salinity measurements by SeaBird microCATs. Blue circles are Aanderaa single point current meters, also measuring salinity. Red circles are current meters without salinity measurements. The green diamonds indicate ADCP (acoustic Doppler Current Profiler) measurements for velocity profiles. This figure is part of an unpublished manuscript (Tsubouchi, 2016), which has been kindly provided by Dr. T. Tsubouchi and is available from the author on request.

To account for the problem of unregular spaced measurements, vessel-based hydrographic data and, additionally, output from the NEMO ocean model is added. The model configuration is comparable to the one of the reanalysis products described above, instead of the horizontal resolution which is in a 1/12 ° configuration. The finer resolution and the concentration of gridlines due to the tripolar grid, results in an effective resolution of approximately 3 kilometres. The vertical resolution is again depth-dependent, with 75 vertical levels and increasing spacing with depth.

Another challenge is the continuous data availability throughout the whole measurement period, lasting from 2004 till 2010. As one can see from Figure 11, there are multiple gaps in the time-series of the individual instruments. Especially at the beginning of the time-series the data coverage is sparse compared to the latter times. Figure 11 is only representative for Davis Strait, however, the time-series for the other straits look similar.

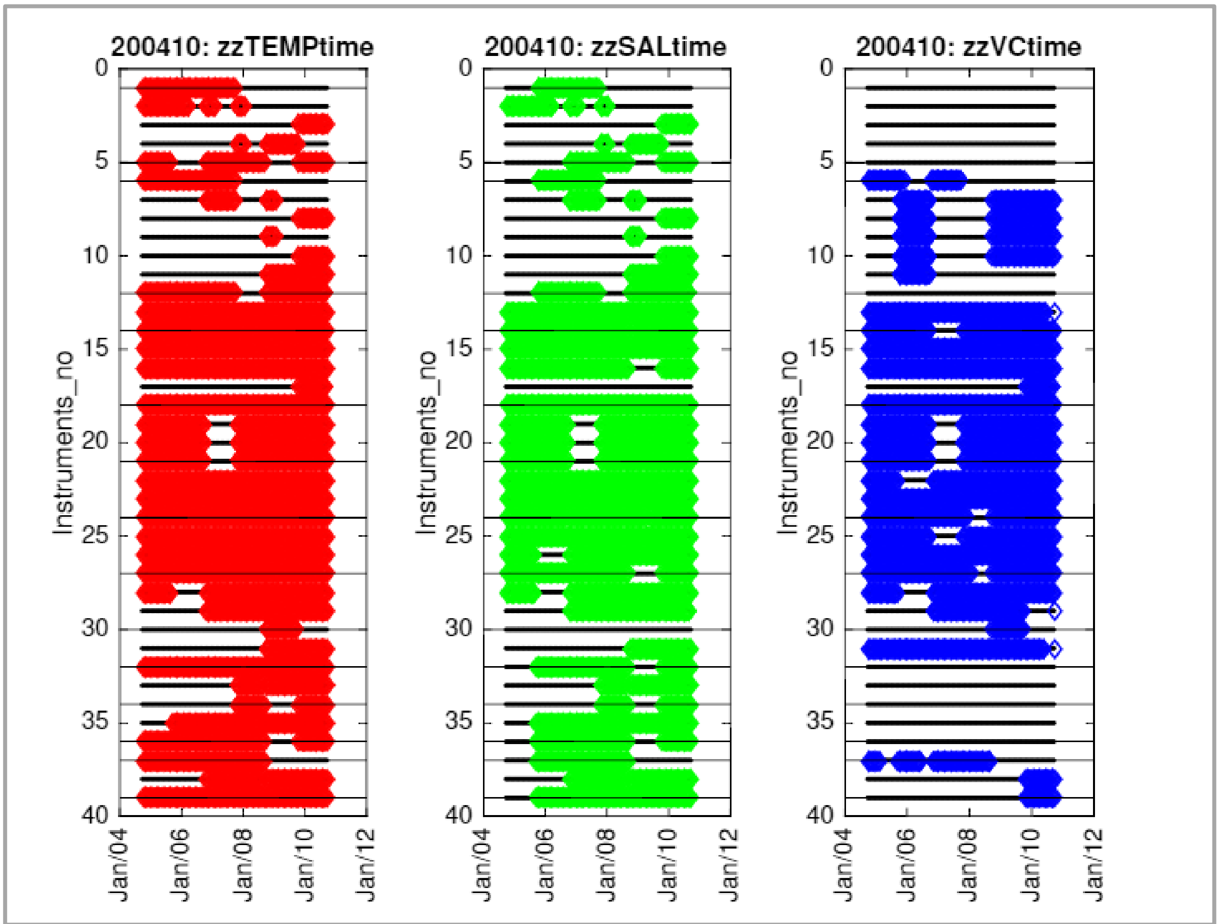

Figure 11: Availability of measurements in Davis Strait. On the vertical axis, the number of the instruments (see Figure 10) is shown and plotted against the time. Red circles indicate temperature measurements, the green ones are salinity measurements and the blue circles are velocity measurements. This figure is part of an unpublished manuscript (Tsubouchi, 2016), which has been kindly provided by Dr. T. Tsubouchi and is available from the author on request.

To account for the gaps in the observations, the data collected by the instruments shown in Figures 9 & 10 is in a first step filtered to remove unwanted tidal signals and faulty time series. In the next step, the data is interpolated, horizontally and vertically as well, to fill the entire cross section of each strait. For each strait and variable, a slightly different method is applied. Simplified, the interpolation process can be described as follows: First a horizontal interpolation at the individual instrument depths is carried out. In a second step the vertical interpolation at each mooring site

is executed. The last part is again a horizontal interpolation, but this time between the mooring locations (Tsubouchi et al., 2017).
By doing so, an ARCGATE grid is made, consisting of 2714 vertical levels and 643 horizontal grid points for temperature and salinity, and 639 grid points for velocity respectively. The derived fields of temperature, salinity and velocity are then averaged to get monthly fields. Those monthly fields are then used by Tsubouchi et al. (2012) to compute the volume, heat and freshwater transports through each strait. For heat and freshwater fluxes, the reference values are obtained by taking the mean temperature and salinity across the Arctic boundary. In addition to these results, in the newer paper of Tsubouchi et al. (2017), the authors used reference values found in literature to compare their results.

2.4.1. Instruments

In this section, a brief overview about the observational instruments and sensors used in the Arctic Ocean and especially in the Arctic Gateway array are given.

2.4.1.1. Acoustic Doppler Current Profiler (ADCP)

ADCP's are instruments anchored on the ocean floor, which are designed to measure ocean currents with high precision and without moving parts. These instruments use the Doppler effect and the assumption that particles in the water are moving with the same speed as the water itself, to detect the direction and the velocity of the water currents above them. The principle is very simple: The ADCP emits a series of high frequency pulses that get reflected by moving particles in the water. If the received frequency is lower than the emitted, the particles are moving away from the profiler. On the other hand, if the frequency is higher, the particles are moving towards the instrument. Since ADCP's are usually equipped with four acoustic transducers, it is possible to measure currents in different depths. Additionally, some research vessels have permanently mounted ADCP's on their outer hull, to conduct continuous measurements. (NOAA, 2008)

2.4.1.2. MicroCAT – CTD Sensors

MicroCAT - CTD Sensors are part of the family of moored instruments. They measure several oceanic quantities at a fixed location over a defined period of time. The abbreviation CTD stands for Conductivity, Temperature, and Depth. Even though, the term

“Depth” is in this case misleading, as CTDs usually measure pressure instead of depth. Since the relationship between pressure and depth can be quite complex (depending on water density, compressibility and local gravity field), it is important to note that both quantities are not the same. Using the CTD data, variables like salinity, density, sound velocity, and other parameters can be calculated. Some CTD’s, also called sondes, have no pressure sensor included, because the deployment depth is known, at least approximately. From this kind of instrument a broad variety of versions exist, some are only suitable for shallow waters with depths not exceeding 350 metres, while others can be deployed in depths reaching 7000 metres. (SeaBird Scientific, 2017)

2.4.1.3. Seaglider

Seagliders are largely autonomous underwater vehicles (AUV), which are designed for long-term measurements of oceanic variables. They use changes in buoyancy in the water and small wings to move forward (Kongsberg, 2017). By doing so, these instruments glide through the water, taking measurements of conductivity (salinity), temperature and pressure as well as other properties like dissolved oxygen or chlorophyll content (Beszczynska-Möller et al., 2011). In contrast to moored instruments, Seagliders can measure at different locations within one measurement campaign. Since Seagliders can execute measurements close to the ice-ocean interface, they are very useful in areas of enhanced sea ice. The data transfer from the Seaglider to the researcher can be made via satellite at the end of the campaign, or every time the glider reaches the ice-free ocean surface. From this type of instrument three different versions are available, the main difference being the maximum diving depth. (Kongsberg, 2017)
In the Arctic Region, Seagliders have been mainly deployed in Davis and Fram Strait to improve the data coverage of temperature and salinity in areas of sparse measurements (Beszczynska-Möller et al., 2011). Nevertheless, these observations are not used in the ARCGATE project.

2.4.1.4. ARGO-floats

In contrast to Seagliders, ARGO is a global array of 3800 free-drifting profiling floats. Each float conducts measurements of temperature and salinity to a maximum depth of 2000 metres in a predefined measurement cycle. This cycle consists of a stepwise dive till the maximum depth is reached and afterwards going up to the surface. At the surface a data transmission via satellite is established and the data gets published hours after its collection. Thanks to the ARGO-program, it is for the first time possi-

ble to have a continuous monitoring of the most important variables of the upper ocean. (GDAC, 2000)
Measurements of the ARGO-program are not used in ARCGATE, but they are very useful for ocean reanalyses, including C-GLORS(v5,v7) and ORAS5 .

2.4.1.5. Expendable bathythermograph (XBT)

Expendable bathythermographs are small sondes usually deployed over the side of a ship, measuring temperature as a function of the pressure (depth). During the dive, the sonde is connected to the ship through small wires to transmit the data back directly. The probe has no pressure sensor included, instead, since the falling speed of the probe in the water is approximately known, the depth and therefore the pressure can be computed. Nevertheless, uncertainties in the falling speed or malfunctions of the acquisition system, can cause significant errors to measured temperatures. Since these biases are of comparable magnitude with the natural temperature variability in the ocean, ignoring them can lead to false conclusions. (Gouretski, 2017; NOAA, 2015)

2.5. Methods

In the following section the methods used will be discussed. The methods are divided into two parts. The first part handles the general setup, while the second part is about diagnostics applied on the ocean reanalysis and observations.

2.5.1. General methods

To compare ocean reanalysis data with observations, all datasets should cover the same area. Since observational data is only available for cross sections in the Arctic Gateways, it was decided to find the points on the reanalysis grid closest to the observations. By doing so, an irregular line of data points is generated. Since all reanalyses used in this thesis use the same tripolar grid, the points are the same as well. The irregularity in this line arises from the fact, that the observation points cross several grid lines of the reanalysis field (compare Fig. 12). In order to calculate ocean transports of volume, heat and freshwater through this line, the fluxes have to be calculated at each grid point.

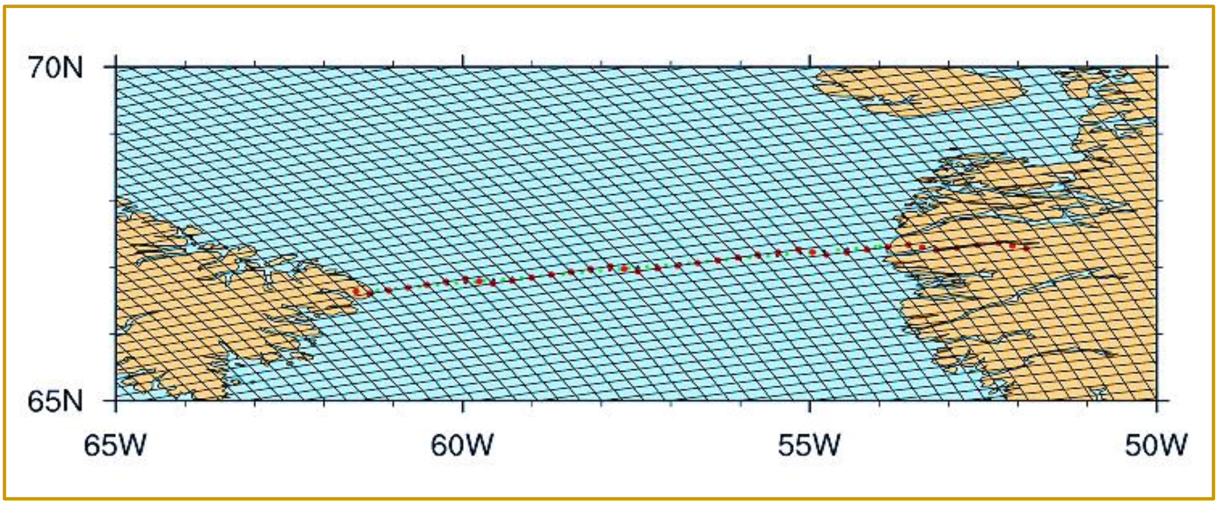

Figure 12: Schematic of Davis Strait model grids. The ARCGATE grid is shown as a line of green dots, while the black lines are the tripolar grid of the reanalysis models for the v-grid. The red dots indicate the closest tripolar grid point to the corresponding ARCGATE points.

To calculate these fluxes, daily (C-GLORS v5, C-GLORS v7) or monthly (C-GLORS v7 – control run, ORAS5) fields of temperature, velocity and salinity are used.
The calculation of volume transports through each Gateway follows equation 9:

$$Volume\ transport = \iint \boldsymbol{v}\ dzdx \qquad Eq.9$$

In this equation $\boldsymbol{v}$ represents the zonal and meridional velocities u and v respectively. To calculate volume fluxes according to equation 9, daily fields of velocity (u and v) are first multiplied with the corresponding depth section (dz_u and dz_v). In the next step, monthly averages of these values are computed. To account for the integral in equation 9, the monthly averages are summed up over the whole depth. In a last step, these results are multiplied with the associated horizontal increment (dx_u and dx_v) and along the line integrated, yielding the monthly means of zonal (u) and meridional volume transports through the cross section bounded by the irregular grid line and the ocean floor.

The computation of the heat transports through the Straits is similar to the computation of volume transports, but additionally, a reference temperature and constants have to be specified (see eq. 10). The reference temperature (θ_{ref}) is set to 0°C, the heat capacity of water at constant pressure ($c_{p(w)}$) is equal to 3990 J/kgK and the density of the ocean water is set constant to ρ = 1026 kg/m^3.

$$Heat\ transport = \iint \rho\, c_{p(w)}(\theta - \theta_{ref})\boldsymbol{v}\, dzdx \qquad Eq.10$$

In comparison to the calculation of volume transports, some additional steps are necessary to calculate heat transports. First, temperature and velocity have to be on the same grid. To achieve this, the temperature fields are interpolated in zonal as well as in meridional direction. After the interpolation, the in-situ temperatures are converted into potential temperatures. Having the potential temperature fields, they can be multiplied with the product of velocity and depth increment (udz_u and vdz_v). Further steps are the monthly averaging and the vertical integration. The last step is again the multiplication with dx_u and dx_v and the integration along the line to receive the monthly values of heat transports through the cross section.

The calculation of freshwater transports follows the same scheme as heat transports, but here, in contrast, the salinity has to be interpolated. Also, a reference salinity (S_{ref}) has to be chosen. To yield comparable results with the observations, the same reference value like in the ARCGATE data is used for all datasets (S_{ref} = 34,662 PSU (Tsubouchi et al., 2012)).

$$Freshwater\ transport = \iint \rho \left(\frac{(S - S_{ref})}{S_{ref}} \right) \boldsymbol{v}\, dzdx \qquad Eq. 11$$

To obtain more intuitive results with respect to freshwater transports, this equation can be multiplied with a factor of (-1). If one is more interested in salt transports instead, the multiplication with the above-mentioned factor can be omitted. Since the net volume transport should be nearly 0 (no volume is accumulated in the Arctic), the only contribution is due to eddy transports (Tsubouchi et al., 2012).

The above obtained transports of volume, heat and freshwater for each Gateway are subsequently used for a first comparison with the ARCGATE dataset, which has these transports already included. To visualize the transports of the reanalysis and ARCGATE data, time series are plotted. Differences between the data sources are furthermore highlighted by comparing averages over the whole period and by computation of a cross correlation.

To get a deeper understanding of the differences and their spatial distribution, another visualization was chosen. A qualitative method for such comparisons can be Hovmoeller diagrams. Albeit their advantage of being very instructive, some additional preparation work is necessary for the generation of these plots. First of all, the reanalysis velocities have to be projected onto the ARCGATE line. By doing so, it can be ensured, that the transports are not along the line, what would cause the transports to disappear. The steps during this preparation work shall be outlined in the following passage.

Since each of the reanalysis products uses a staggered grid, it is difficult to define a velocity vector in each grid point. This is due to the fact, that there is for example no information about meridional velocities (v^u) on the u-grid. This lack of information has to be compensated by an interpolation of the v-values onto the u-grid. The velocity vector at an arbitrary u-grid point can then be written as follows:

$$\boldsymbol{v}^u = u^u \cdot \boldsymbol{e}_{1,u} + v^u \cdot \boldsymbol{e}_{2,u} \qquad Eq.12$$

The vectors $\boldsymbol{e}_{1,u}$ and $\boldsymbol{e}_{2,u}$ in equation 12 represent the Cartesian unit vectors and are calculated as the normed vectors between two neighbouring temperature grid points and two vorticity (f) grid points respectively. Of course, the same is true for the v-grid. A schematic illustration of these considerations can be seen in Figure 13.

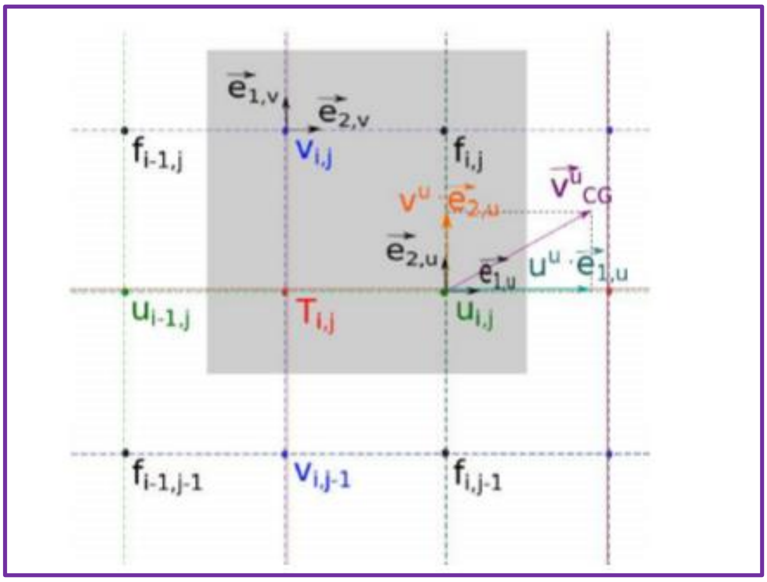

Figure 13: Illustration of a staggered NEMO grid. The red points belong to the T-grid, green points to the u-grid, blue colours indicate the v-grid and black belongs to the f-grid. The grey area indicates the grid points with the same indices (i,j).
The unit vectors of the u and v-grid are shown in black arrows. Additionally, the velocity vector and its components at a specific u-grid point are shown. Taken from Madec (2016, p.52), adapted version from Pietschnig, 2016.

The next step is the implementation of a normal vector $\boldsymbol{n}_{AG}$ onto the velocity vector can be projected. This vector can be easily found by calculating the distance and the Cartesian direction between the ARCGATE points ($\boldsymbol{e}_{AG}$). Subsequently, one has to compute the cross product of $\boldsymbol{e}_{AG}$ with its position vector, yielding $\boldsymbol{n}_{AG}$. For each point on the irregular reanalysis line a separate normal vector has to be calculated.
With the normal vector found, the projection of the velocity vector onto the normal vector can be written as:

$$\boldsymbol{v}_{projected} = \boldsymbol{v} \cdot \boldsymbol{n}_{AG} \qquad Eq.13$$

After the projection is calculated, the monthly values can be used for the computation of the transports through each gateway. To make the values obtained from the reanalysis dataset and the ARCGATE dataset comparable, they have to be brought to the same resolution. This is done by thinning out the ARCGATE line and, at the same time, increasing the vertical resolution of the reanalysis to match that of the ARCGATE. To do so, the vertical levels of the model data have to be converted into pressure levels. For this thesis, a set of two different Hovmoeller plots is generated. The first one – a time versus depth representation – is generated by integrating over all grid points along each gateway, while the second diagram is created by integration along the vertical axis.

2.5.2. Time series analysis

The first part of this subsection covers the creation of time series plots for all datatypes. Since the time series of each of the datasets reveal some special characteristics, this subitem deals with some additional diagnostics applied on all datasets. These diagnostics, also known as time series analysis, covers all methods for describing data in which the observations or data points are organized in time (von der Lippe, 1993).
By dealing with such time series, it is useful to calculate the mean seasonal component. This allows the seasonal influences to be isolated from the whole time series. Isolating and removing these influences yields time series of the anomalies, which are suitable for a further and deeper analysis. The seasonal component can be easily computed for every single month by calculating the monthly mean value of a variable (e.g. temperature) of this calendar month over a given period (see Eq. 14, modified after von der Lippe (1993), p. 417).

$$\bar{\bar{x}}_i = \frac{1}{n}\sum_{j=1}^{n} \bar{x}_i \qquad Eq. 14$$

The expression $\bar{\bar{x}}_i$ represents the monthly mean of the variable of interest, the subscript i denotes the month of interest. The variable n stands for the number of years in the dataset. Afterwards, the calculation of $\bar{\bar{x}}_i$ can be repeated for all months of the year (von der Lippe, 1993). In a second step, these values – the climatology- can be subtracted from the original time series. The result is an anomaly time-series, which can be used for further analysis.
To investigate the periodic behaviour of these anomaly time-series, they can be expressed as a combination of cosine (or sine) waves with slightly different periods and amplitudes (von der Lippe, 1993; p.432).

$$x_t = \sum_{j=1}^{n/2} \left[\beta_1 \left(\frac{j}{n}\right) cos(2\pi\omega_j t) + \beta_2 \left(\frac{j}{n}\right) sin(2\pi\omega_j t)\right] \qquad Eq. 15$$

(modified after von der Lippe, 1993; p. 433)

In *Eq.15* n is the number of data points and the ω_j are a set of possible frequencies, the so-called harmonics. The parameters β_1 and β_2 are regression parameters. This decomposition has not to be done manually; instead, a built-in function of NCL can be used. The NCL-function *specx_anal* performs this transformation via a Fast Fourier Transform (FFT) (NCAR, 2017).

By looking at the time series plots in Section 3, it is easy to see, that there is lots of high frequency noise in all parameters (volume, heat and freshwater transports) and all datasets (reanalysis and observations). Since these high frequency variations hinder an effective comparison of the reanalysis data with the observations, it was decided to use a low-pass filtering to remove this high frequency noise. At this point it is worth noting, that such a filter should also be applied to the anomaly timeseries instead of to the original time series. Numerical low-pass filtering is used to suppress short-term variations and therefore high frequencies, while longer-term fluctuations become clearer. To examine the filtering, a range around any time value must be specified. Within this range, surrounding values used to compute a weighted average (previous and consecutive time steps (Schönwiese, 2006)). To compute the weights, also a built-in NCL function was used. The function *filwgts_lanczos* creates a set of weights for each individual time series with user-specific characteristics (NCAR, 2017). After the weights and therefore the mean at one point is computed, the filter area is moved to the next data point. For this reason, this method is called "running mean". One drawback of this method is, that at the edges of the time series, where no previous or consecutive data is available, the filtering cannot be applied. Usually these sections of the time series are cut off to avoid erroneous values at both ends (Schönwiese, 2006).

$$\overline{x_t} = \frac{1}{2n+1} \sum_{i=-n}^{n} \omega_{t-i} x_{t-i} \qquad \forall\, t \in\; [n, k-n] \qquad Eq.16$$

In this equation n represents the number of data points used prior and after the central point for the calculation of the weighted running mean. The ω_i are a symmetrical set of weights computed with the NCL *filwgts_lanczos* function.

Next, the time series of the individual straits are reviewed. This is done by correlating the straits against each other. By doing so, it is possible to investigate the influence of an inflow in one strait on the other straits and vice-versa. The cross-correlation between two datasets x and y, can be computed according to Rodgers & Nicewander (1988) with the following equation:

$$r_{x,y} = \frac{\sum xy - \sum x \cdot \sum y}{\sqrt{[\sum x^2 - (\sum x)^2][\sum y^2 - (\sum y)^2]}} \qquad Eq.17$$

An alternative formulation of this equation, again given by Rodgers & Nicewander (1988), can be written as:

$$r_{x,y} = \frac{Cov(x,y)}{\sigma_x \cdot \sigma_y} \qquad Eq.18$$

With *Cov(x,y)* being the covariance between x and y, and σ_x and σ_y indicating the standard deviation of x and y respectively. Instead of computing these correlations manually, again an NCL-function (*escorc*) was used in this thesis. This function computes the Pearson cross-correlations at lag 0 (with no time shift between the time series (NCAR, 2017)). They make the correlations visible and the values of the straits are plotted as scatter plots against each other. In these plots, regression lines indicate the amount of correlation.

3. Results and Discussion

In this chapter, time-series plots, Hovmoeller plots and the diagnostic plots obtained from both, reanalysis and observations, are shown. Similarities and differences between these datasets are discussed, attempting to find possible explanations for the differences. For clarity reasons, this section is furthermore split into three parts, volume transports, heat transports and freshwater transports.

3.1. Volume transports

The volume transports into and out of the Arctic Ocean, obtained from all datasets should be discussed first. As already described in the previous chapter, volume transports of the Ocean reanalysis are computed on the tripolar grid, while the ARCGATE transports are included in the data.

3.1.1. Time Series

Starting with time-series plots, a first comparison between volume transports of the different ocean reanalysis and the ARCGATE observations should be made.

3.1.1.1. C-GLORSv5

Figure 14 shows the time series of volume transports through each of the four Arctic Gateways as well as the net transport obtained from C-GLORSv5 Ocean Reanalysis and ARCGATE observations. Although reanalysis data would be available for a longer period, this plot shows only data from the period where both datasets are available (10/2004 – 05/2010 (aka ARCGATE-period)). To distinguish between ARCGATE and C-GLORSv5 transports, ARCGATE transports are drawn in dashed lines, while reanalysis transports have solid lines. Additionally, the transports through the individual Straits have different colours. Transports through Davis Strait are coloured in red, Fram Strait in green, BSO in blue and Bering Strait transports are cyan. Net transports of both data sources are shown in black. Transports into the Arctic Ocean are represented by positive values, while transports out of the Arctic are negative. In addition to Figure 14, a table with average values, standard deviation of the differences and correlation coefficients for the individual straits is shown. The calculated uncertainty bounds represent the standard deviation of the anomaly of the time-series.

Looking at Figure 14, one can see, that the general patterns are qualitatively well captured by the reanalysis. Largest volume exports are found in Davis Strait, while volume import is mainly through Barents Sea Opening (BSO). Minor contributions to in- and outflow of the Arctic Ocean are from Bering Strait and Fram Strait respectively. Since volume is conserved, the net transport is close to zero in both datasets (-0,10 $\pm$ 0,16 *Sv* compared to -0,14 $\pm$ 0,02 *Sv* from ARCGATE). Since the method for volume conservation in ARCGATE is applied for every month, there is less variation of the net volume transport in the observation-based dataset than in the ocean reanalysis.

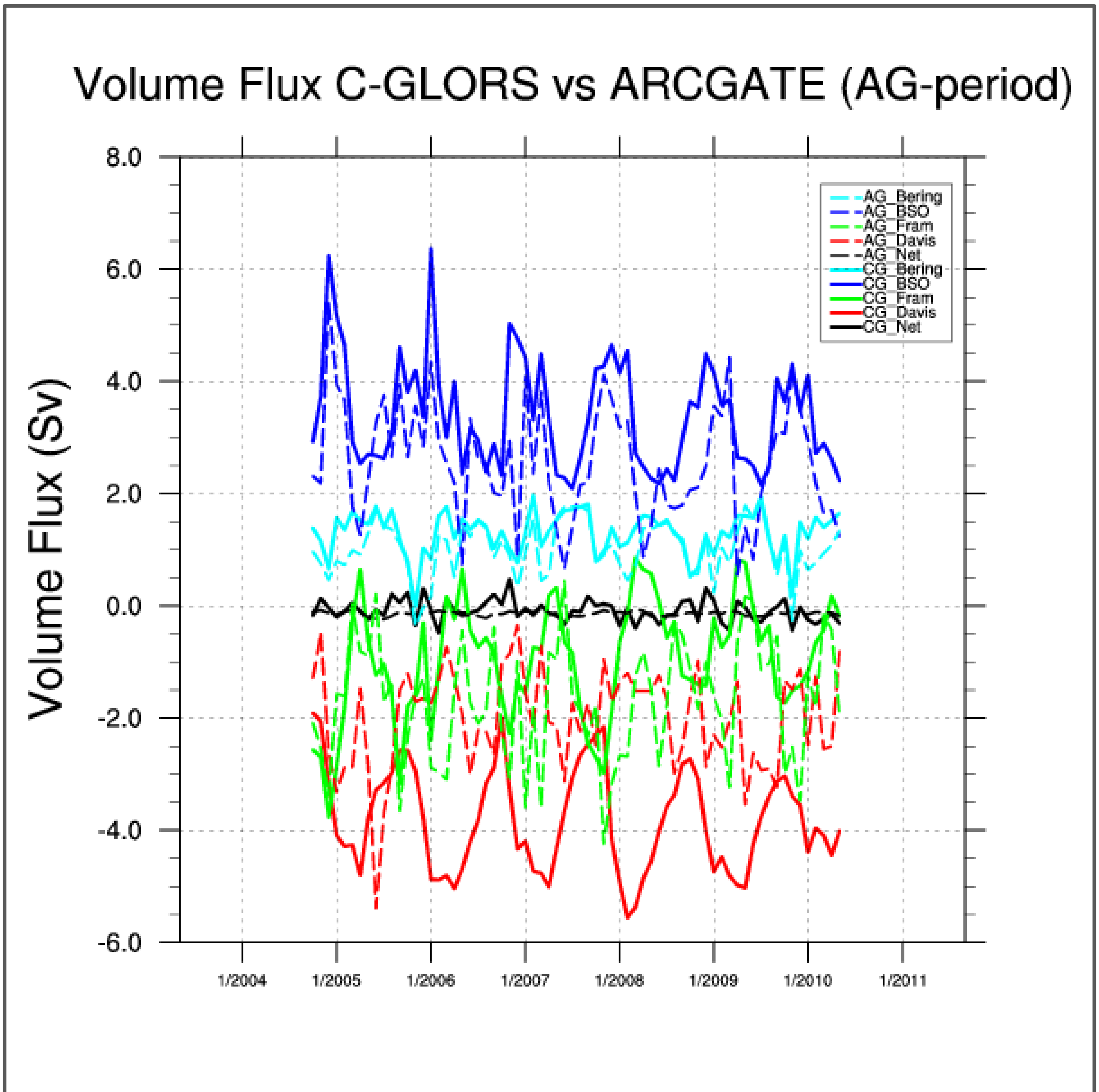

Figure 14: Volume transports from C-GLORSv5 (solid lines) and ARCGATE (dashed lines) for the period 10/2004 – 05/2010. Davis Strait is plotted in red, Fram Strait in green, Bering Strait is coloured in cyan and BSO is shown in blue. Net transports are also plotted (black). The units are Sverdrup (Sv) with 1 Sv = $10^6\ m^3/s$

The negative values of volume transports can be explained through river runoff, ice melt and precipitation exceeding the evaporation rate. Taking a closer look at the individual straits, it is noticeable that the coincidences are not the same everywhere; instead, each of the four gateways should be treated separately.

To get a better understanding of when the largest differences occur during what time of the year, the seasonal cycle of both datasets is shown additionally in Figure 15. Despite the C-GLORSv5 time-series is much longer then the observation-based one, the seasonal cycle is computed over the same period (ARCGATE-period).

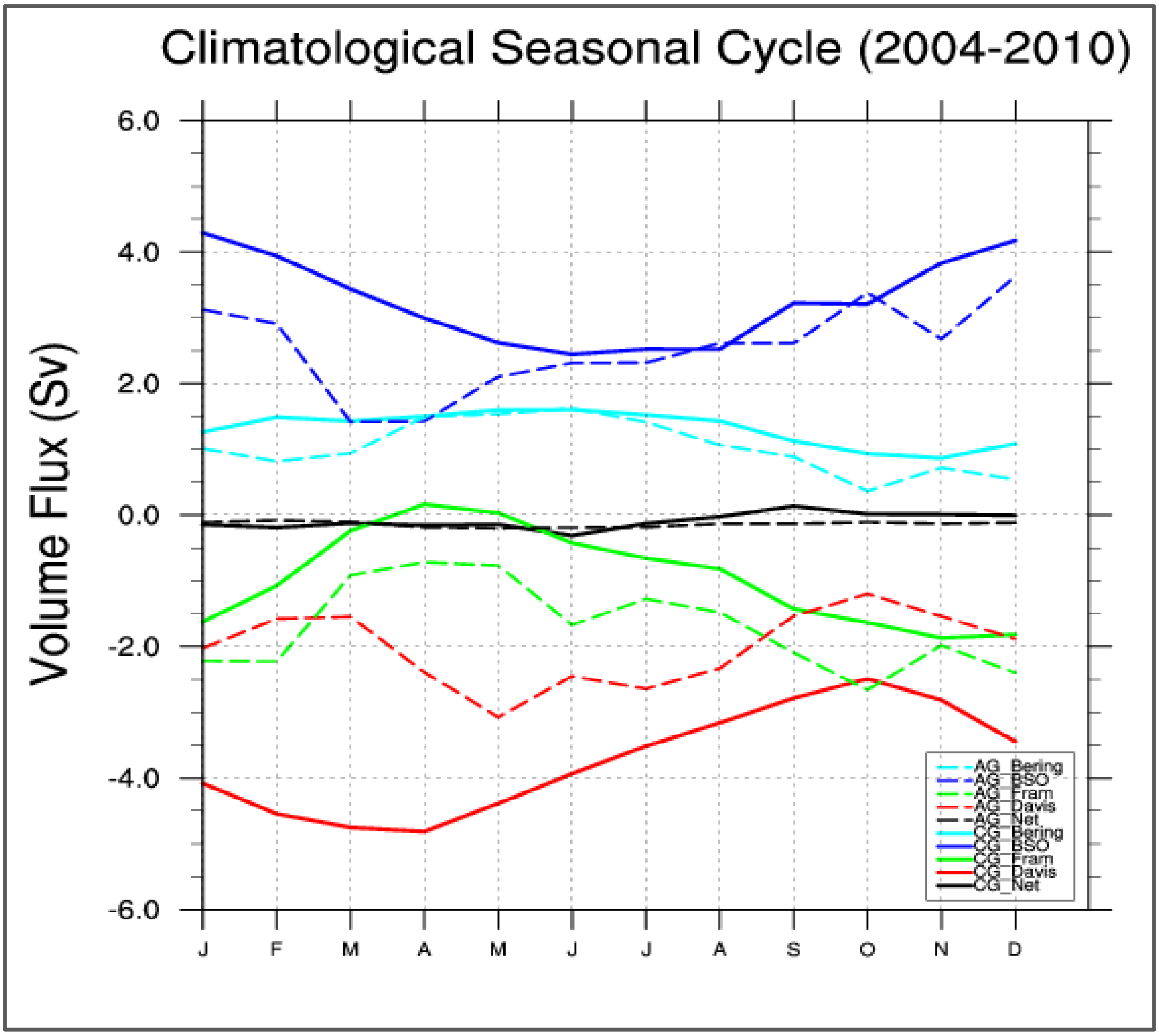

Figure 15: Seasonal cycle of the volume transports obtained from C-GLORSv5 (solid lines) and ARCGATE (dashed lines), calculated for the period 10/2004 – 05/2010. Davis Strait is plotted in red, Fram Strait in green, Bering Strait is coloured in cyan and BSO is shown in blue. Net transports are also plotted (black). All units are Sverdrup (Sv).

Again, the agreement between reanalysis and ARCGATE data is qualitatively good; nevertheless, this view set uncovers larger discrepancies, especially in BSO and Davis Strait in late winter and early spring. Despite these differences, it is noteworthy, that for the rest of the year the fluxes in BSO agree very well, while Davis Strait volume exports are overestimated by C-GLORSv5 through the whole year. Good agreement of the annual variation can be found in Fram Strait, even though the reanalysis is underestimating the volume export by nearly 1 Sv throughout the year. High analogies in the time-series are also present for the comparison of Bering Strait values.
Although the differences are small, a look at the net transports reveals some interesting facts. While the ARCGATE net volume transport is almost constant, a clear seasonality can be seen in the C-GLORSv5 time-series. In the following paragraphs, the differences in the individual straits are outlined in detail and the values are compared to literature.

Table 2: Average values of volume transport through the different straits obtained from C-GLORSv5, ARCGATE and literature. Correlation coefficient (R) and STDDEV are calculated between ARCGATE and C-GLORSv5. All average values (AVG) and STDDEV are in Sv, the R is unitless.

	C-GLORSV5 (AVG)	ARCGATE (AVG)	R	STDDEV (DIFF)	LITERATURE (AVG)
Davis Strait	-3,72 ± 0,51	-2,0 ± 0,70	0,00	1,32	-2,3 ± 0,7
Fram Strait	-0,96 ± 0,72	-1,71 ± 0,90	0,51	1,12	-1,75±5,01
BSO	3,25 ± 0,65	2,54 ± 0,77	0,73	0,76	2,0 ± 0,4
Bering Strait	1,33 ± 0,29	1,02 ± 0,34	0,81	0,29	0,8 ± 0,2

For **Bering Strait**, the C-GLORSv5 derived volume transports match those of the ARCGATE dataset within the uncertainty bounds, although the C-GLORSv5 value is about 30% higher. Even “extreme” events like the ones in fall and early winter 2005 or in late 2009 are captured by this ocean reanalysis. The good overall match between these two data sources can also be seen in Figure 15 as well as in Table 2. By comparing the total time-series and the seasonal cycle values obtained from reanalysis and observations with literature estimates, one can also find good agreement. The average volume transport through Bering Strait was estimated by Woodgate and Aagaard (2005) for the 1990-2004 period, using only one mooring site. This mooring site, located in the centre of the Strait, is believed to account for the flows through both channels of the Bering Strait. Woodgate and Aagaard estimated the volume transport with $0{,}8 \pm 0{,}2\ Sv$. The high degree (~25%) of uncertainty arises from absence of other measurements and the fact, that boundary currents are neglected. The ARCGATE average over the whole period is $1{,}02 \pm 0{,}34\ Sv$ and therefore matching the literature within its uncertainty range, while C-GLORSv5 is slightly overestimating the inflow through Bering Strait ($1{,}33 \pm 0{,}29\ Sv$). Also, the seasonal development of the volume transport reflects literature values in a qualitative way. Woodgate and Aagaard (2010) estimate the seasonal cycle to start with values of 0,4 Sv volume inflow in January, increasing to 1,3 Sv in June and then decreasing again to about 0,5 Sv in December. A similar trajectory can also be found in both datasets, albeit the values are higher. The discrepancy between literature and ARCGATE values can again be explained with the limited amount of observations used by Woodgate and Aagaard (2010) in their work.

Barents Sea Opening estimates of CGLORSv5 are also matching those of ARCGATE, except in spring and early summer the fluxes in the ARCGATE dataset are 50% smaller. Since CGLORSv5 is not able to detect this feature, it is overestimating the average inflow into the Arctic Ocean (3,25 $\pm$ 0,65 Sv) compared to the ARCGATE estimates (2,54 $\pm$ 0,77 Sv) and literature values by Smedsrud et al. (2010) with 2,0 $\pm$ 0,4 Sv. By comparing the seasonal cycle of reanalysis and observation-based data, again two different periods can be defined. In the first part of the year, when the inflow through BSO is slowly decreasing, C-GLORSv5 is overestimating the volume transport quite significantly (up to a factor of 2), while in the second half of the year the transports match very well. Nevertheless, C-GLORSv5 and ARCGATE estimates are higher than literature values by Smedsrud (2010), who found Arctic inflow to have a minimum of 1,3 Sv in April and a maximum of 2,8 Sv in January. The overassessment of the inflow by the ocean reanalysis may be explained by a significant outflows through the Bear Island trench (0,9 Sv (Skagseth, 2008)) and the Bear Island Current (~0,3 Sv (Blindheim, 1989)), which are only partially captured in the reanalysis data (see section 3.1.2). Subtracting these values from the C-GLORSv5 values, one would receive comparable results.

Concerning the outflow of the Arctic Ocean, Fram Strait and Davis Strait are important. By looking at Figure 14, one can see, that the discrepancies between CGLORSv5 and ARCGATE are much bigger for these two Straits. Beginning with **Fram Strait**, one can see, that the agreement of both datasets has a high variability. In question of the average values, C-GLORSv5 is underestimating the outflow compared to ARCGATE and literature by approximately 0,8 Sv (Literature values are taken from Fieg, Fahrbach, Gerdes, Beszczynska-Möller, & Schauer (2010), (mooring-derived estimates)).
Despite the larger discrepancies in the time-series plots, the seasonal cycle matches qualitatively good, having a maximum volume export in late fall or early winter and minimum transports in spring. Quantitatively, the seasonal cycle reveals the underestimation by C-GLORSv5 compared to ARCGATE by up to 50%. A possible explanation for the differences in time-series as well as in the seasonal cycle, may be that the ocean reanalysis is only partly eddy resolving. Since Fram Strait transports are dominated by two opposing and comparable strong currents (WSC and EGC), the inability of capturing recirculation patterns can cause these differences. Again, both climatologies can be compared with literature values. Literature values are obtained by a combination of observation-based seasonal cycles of the two main currents in Fram Strait (WSC (Beszczynska-Mo ̈ller and EGC (de Steur et al., 2014)). While the phase

of minimum export in this combined dataset can be found again between March and May, maximum exports are shifted to February and July.

To complete all gateways, **Davis Strait** is examined next. From both, Figure 14 and Figure 15, one can see, that the biggest differences of all Straits can be found in Davis Strait. Concerning the entire time-series (Fig. 12), the C-GLORSv5 derived dataset shows a clear and well developed seasonal variability, what cannot be found in the ARCGATE data, causing differences up to 4 *Sv* at some points in the time-series. Matching the average values computed over the whole period, one can also see these huge differences. The C-GLORSv5 derived estimate for volume export is given by -3,72 ± 0,51 *Sv*, while the ARCGATE estimate yields -2,0 ± 0,7 *Sv*. Literature values taken from Curry et al., (2011) (-2,3 ± 0,7 *Sv*), match those of ARCGATE very well, indicating that the source of the discrepancies may be the ocean reanalysis. The large discrepancies become even more clear by looking at the correlation coefficient and the standard deviation of the difference between both datasets in Table 2 (R = 0,00 means no correlation at all).
Investigating the seasonal cycle (Fig. 13), there is hardly any agreement between C-GLORSv5 and ARCGATE, neither qualitatively nor quantitatively. A comparison of these cycles with the one obtained by Curry et al. (2011), reveals slight qualitative conformity between C-GLORSv5 and their dataset, nevertheless, the absolute values are quite different.

3.1.1.2. ORAS 5

Let us now compare ARCGATE and ECMWF's ocean reanalysis ORAS5. As already explained in chapter 2 of this thesis, the horizontal grid and therefore the horizontal resolution of ORAS5 and C-GLORSv5 are the same. However, a different version of the ocean model NEMO was used for the ECMWF ocean reanalysis. Another difference is the vertical resolution, which is increased by 50 % in the ORAS5 reanalysis.
Taking a quick look at Figure 16, again the general patterns are qualitatively well captured by the reanalysis. Compared to the C-GLORSv5 reanalysis, also some improvements are visible. This is especially true for Davis Strait, albeit the match between ARCGATE and ORAS5 is still only modest. Further improvement compared to the former reanalysis can be seen in Fram Strait and Bering Strait. At this point it is noteworthy, that there is a nearly perfect match between volume transports through Bering Strait in ARCGATE and ORAS5. Hardly any changes or improvements can be found for Barents Sea Opening and the net transports.
In addition to Figure 16, table 3 displays average values, computed over the whole period, as well as the correlation coefficients for the individual straits and the standard deviation of the difference between both datasets.

Table 3: Average values of volume transports for ORAS5, ARCGATE and literature for the different Straits. Correlation coefficient (R) and STDDEV are computed between ARCGATE and ORAS5. All average values (AVG) and STDDEV are in Sv, R is unitless.

	ORAS5 (AVG)	ARCGATE (AVG)	R	STDDEV (DIFF)	LITERA-TURE (AVG)
Davis Strait	-3,15 ± 0,42	-2,0 ± 0,7	0,22	1,01	-2,3 ± 0,7
Fram Strait	-1,73 ± 0,73	-1,71 ± 0,90	0,58	0,97	-1,75±5,01
BSO	3,42 ± 0,74	2,54 ± 0,76	0,73	0,80	2,0 ± 0,4
Bering Strait	1,31 ± 0,39	1,02 ± 0,34	0,92	0,20	0,8 ± 0,2

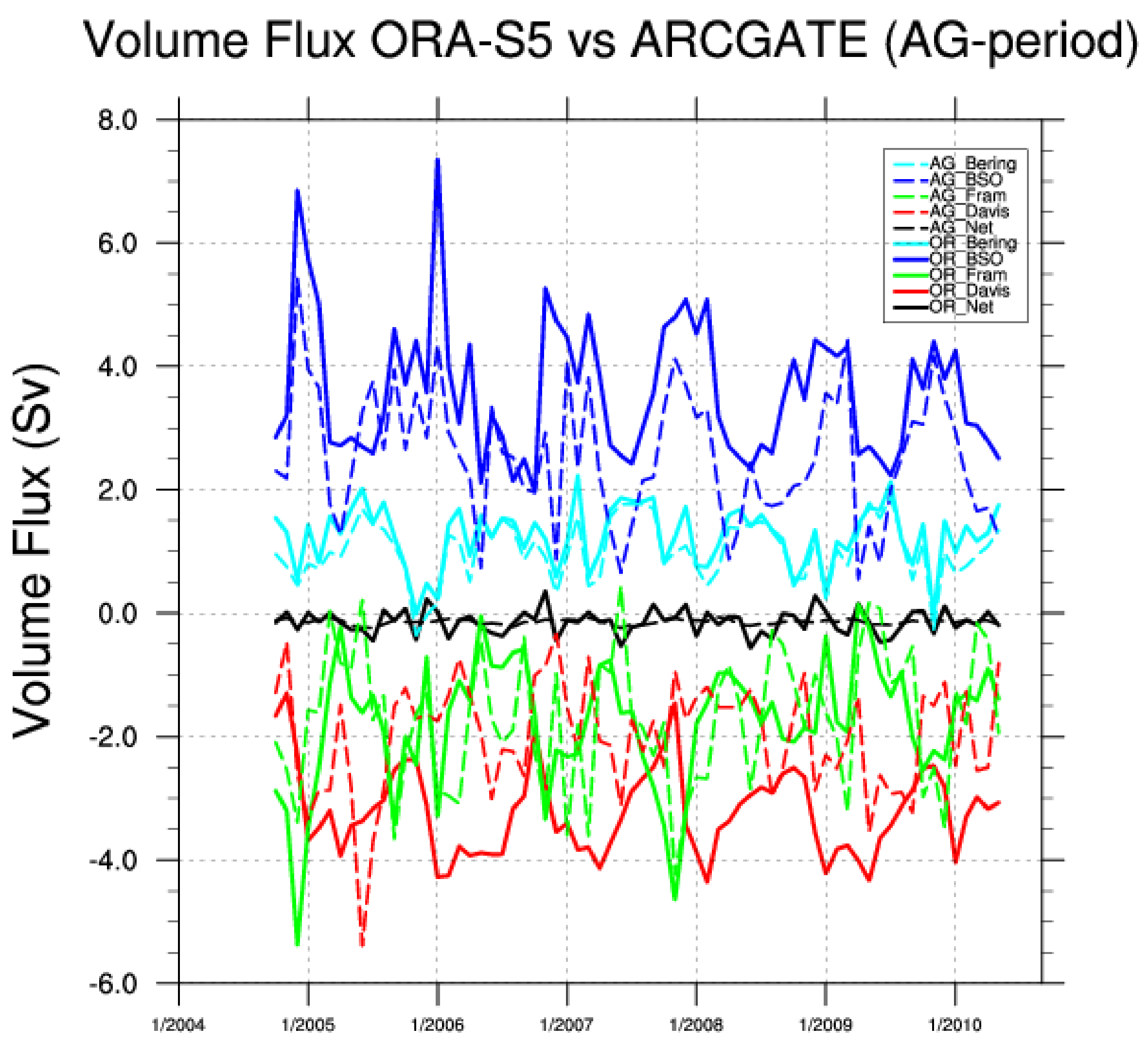

Figure 16: Volume transports from ORAS5 (solid lines) and ARCGATE (dashed lines) for the period 10/2004 – 05/2010. Davis Strait is plotted in red, Fram Strait in green, Bering Strait is coloured in cyan and BSO is shown in blue. Net transports are also plotted (black). The units are Sverdrup (Sv) with 1 Sv = $10^6 \, m^3/s$

In the following paragraph the differences of the individual straits between C-GLORSv5 and ORAS5 are highlighted and possible explanations are given.

Starting again with **Bering Strait,** one can see the excellent match between the two datasets. Albeit this qualitative agreement, the average values still differ by about 0,3 *Sv*. Compared to the literature value obtained by Woodgate and Aagaard (2010), the difference is about 0,5 *Sv*. Nevertheless, the high value of the correlation coefficient and the low standard deviation of the difference between ORAS5 and ARCGATE indicate, that there is also quantitatively a good overall agreement for Bering Strait.
This is also true for the seasonal cycle (Fig 17). The seasonal cycle of ORAS5 was computed over the whole period and conforms with the ARCGATE cycle very well. Only slight overestimations of Arctic inflow can be seen during winter and late summer. This overestimation compared to ARCGATE is the reason for the discrepancy of 0,3 *Sv* mentioned above.

For **Barents Sea Opening** the situation is different. There are some small deteriorations compared to C-GLORSv5. This becomes even clearer by comparing Table 2 and Table 3. While the former ocean reanalysis estimates the average volume transport through BSO with 3,25 ± 0,65 *Sv*, the ECMWF ocean reanalysis derived average values are 3,42 ± 0,74 *Sv*. This results in a significant overestimation of Arctic inflow compared to literature values by nearly 1,4 *Sv* or 75 % (Smedsrud et al., (2010)). The correlation coefficient is the same for both reanalysis, meaning they capture the overall patterns with the same efficiency.
The climatology of ORAS5 also reveals some noteworthy mismatches. Compared to ARCGATE, the biggest differences can be found in winter and early spring, when the inflow is significantly overestimated by the reanalysis (up to 50%). For the rest of the year, the seasonal cycles agree well. The reason for this huge discrepancy may be again the outflow in the North of the Strait, which might not be captured sufficiently well (compare to Section 3.1.1.1).

For **Fram Strait**, one can see a major qualitative improvement compared to C-GLORSv5. This is also true for the average values. While C-GLORSv5 was underestimating the outflow compared to ARCGATE and literature by approximately 0,8 *Sv,* there is nearly a perfect match between ORAS5 and ARCGATE (and literature). Looking at the correlation coefficient and the standard deviation in Table 3, one can also see this improvement. Both values have improved, the standard deviation has decreased considerably and the correlation coefficient increased slightly. The fact, that there is only a slight increase in correlation coefficient, may be explained by the non-eddy-resolving configuration of the ocean reanalysis. Turning now to the climatology, both datasets, ORAS5 and ARCGATE, match very well. Nevertheless, the differences to the literature derived seasonal cycle are the same as for C-GLORSv5 described above.

Although there are visible improvements for **Davis Strait** compared to C-GLORSv5 too, the degree of agreement with the ARCGATE dataset is still very low. This is true for the general patterns of the time-series and for the average values as well. ORAS5 derived volume transports indicate an average outflow of -3,15 ± 0,42 *Sv*, what is approximately 0,8 *Sv* or 70% higher than comparable literature values from Curry et al. (2011) and about 1 *Sv* higher than the ARCGATE estimates. Despite these huge differences, the values derived by ORAS5 match those of ARCGATE better than the C-GLORSv5 values. This is especially true for the correlation coefficient (0,22). Concerning the seasonal cycle (Fig. 17), some qualitative agreement between ORAS5 and ARCGATE can be found. Nevertheless, the absolute values of both datasets are quite different. Therefore, the comparison of these climatologies with the seasonal cycle obtained by Curry et al. (2011), reveals only minor conformities.

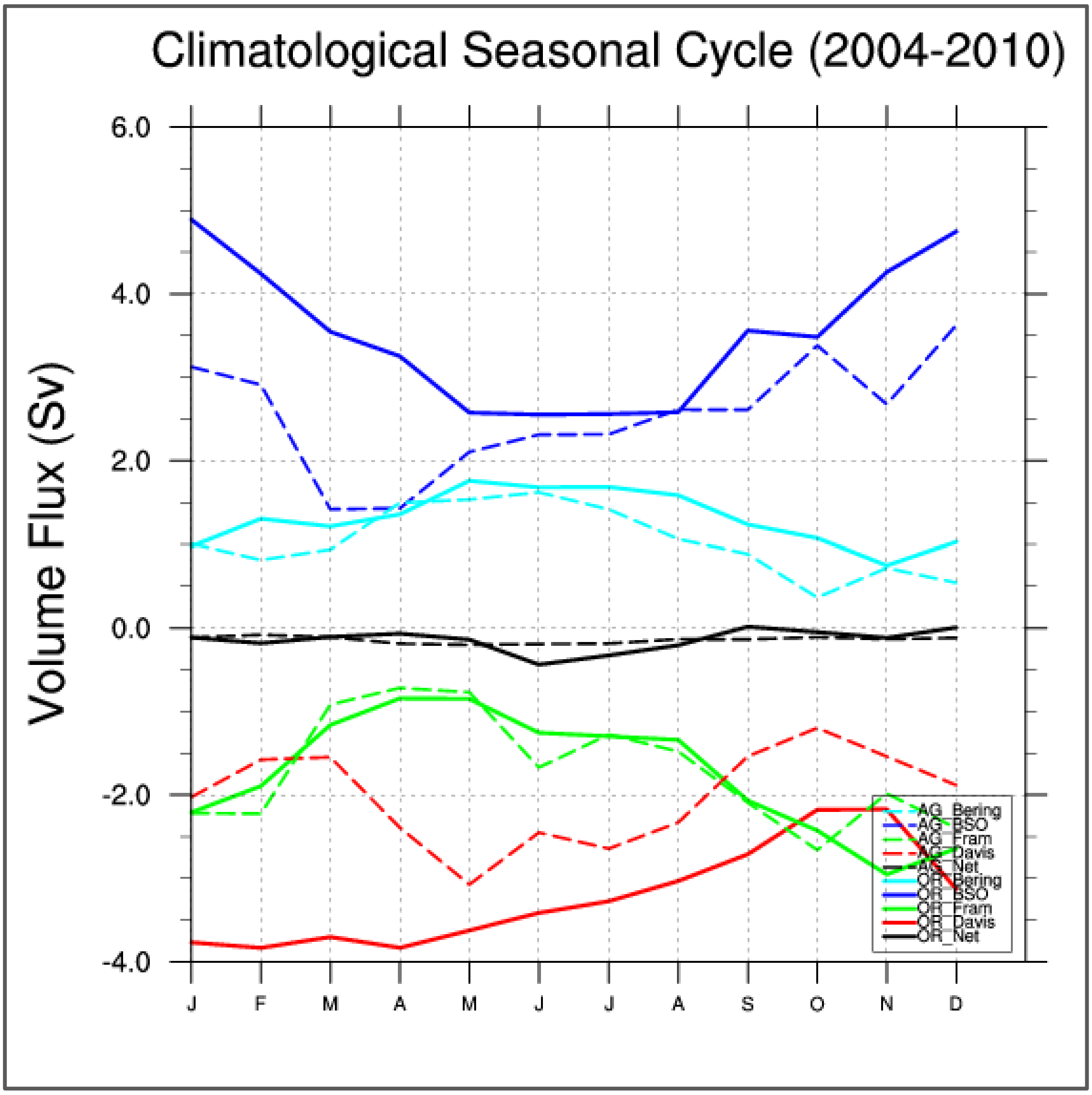

Figure 17: Seasonal cycle of the volume transports obtained from ORAS5 (solid lines) and ARCGATE (dashed lines), calculated for the period 10/2004 – 05/2010. Davis Strait is plotted in red, Fram Strait in green, Bering Strait is coloured in cyan and BSO is shown in blue. Net transports are also plotted (black). All units are Sverdrup (Sv).

3.1.2. Hovmoeller diagrams

In the following section, Hovmoeller-diagrams of volume transports for each of the Arctic gateways are shown. For each of the straits, two different figures are made, one showing a time versus width visualization, the other a time versus depth visualization. The aim of these plots is to get a deeper understanding of the differences between the datasets and their spatial distribution.

Starting again with **Bering Strait**, it was shown in the previous section, that the differences between the individual datasets are very small. Looking at Figure 18, one can also see this.

There is an overall good agreement between ARCGATE and both reanalysis, even extreme events like the negative volume transport in late 2005 are captured by the reanalysis. Albeit this good agreement, small differences can be seen. This especially true for the location of the transports within the Strait. While ARCGATE and C-GLORSv5 data show most of the volume transport is through the Russian side of Bering Strait, there are also minor peaks on the Alaskan side of the Strait in ORAS5. The Diomede Island, dividing Bering Strait into two channels, may explain this second peak. This feature seems to be captured by ORAS5, indicated by a minimum in transports, while both other datasets do not show this pattern. Further differences can be found by looking at the seasonality of the transports, which agree slightly better for ORAS5 than for C-GLORSv5 (Note, that the quantitative values have already been discussed in the previous section).

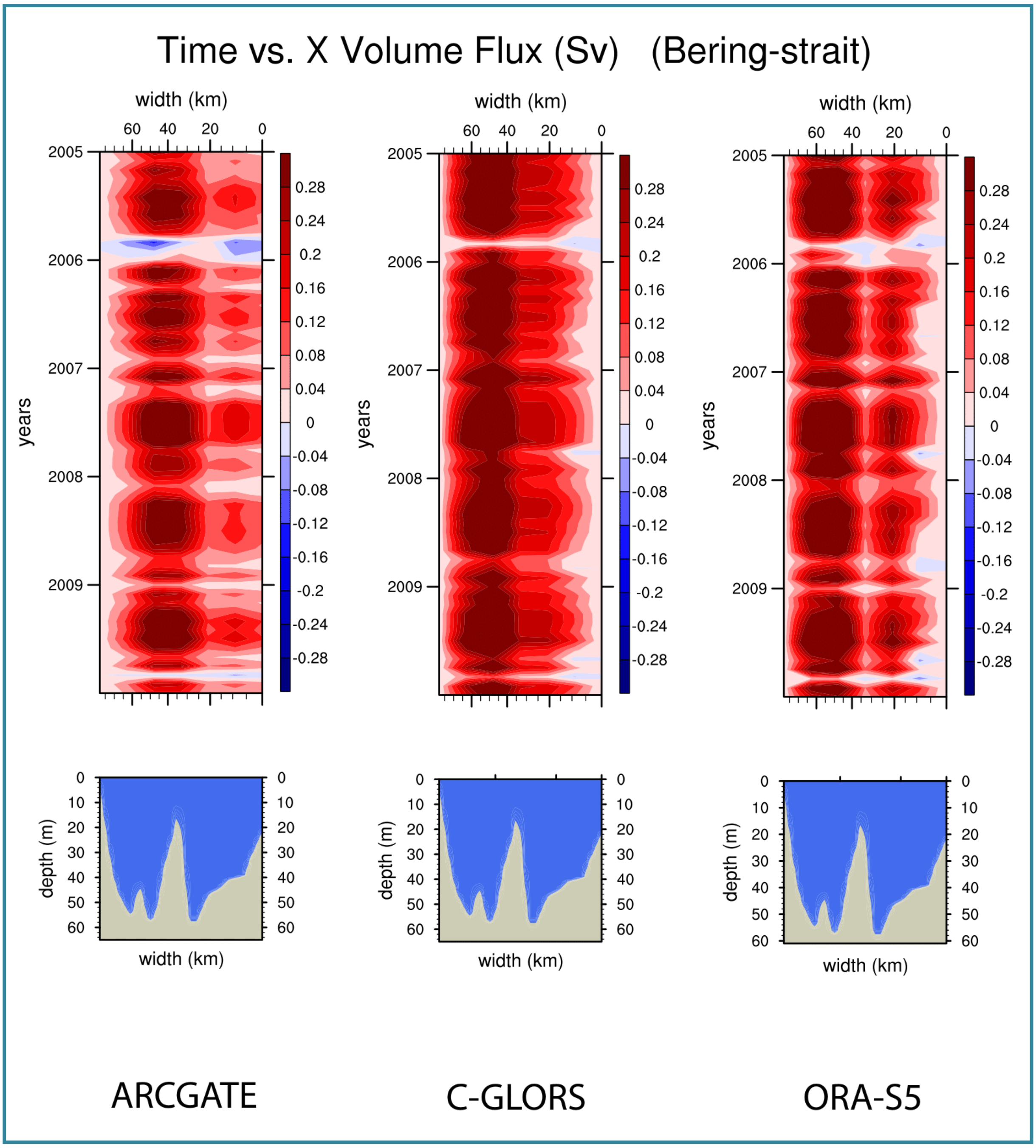

Figure 18: Time versus width Hovmoeller diagram for Bering Strait. ARCGATE is shown to the left, C-GLORSv5 in the middle and ORAS5 is on the right side. In the bottom section the bathymetry of Bering Strait is plotted. The values are normalized to the data points in the strait.

Turning now to the vertical distribution of the transports, Figure 19 reveals also some interesting points. While the depth structures of ARCGATE and ORAS5 are quite similar, C-GLORSv5 shows less transport in depths less than 35 metres. One can speculate that the reason for this mismatch might be the lower vertical resolution of the C-GLORSv5 reanalysis compared to ORAS5.

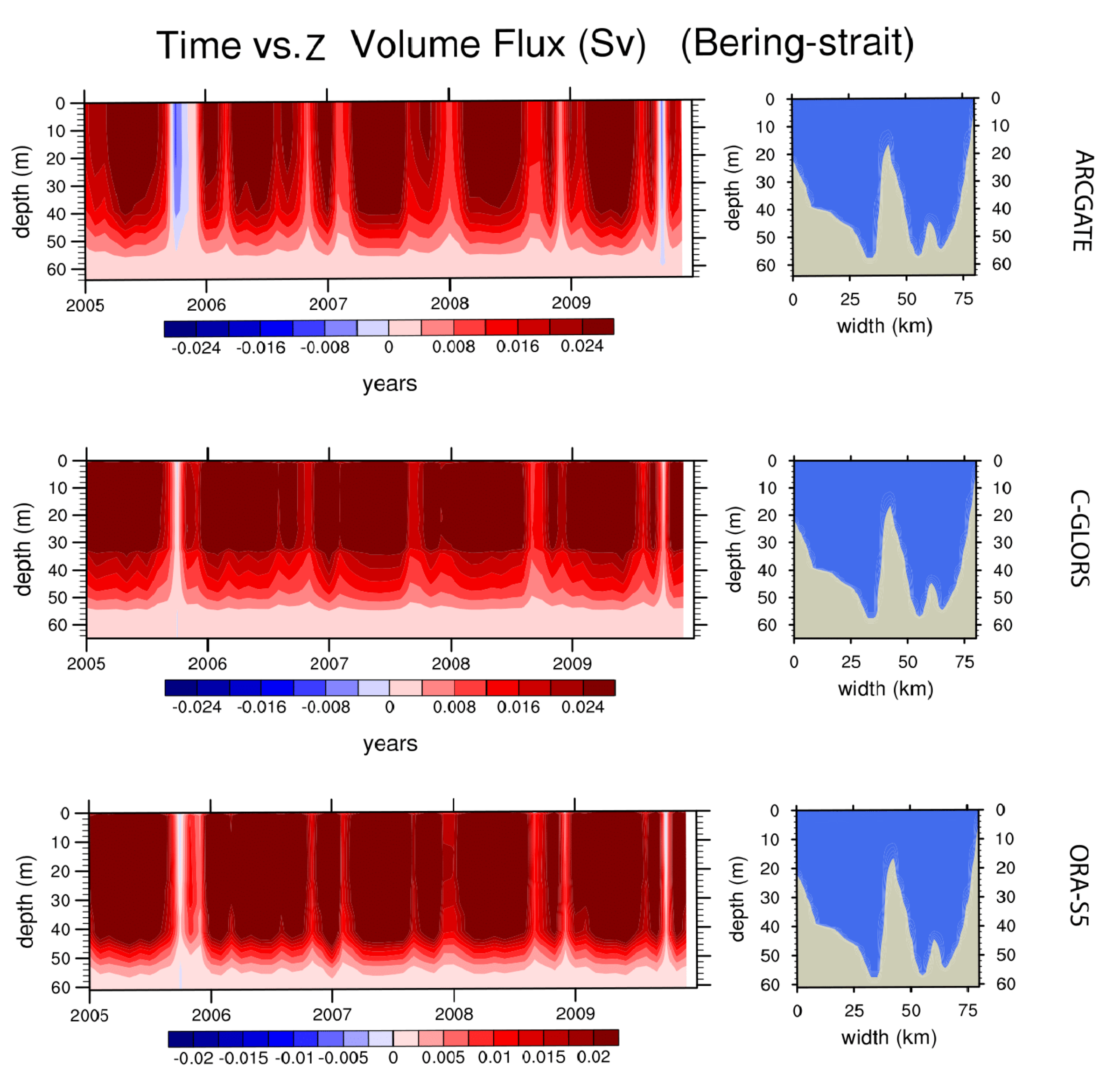

Figure 19: Time versus depth Hovmoeller diagram for Bering Strait. ARCGATE is shown at the top, followed by C-GLORSv5 in the middle and ORAS5 at the bottom. To the right of the plots, the bathymetry of Bering Strait is plotted. The values are normalized to the data points in the strait.

For **BSO** the time-series plots show some larger discrepancies between the datasets. These discrepancies can also be found in the Hovmoeller diagrams (see Fig. 20). Especially the region around Bear Island uncovers differences between observations and reanalysis. While ARCGATE data shows predominantly volume outflow (negative values), both reanalysis products show an additional inflow-branch in this region. Additional to the already mentioned lower outflow around Bear Island, this positive inflow might be another explanation for the overestimation of volume inflow by both reanalysis as described in the previous section. The rest of Figure 20 reveals only slight differences between the data; seasonality and location of the transports are captured very well by C-GLORSv5 and ORAS5. Taking again a look at the vertical structure, one can see at which depths the datasets agree better and where they are less accurate.

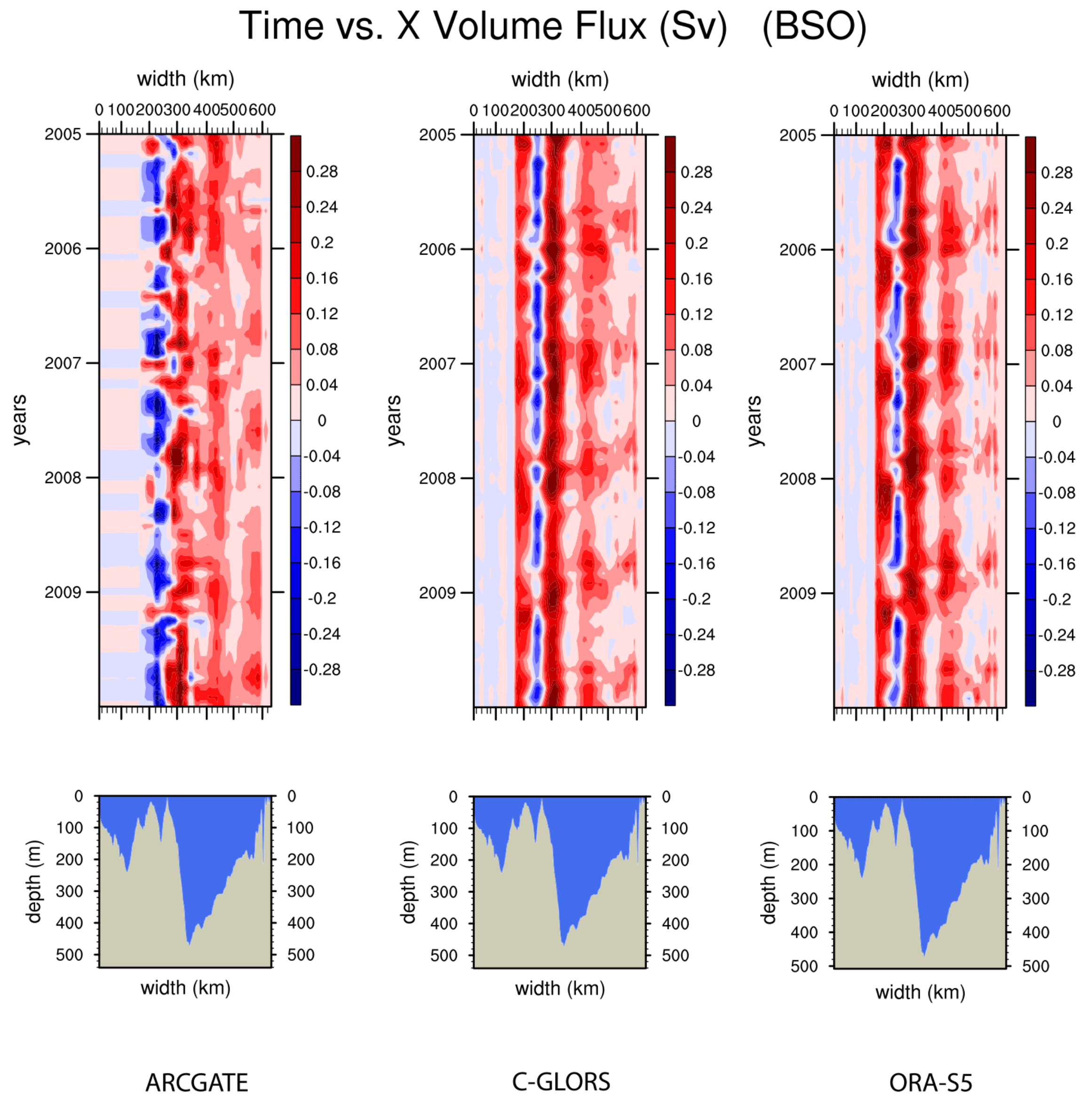

Figure 20: Time versus width Hovmoeller diagram for Barents Sea Opening. ARCGATE is shown to the left, C-GLORSv5 in the middle and ORAS5 is on the right side. In the bottom section the bathymetry of BSO is plotted.

While the transports near the surface match those of ARCGATE very well, Figure 21 shows bigger discrepancies at depths below 200 metres. This is particularly true for ORAS5, which indicates higher volume inflow at greater depths than C-GLORSv5 and ARCGATE.

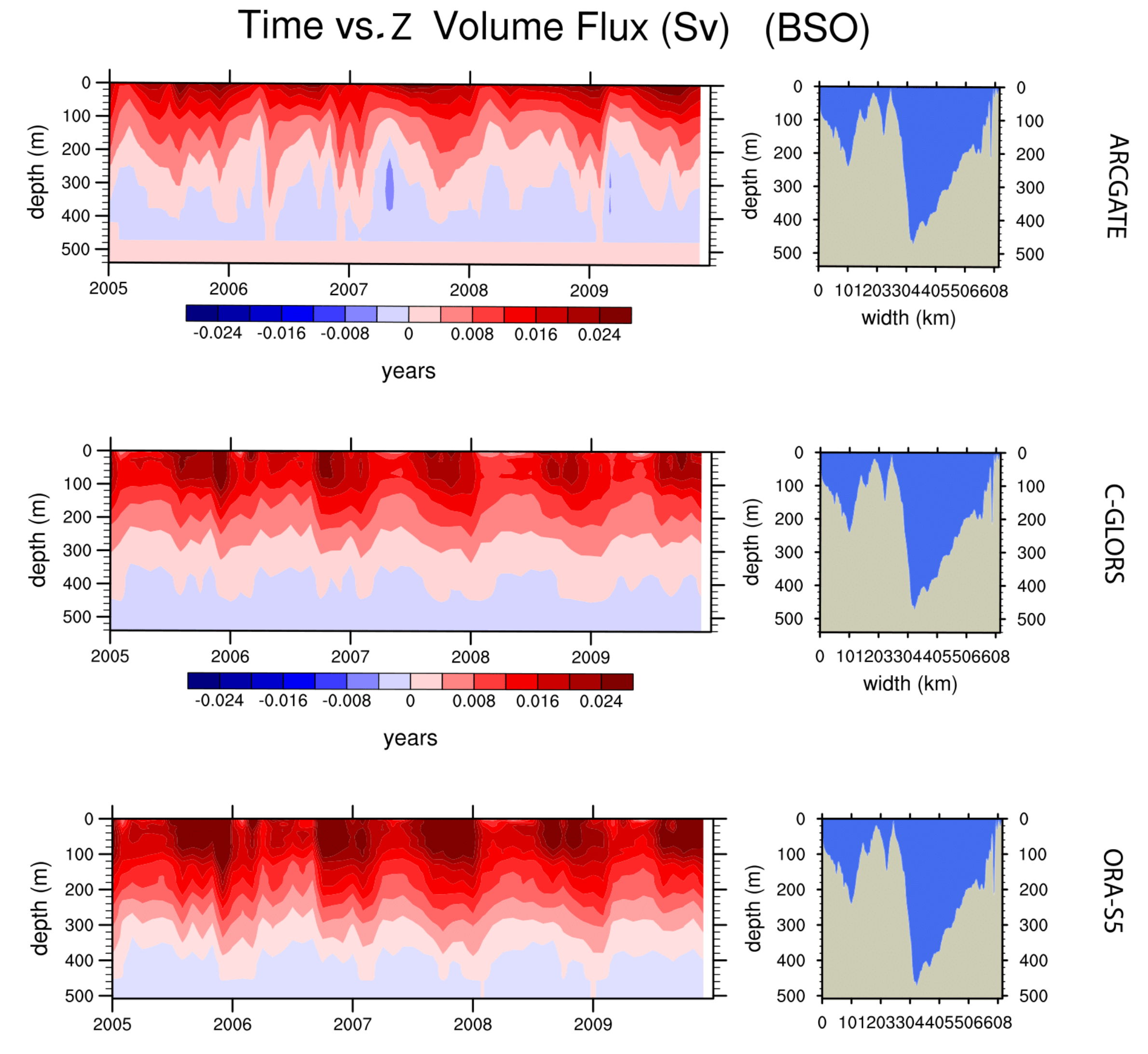

Figure 21: Time versus depth Hovmoeller diagram for Barents Sea Opening. ARCGATE is shown in the top-panel, followed by C-GLORSv5 in the middle and ORAS5 at the bottom. To the right of the plots, again the bathymetry of BSO is plotted.

The Hovmoeller diagrams for **Fram Strait** also show some differences between the datasets. Although it is shown in the time-series plots, that the general flow pattern Fram Strait is captured in all datasets (inflow through the West Spitzbergen Current and large outflows through East Greenland Current) in a similar way, Figure 22 represents various discrepancies in the boundary section between WSC and EGC in the middle of Fram Strait. The structure of strong in- and outflow regions in striking distance, indicate the presence of eddies in this region. While ARCGATE is at least partly eddy resolving, both ocean reanalyses are not able to represent this small-scale features reasonably well. It is also noteworthy, that both reanalysis indicate a seasonality in these features, which is not represented in the ARCGATE data.

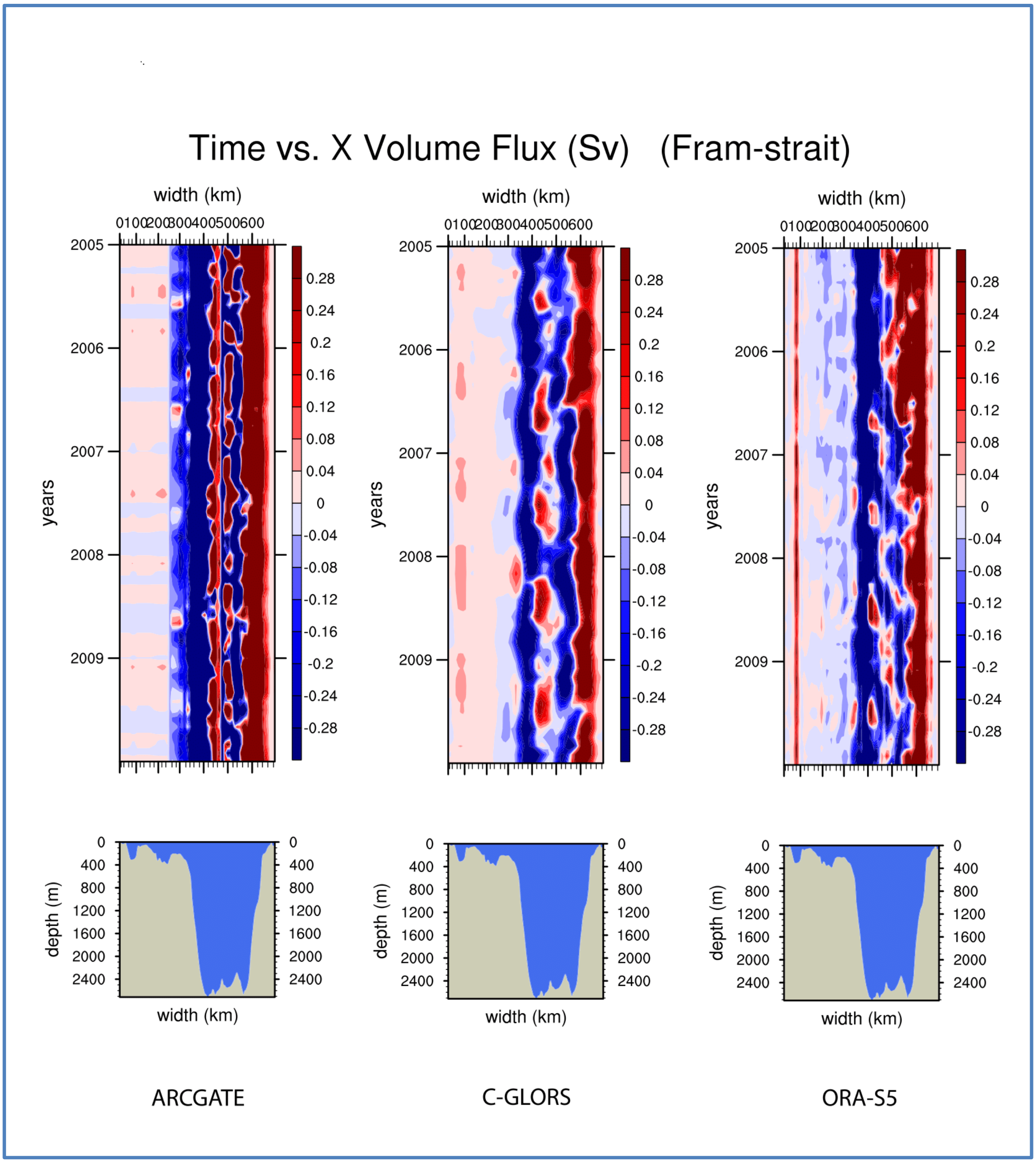

Figure 22: Time versus width Hovmoeller diagram for Fram Strait. ARCGATE is shown to the left, C-GLORSv5 in the middle and ORAS5 is on the right side. In the bottom section the bathymetry of Fram Strait is plotted.

Another interesting difference between reanalysis and observation-based data can be found near Greenland on Belgica Bank. Both reanalyses indicate inflow through some parts of this region; especially in ORAS5 the inflow is significant. By comparing this to the ARCGATE derived data, one can see, that there is hardly any inflow captured by observations on Belgica Bank. This discrepancy can easily be explained by the lack of observational instruments in the region of Belgica Bank.
Turning now towards the vertical structure of the datasets, also some disagreements between observations and reanalyses become visible. The most obvious difference can be seen for depths below 2000 metres. While ARCGATE is indicating predominant outflow in these depths, both reanalysis products show transports near zero and inflow during spring and summer months respectively.

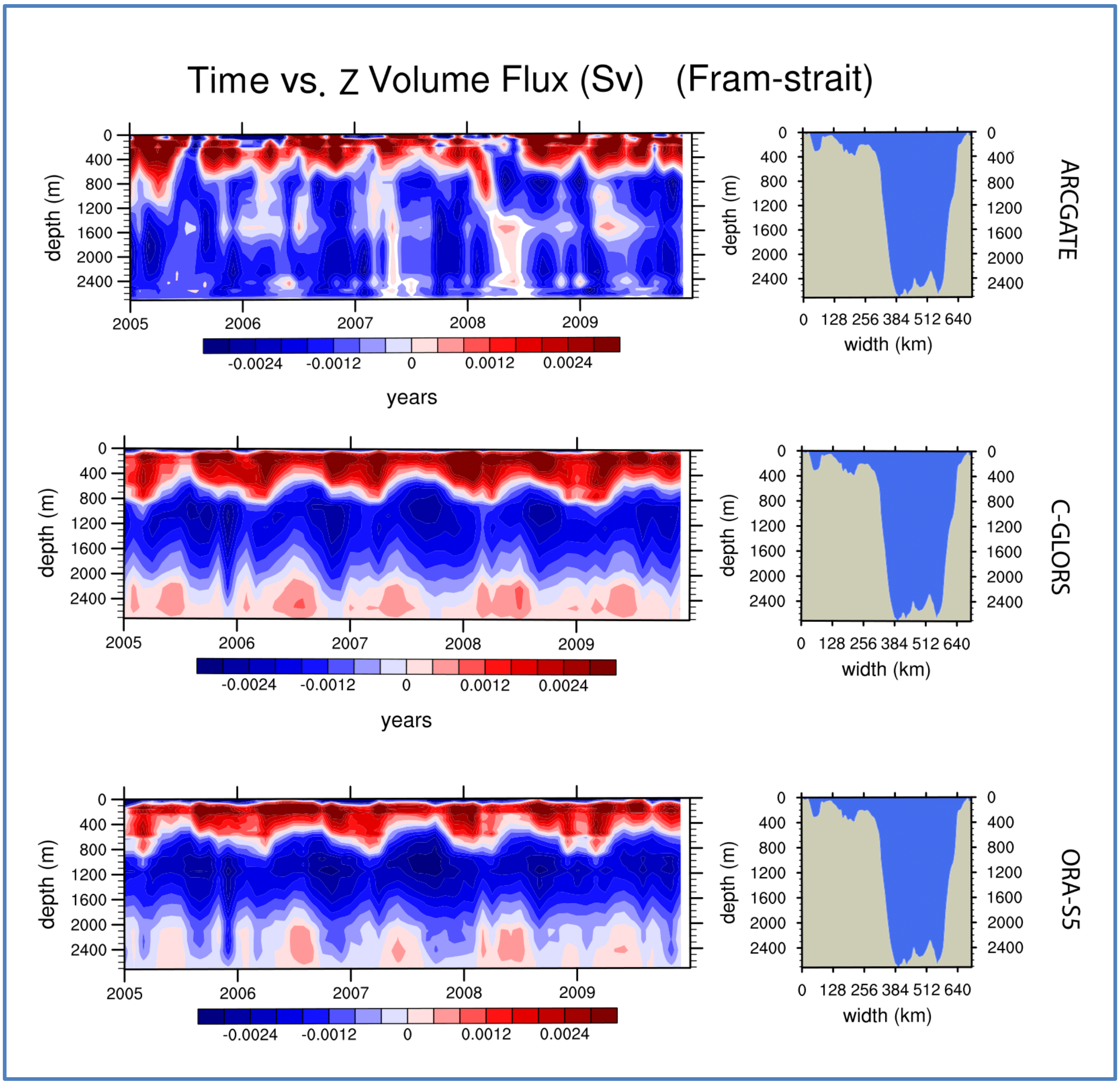

Figure 23: Time versus depth Hovmoeller diagram for Fram Strait. ARCGATE is shown in the top-panel, followed by C-GLORSv5 in the middle and ORAS5 at the bottom. To the right of the plots, again the bathymetry of Fram Strait is plotted.

Near the surface some differences appear in Figure 23. While in C-GLORSv5 as well as in ORAS5 the surface volume transports are negative (integrated along the whole width of the Strait), ARCGATE shows periods of positive volume transports into the Arctic Ocean. Another difference can be seen in depths between 400 and 1200 metres. A clear seasonality of the volume transport into the Arctic is visible in the reanalysis-based datasets, with inflow reaching maximum depths around 900 to 1000 metres in summer and only 500 metres on average during the colder seasons. This seasonality cannot be found in an analogous way in the observation-based data.

The biggest differences can be found for **Davis Strait** plots. Starting again with the horizontal structures (Fig.24), the source of the discrepancies revealed in the time-series plots becomes visible.

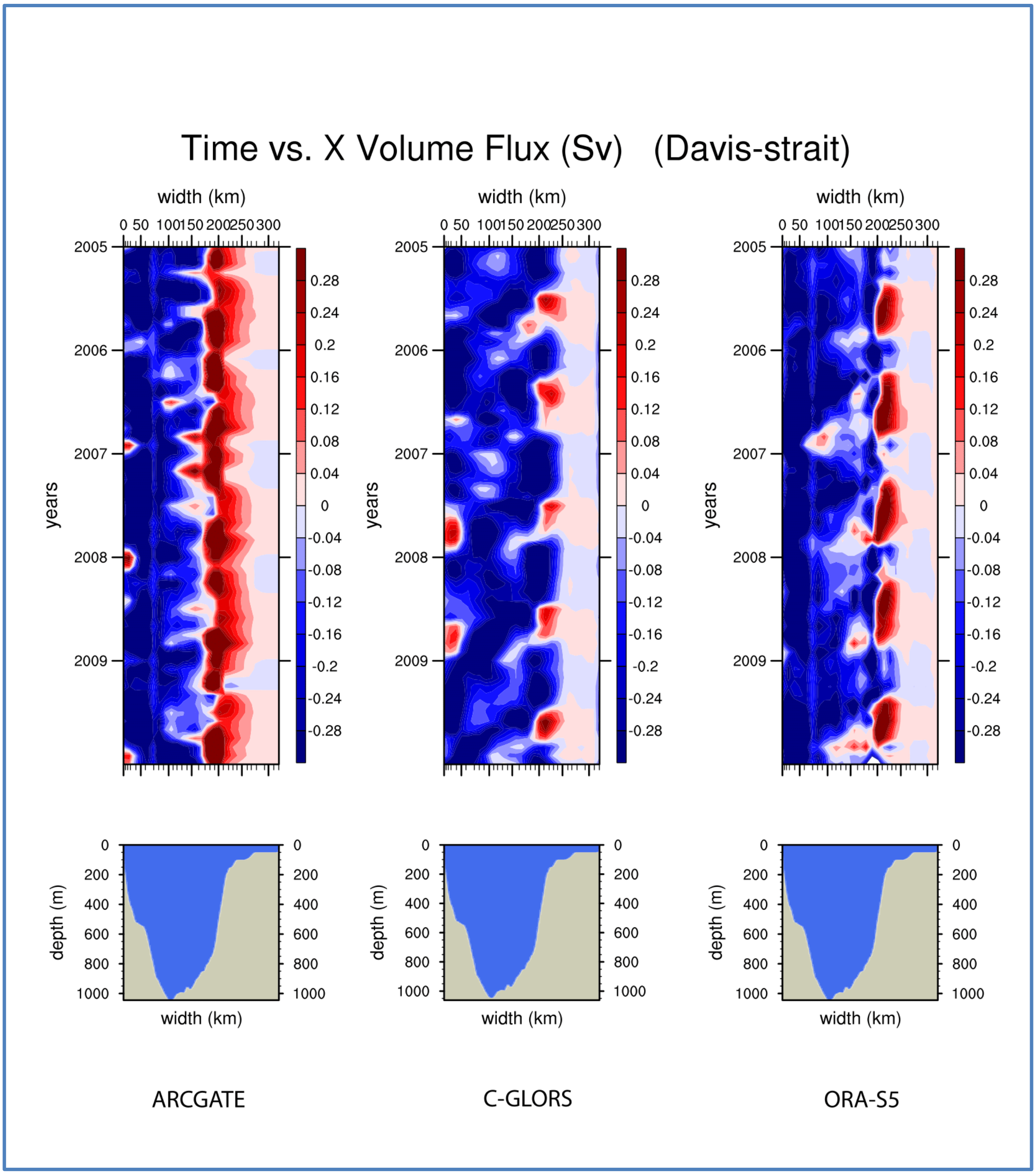

Figure 24: Time versus width Hovmoeller diagram for Davis Strait. ARCGATE is shown to the left, C-GLORSv5 in the middle and ORAS5 is on the right side. In the bottom section the bathymetry of Davis Strait is plotted.

For Davis Strait, negative volume transports are predominant. Nevertheless, there are some regions of inflow into the Arctic Ocean, for example near Greenland through the West Greenland Current (WGC) and the West Greenland Shelf (WGS), opposing the outflow. The inflow through WGC is clearly represented in ARCGATE, while there is only seasonal appearance in the other two datasets. Since both reanalysis only compute transports in the slope region during the warmer season, one may speculate, that there is too much sea ice moulded, resulting in an inhibition of northward transports in this region. Although the agreement between reanalysis and observations in this region is low, an improvement can be seen referable to the higher vertical resolution used in ORAS5 compared C-GLORSv5. The inflow period is extended over several months and additionally the magnitude of the transports is increased in the WGS region.

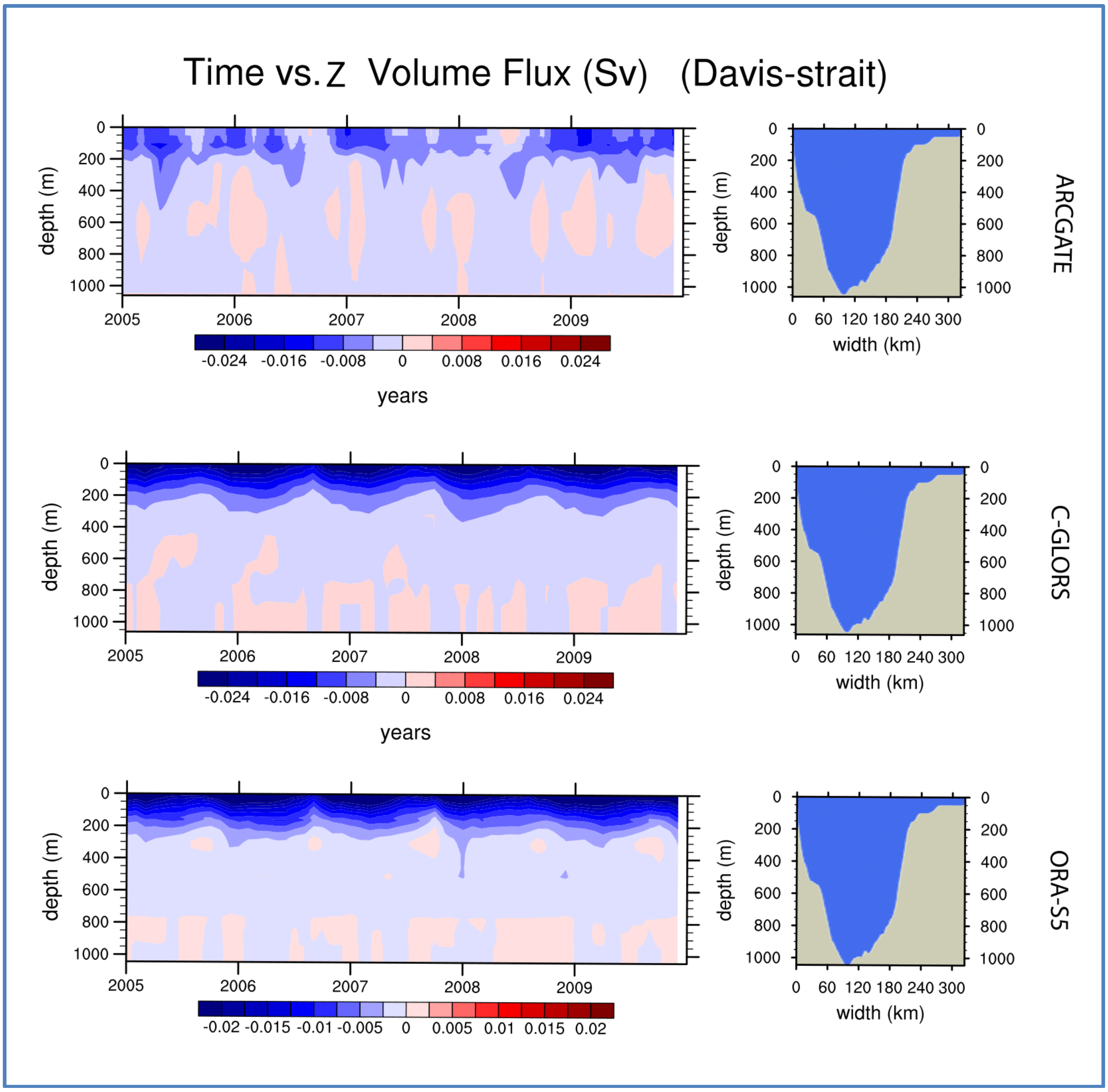

Figure 25: Time versus depth Hovmoeller diagram for Davis Strait. ARCGATE is shown in the top-panel, followed by C-GLORSv5 in the middle and ORAS5 at the bottom. To the right of the plots, again the bathymetry of Davis Strait is plotted.

Concerning the comparison of the vertical structure of all three datasets in Figure 25, the differences are small and concentrated to the upper 200 metres of the Strait. The integration along the width of the Strait shows again a very smooth distribution with slight seasonal variability for reanalysis, whilst the ARCGATE data shows a much smaller outflow and a noisier seasonal cycle. This behaviour can be explained with the above-mentioned inflow through WGC, which causes larger fluctuations to the net transport.

3.2. Heat Transports

The heat transport into and out of the Arctic Ocean plays an important role in terms of arctic amplification (see introduction chapter) and therefore the results obtained in this thesis will be outlined in detail in this section. Again, the transports received from ocean reanalyses are computed on the tripolar grid, while the ARCGATE transports are included in the data.

3.2.1. Time Series

3.2.1.1. C-GLORSv5

To get a qualitative and quantitative overview over the heat transports through the different Straits and the net transports, time-series plots are shown first. Figure 26 compares heat transports derived from the ocean reanalysis C-GLORSv5 with the ARCGATE observation-based estimates.

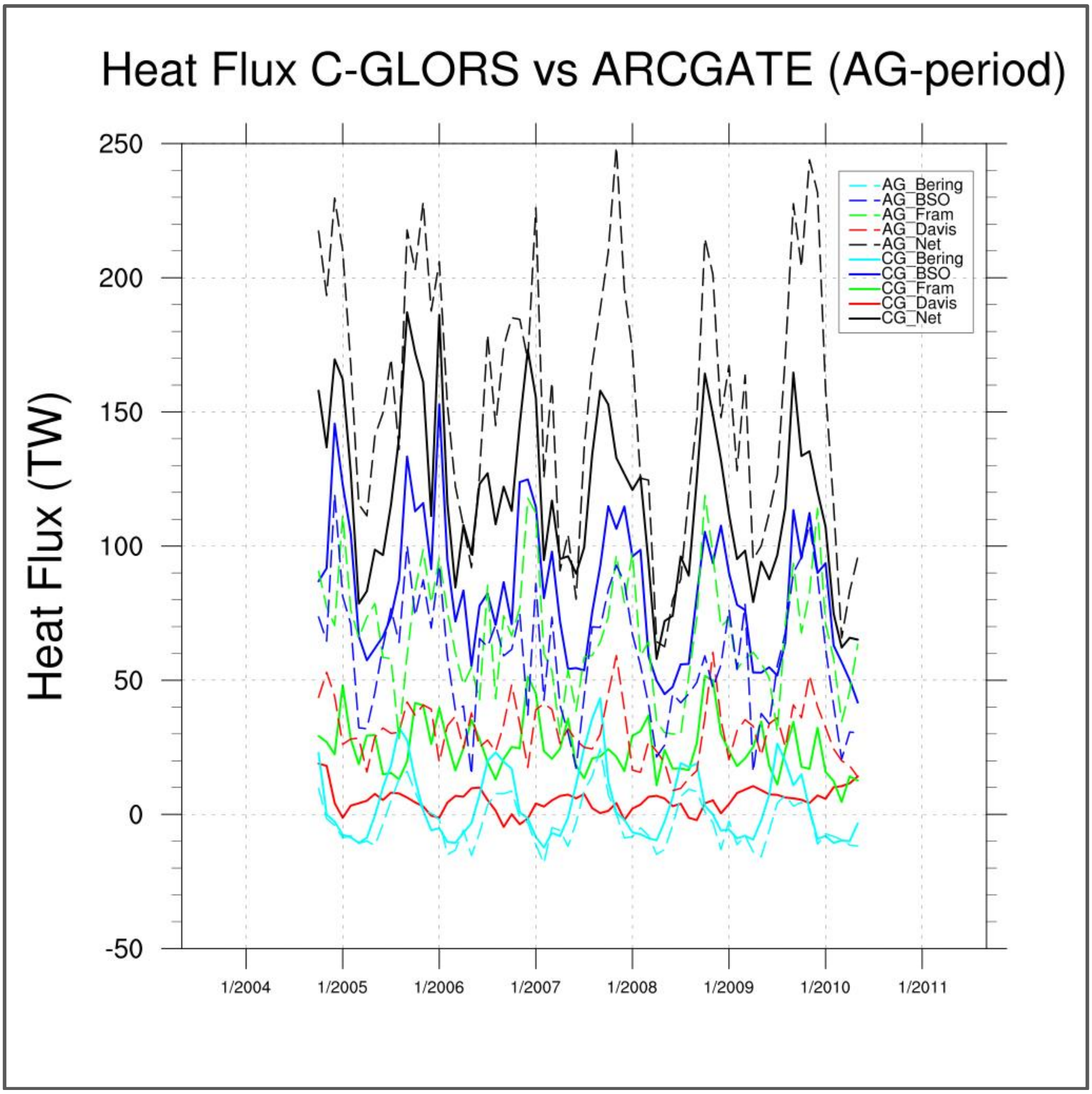

Figure 26: Heat transports from C-GLORSv5 (solid lines) and ARCGATE (dashed lines) for the period 10/2004 – 05/2010. Davis Strait is plotted in red, Fram Strait in green, Bering Strait is coloured in cyan and BSO is shown in blue. Net transports are also plotted in black. All units are Terawatts (*TW*).

Again, both datasets cover the same period of time (10/2004 – 05/2010), despite the fact that C-GLORSv5 would have been available for a much longer period.
The plot setup is the same as in the volume transport section; meaning ARCGATE transports are drawn in dashed lines, while reanalysis transports have solid lines. The

colours of the individual Straits are the same as well. The sign convention is self-evident. Positive values represent heat transport into the Arctic, while transports out of the Arctic have negative values. For a quantitative discussion, an extra table with average values, standard deviations of the differences and correlation coefficients for the individual straits is shown.

A look at Figure 26 reveals some interesting results of the comparison between ocean reanalysis and observations. One can see, that the general patterns are captured by the reanalysis, nevertheless also large differences can be seen. A qualitatively good agreement can be found for Bering Strait for example. Also, the behaviour as a temporal heat sink is clearly visible from the time-series. The largest heat transports into the Arctic Ocean are, as literature lets expect, found in Fram Strait and Barents Sea Opening. Minor contributions to the heat transport are observed for Davis Strait. The net transport reveals the biggest differences between both datasets, nevertheless, they agree within their uncertainty bounds (114,81 ± 20,74 *TW* compared to 154,31 ± 24,05 *TW* from ARCGATE). To explain this large discrepancy a closer look at the individual straits has to be made.

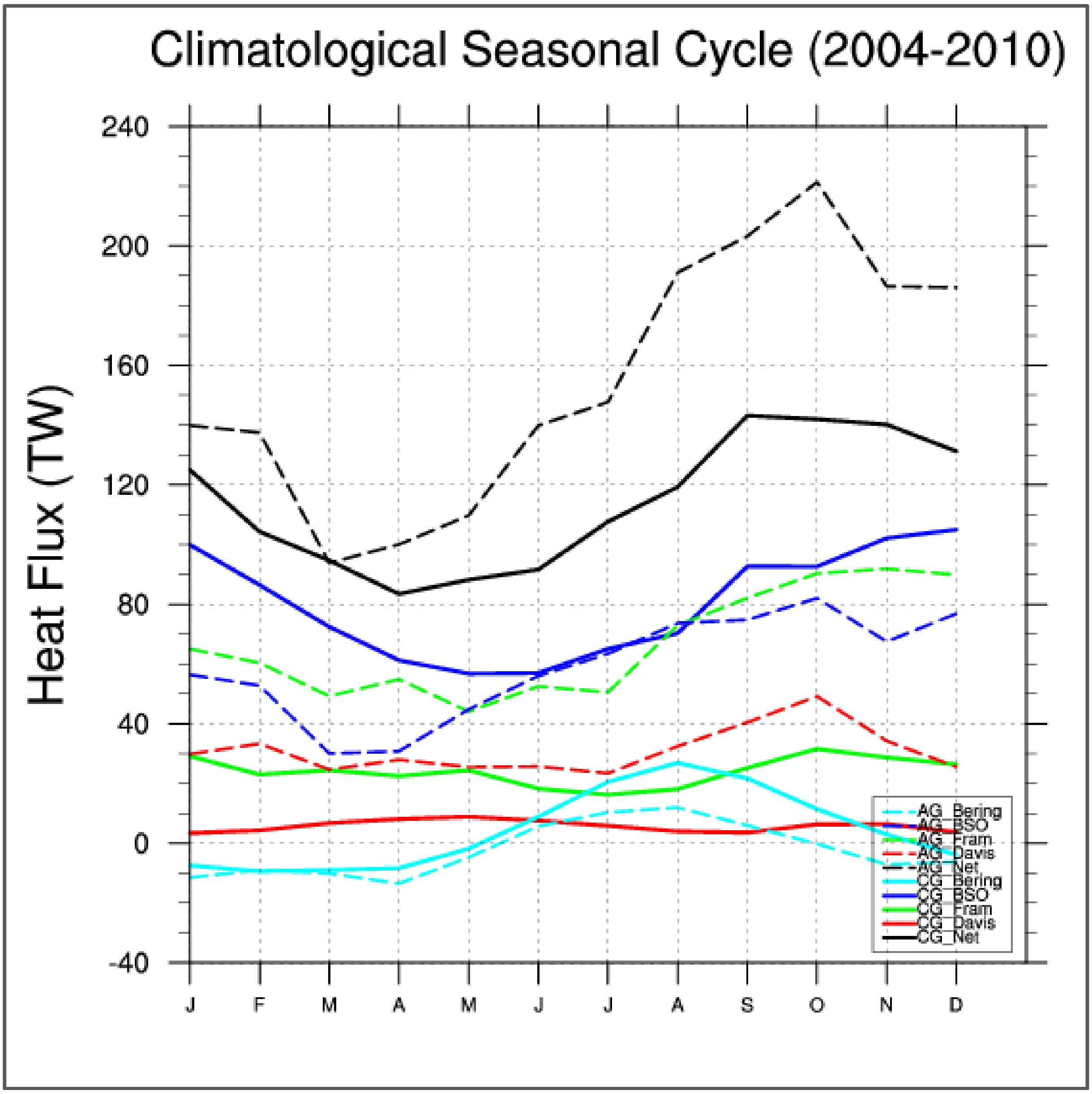

Figure 27: Seasonal cycle of the heat transports obtained from C-GLORSv5 (solid lines) and ARCGATE (dashed lines), calculated for the period 10/2004 – 05/2010. Davis Strait is plotted in red, Fram Strait in green, Bering Strait is coloured in cyan and BSO is shown in blue. Net transports are also plotted in black. All units are Terawatt (*TW*).

To get a better understanding of the seasonal distribution of the discrepancies between the data, again an additional seasonal cycle plot for C-GLORSv5 and ARCGATE is shown in Figure 27. There is some agreement between reanalysis and the ARCGATE data, nevertheless in detail large discrepancies can be found in all straits except Bering Strait. For BSO, two different seasons can be distinguished. During the summer the agreement is good, while during the rest of the year differences up to 40 *TW* occur. Davis Strait heat transport is underestimated throughout the year, whilst for Fram Strait the opposite is true. Heat transports through Fram Strait are underestimated in fall and early winter by nearly 60 *TW*. High analogy between observation-based values and reanalysis is present for the comparison of Bering Strait estimates, with only slight overestimation by the ocean reanalysis in summer (~10 *TW*).

Concerning the net heat transport into the Arctic, some interesting facets can be seen in Figure 27. While large differences are present in late summer and fall, better agreement is shown for the first half of the year. Overall the seasonal cycle is double as large in ARCGATE compared to C-GLORSv5 (and ORAS5 – see section 3.2.1.2).
In the following paragraphs, the differences in the individual straits are outlined in detail and the values are compared to literature.

Table 4: Average values for C-GLORSv5, ARCGATE and literature for the different straits. Additionally, the correlation coefficient (R) and STDDEV between ARCGATE and C-GLORSv5 is computed. All average values (AVG) and STDDEV are in *TW*, R is unitless.

	C-GLORSV5 (AVG)	ARCGATE (AVG)	R	STDDEV (DIFF)	LITERATURE (AVG)
Davis Strait	6,62 ± 3,97	30,94 ± 7,83	0,09	11,56	20 ± 9
Fram Strait	24,61 ± 9,67	67,21 ± 14,75	0,70	17,09	36 ± 6
BSO	79,44 ± 15,66	58,92 ± 15,18	0,78	16,68	70 ± 5
Bering Strait	4,14 ± 4,51	-2,78 ± 3,77	0,89	6,81	10 -20

Starting again with **Bering Strait**, the C-GLORSv5 derived heat transports match those of the ARCGATE dataset very well. Despite this good overall agreement, there are also periods of slight overestimation by the reanalysis. Especially during summer, the heat inflow calculated by C-GLORSv5 is on average 5 to 10 *TW* higher than in the observations. On average over the whole period the difference is about 7 *TW,* with ARCGATE derived average heat transports for the period being negative. Nevertheless, the high correlation coefficient in Table 4 indicates a good match over the whole ARCGATE-period. By comparing time-series values obtained from C-GLORSv5 ocean reanalysis and observations with literature estimates, one finds some mismatches between the datasets. While Woodgate (2010) estimates heat transports through Bering Strait with 10 to 20 *TW*, both, reanalysis and observations, show lower values. At this point it is noteworthy, that for the literature values a different reference temperature was used. Comparing the seasonal cycle, there is a good qualitative match between ARCGATE and C-GLORSv5, although there is an overestimation of heat transport into the Arctic by C-GLORSv5 during the summer months. The agreement between the investigated datasets and literature obtained by Woodgate (2017) is also qualitatively good, quantitatively the comparison is hampered by differences in the used reference values.

Barents Sea Opening time-series and seasonal cycle plots (Fig 26 & 27) show reasonable agreement between ARCGATE and C-GLORSv5 at least for some parts of the year. Especially during summer the agreement is good. This high degree of accordance can also be seen by the relatively high correlation coefficient in Table 4. Bigger differences between the data arise in the colder part of the year, from September to April, when C-GLORSv5 overestimates the transport of heat into the Arctic (see Fig. 27). On average, the reanalysis-derived transport exceeds those of ARCGATE by approximately 20 *TW*. Comparing these values with literature estimates obtained by Smedsrud et al. (2010) reveals also some interesting findings. With literature values being around 70 ± 5 *TW*, they are exactly in between the two other data sources. The seasonal cycle of BSO heat transport provided by Smedsrud et al. (2010) reveals qualitative good agreement to the ARCGATE-derived one. The smallest values can be found in April with approx. 35 *TW*, the largest during winter. The minimum values are nearly the same, while ARCGATE shows lower transports in winter. These lower transports result in an overall underestimation. The C-GLORSv5 seasonal cycle shows a slightly shifted minimum in transports towards summer, whereas the maximum transports are also in January. However, the reanalysis estimates are much higher throughout the year and therefore the transports are overestimated compared to literature and ARCGATE.

The next paragraph deals with the comparison of **Fram Strait** data. Looking at Figure 26, one can see significant underestimation of heat transports into the Arctic Ocean through Fram Strait by C-GLORSv5 throughout the whole period. This is also true for the seasonal cycle plot (Fig. 27). Regarding the mean values, a huge discrepancy can be observed. While ARCGATE indicates heat transports of approximately 67 *TW* on average, C-GLORSv5 transports are only about one third. Despite these huge difference, the correlation coefficient is high. This high correlation suggests, that the temporal patterns of both datasets are similar. Turning now towards the comparison with literature values, Schauer & Beszczynska-Möller (2009) found mean heat transport through Fram Strait of 36 ± 6 *TW*, which are much closer to the C-GLORSv5 estimates. Concerning the seasonal cycle in Figure 27, there are also some differences. While the observation-based dataset shows a clear seasonal cycle, the reanalysis shows hardly any variation through the year. Additionally, the ARCGATE values are again always higher than C-GLORSv5-based transports. A comparison with literature values obtained by Schauer, Fahrbach, Osterhus, & Rohardt (2004) for the years 1998 and 1999 shows qualitative good agreement with ARCGATE seasonal cycle (minimum during summer, maximum during winter), quantitatively there is hardly any match with ARCGATE nor C-GLORSv5.

To complete this section, **Davis Strait** heat transports are compared. Figure 26 reveals large discrepancies between ARCGATE and C-GLORSv5, both qualitatively and quantitatively. While observation-based transports show large variations throughout the years, C-GLORSv5 heat transports are nearly constant or partly opposing the ARCGATE ones. This can be also seen in Figure 27. The quantitative differences become also visible by looking at the average values in Table 4. While the observation-based transports agree with literature values by Curry et al. (2011) within their uncertainty range, the transports obtained by reanalysis are significant lower. This is also true for the comparison of the climatology with literature estimates. Lee, Curry, Gobat, Petrie, & Azetsu-Scott obtain a seasonal cycle very close to the ARCGATE climatology, while C-GLORSv5 transports are smaller and without any variability during the year. The huge difference between literature and ocean reanalysis may be explained again by the inability of the reanalysis to correctly capture the inflow through WGC and the WGS.

Comparing time-filtered anomaly time-series of both datasets and subsequently their correlation, one can find similar patterns to the ones described above. This is especially true for BSO and Bering Strait, while for the other two straits some differences arise. The correlation for Davis Strait is much higher than in the full time-series. At the same time, the correlation for Fram Strait decreases significant. Nevertheless, the overall anomaly correlation is good as shown in Figure 28.

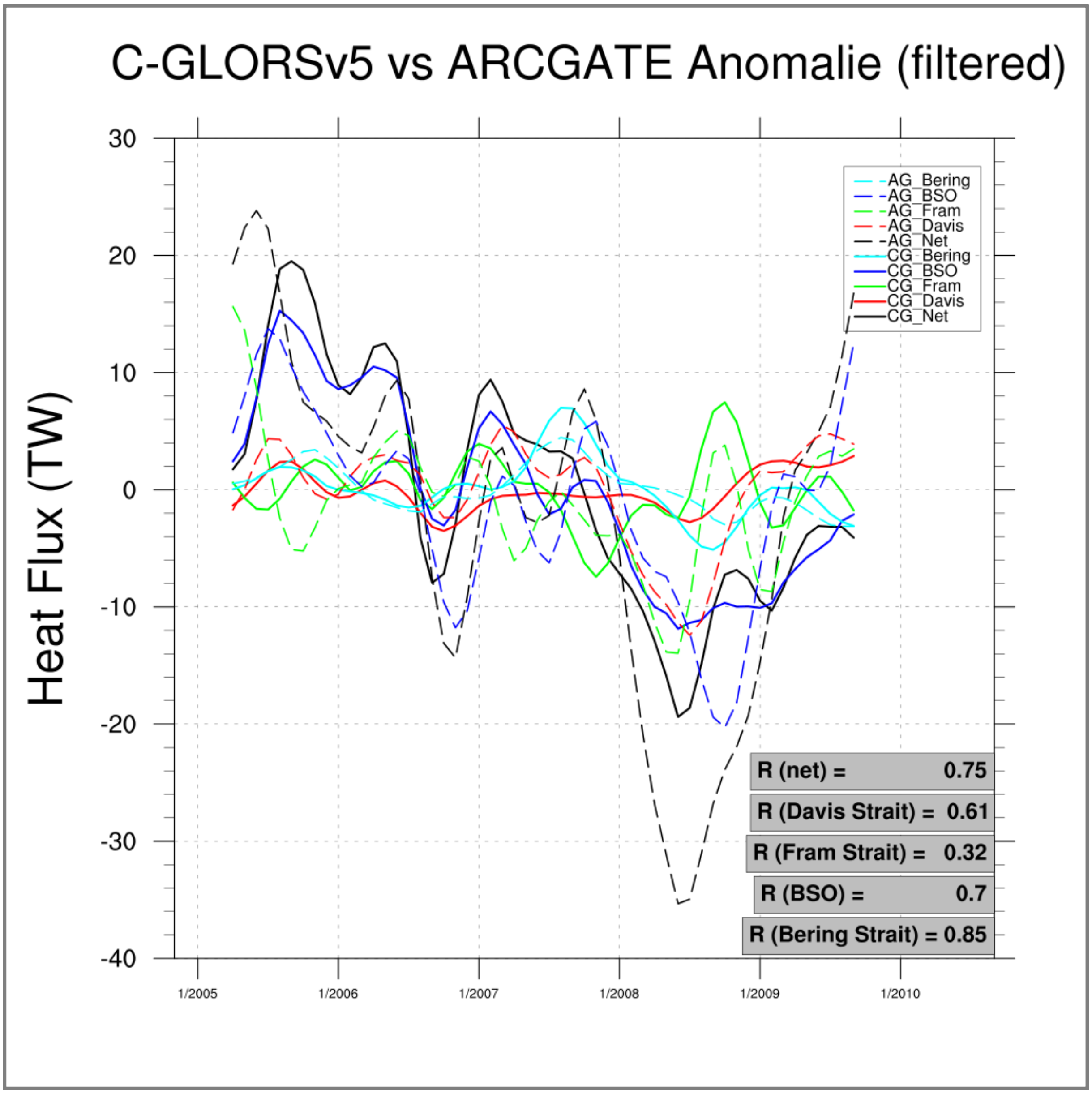

Figure 28: Anomaly time-series of the heat transports from C-GLORSv5 (solid lines) and ARCGATE (dashed lines), calculated for the period 10/2004 – 05/2010. Davis Strait is plotted in red, Fram Strait in green, Bering Strait is coloured in cyan and BSO is shown in blue. Net transports are also plotted in black. All units are Terawatt (*TW*).

3.2.1.2. ORAS5

Next, the comparison between ARCGATE and the ECMWF ocean reanalysis ORAS5 regarding heat transports will be discussed. Taking a quick look at Figure 27, one can see that there is some better agreement between observations and reanalysis than it is for C-GLORSv5. This is especially true for Barents Sea Opening, albeit the match between ARCGATE and ORAS5 is still not the best. Comparing Fram Strait net transports, further improvements can be seen (133,76 $\pm$ 21,74 *TW* compared to 154,31 $\pm$ 24,05 *TW* from ARCGATE). Hardly any improvement is visible for Davis Strait, while for Bering Strait a slight deterioration can be seen.

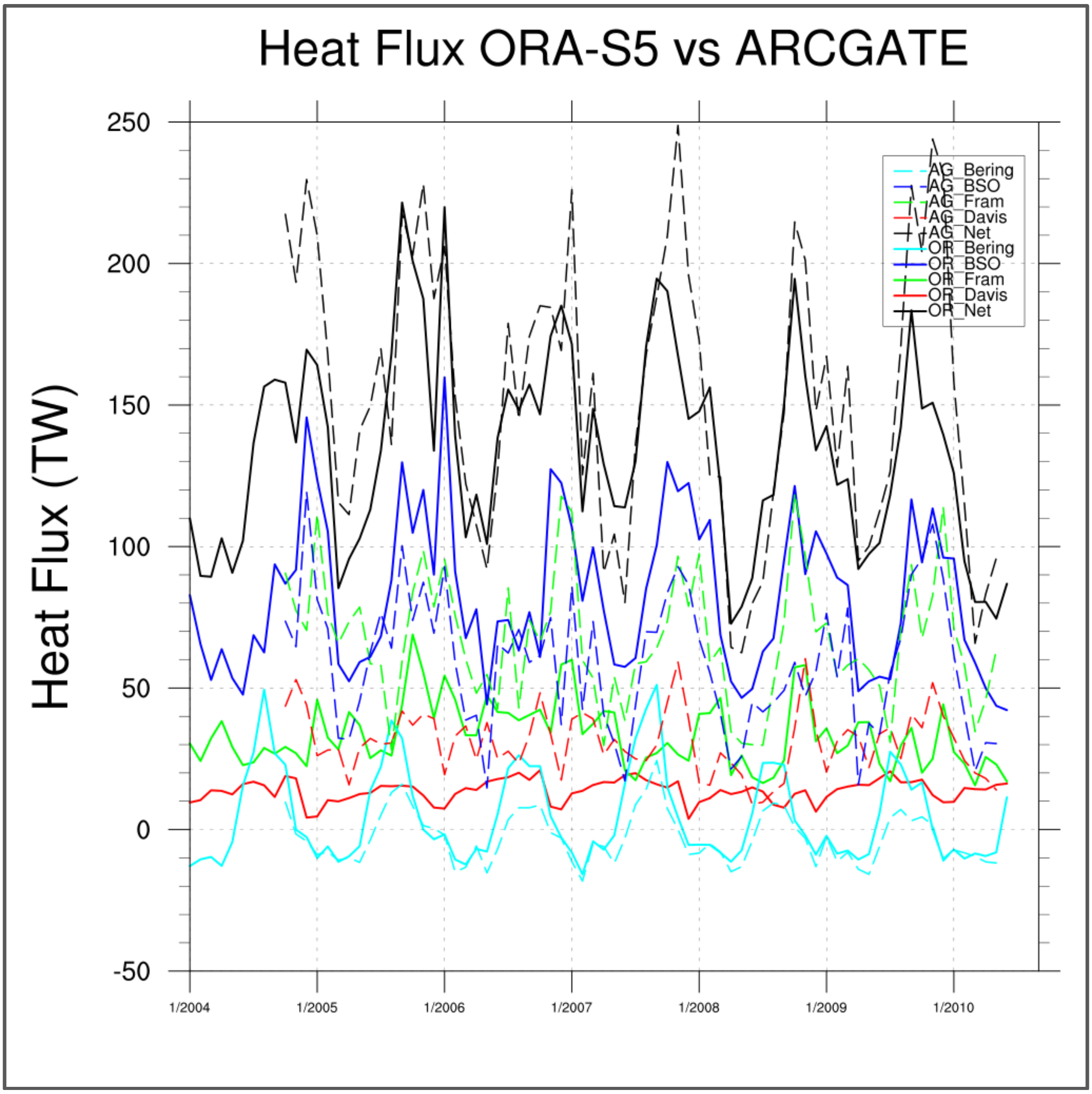

Figure 29: Heat transports from ORAS5 (solid lines) and ARCGATE (dashed lines) for the period 10/2004 – 05/2010. Davis Strait is plotted in red, Fram Strait in green, Bering Strait is coloured in cyan and BSO is shown in blue. Net transports are also plotted in black. All units are Terawatts (*TW*).

Regarding the average values for **Bering Strait**, the difference between ARCGATE and ORAS5 has increased with respect to C-GLORSv5. Nevertheless, the qualitative match between reanalysis and literature values is better for ORAS5 than for C-GLORSv5 (a quantitative comparison is hampered by different reference temperatures). Despite the bigger differences between observations and reanalysis, the correlation between these two datasets has further improved. This fact can be seen in Figure 29 as well, however, the overestimation of heat transports compared to ARCGATE is bigger for ORAS5 in late summer and fall. The agreement between the investigated climatologies and literature seasonal cycle obtained by Woodgate (2017) is also qualitatively good, with slight improvements compared to C-GLORSv5.

Qualitative improvement can be seen for **Barents Sea Opening** in Figure 29, although none of the values in Table 5 have improved. Average values for BSO are slightly higher for ORAS5 than for C-GLORSv5 and therefore the standard deviation is also higher. Since the changes are very small, still both datasets, ARCGATE and ORAS5 agree with literature estimates within their uncertainty range.

The comparison of the seasonal cycles in Figure 30 with literature values provided by Smedsrud et al. (2010) reveals hardly any difference to the comparison with C-GLORSv5. The ORAS5 climatology shows a slightly shifted minimum in transports towards summer compared to literature. The maximum transports can also be found January. Since ORAS5 estimates are higher throughout the year, heat transports are overestimated compared to literature and ARCGATE.

For **Fram Strait,** Figure 29 shows some improvements compared to C-GLORSv5. Albeit this enhancement, there is still a significant underestimation of heat transports into the Arctic Ocean through Fram Strait by ORAS5. Comparing again the average values for the whole AG-period, there is a slightly better match. This is also confirmed by the lower standard deviation in Table 5. Simultaneously, the correlation between ARCGATE and ORAS5 has decreased, indicating that the temporal patterns are captured better by the CMCC ocean reanalysis. Since heat transports in ORAS5 are higher than in C-GLORSv5, there is even better agreement with literature values obtained by Schauer & Beszczynska-Mo ̈ller (2009) (36 ± 6 *TW*). Concerning the seasonal cycle in Figure 30, there are also some differences. Although the transports are higher, still only slight variations can be seen in the ORAS5 dataset. In contrast, a climatology obtained by Schauer, Fahrbach, Osterhus, & Rohardt (2004) for the years 1998 and 1999 shows a clear minimum during summer and a maximum during winter.

Davis Strait heat transports are discussed next. Like Figure 26, Figure 29 also reveals large discrepancies between ARCGATE and the ocean reanalysis. Although there are only minor visible improvements compared to C-GLORSv5, ORAS5 mean values for the entire period are much closer to the observations. This is also true for the standard deviation, which has decreased. The comparison between the climatologies can also be seen in Figure 30. A comparison of the ORAS5 climatology with literature estimates by Lee, Curry, Gobat, Petrie, & Azetsu-Scott reveals better results as for C-GLORSv5, nevertheless the transports throughout the year are still very different. The slight improvements compared to the CMCCs ocean reanalysis can also be seen by looking at the correlation coefficient in Table 5.

For a quantitative comparison, Table 5 provides again mean values of all straits for ARCGATE and ORAS5, as well as estimates found in literature. Additionally, the correlation coefficient and the standard deviation between ARCGATE and ORAS5 for all gateways are shown.

Table 5: Average values for ORAS5, ARCGATE and literature for the different straits, additionally correlation coefficient (R) and STDDEV are computed. All average values (AVG) and STDDEV are in *TW*.

	ORAS5 (AVG)	ARCGATE (AVG)	R	STDDEV (DIFF)	LITERATURE (AVG)
Davis Strait	14,00 ± 3,22	30,94 ± 7,83	0,15	11,21	20 ± 9
Fram Strait	32,61 ± 10,20	67,21 ± 14,75	0,60	18,13	36 ± 6
BSO	81,20 ± 16,66	58,92 ± 15,18	0,78	17,38	70 ± 5
Bering Strait	5,95 ± 5,48	-2,78 ± 3,77	0,92	8,12	10 -20

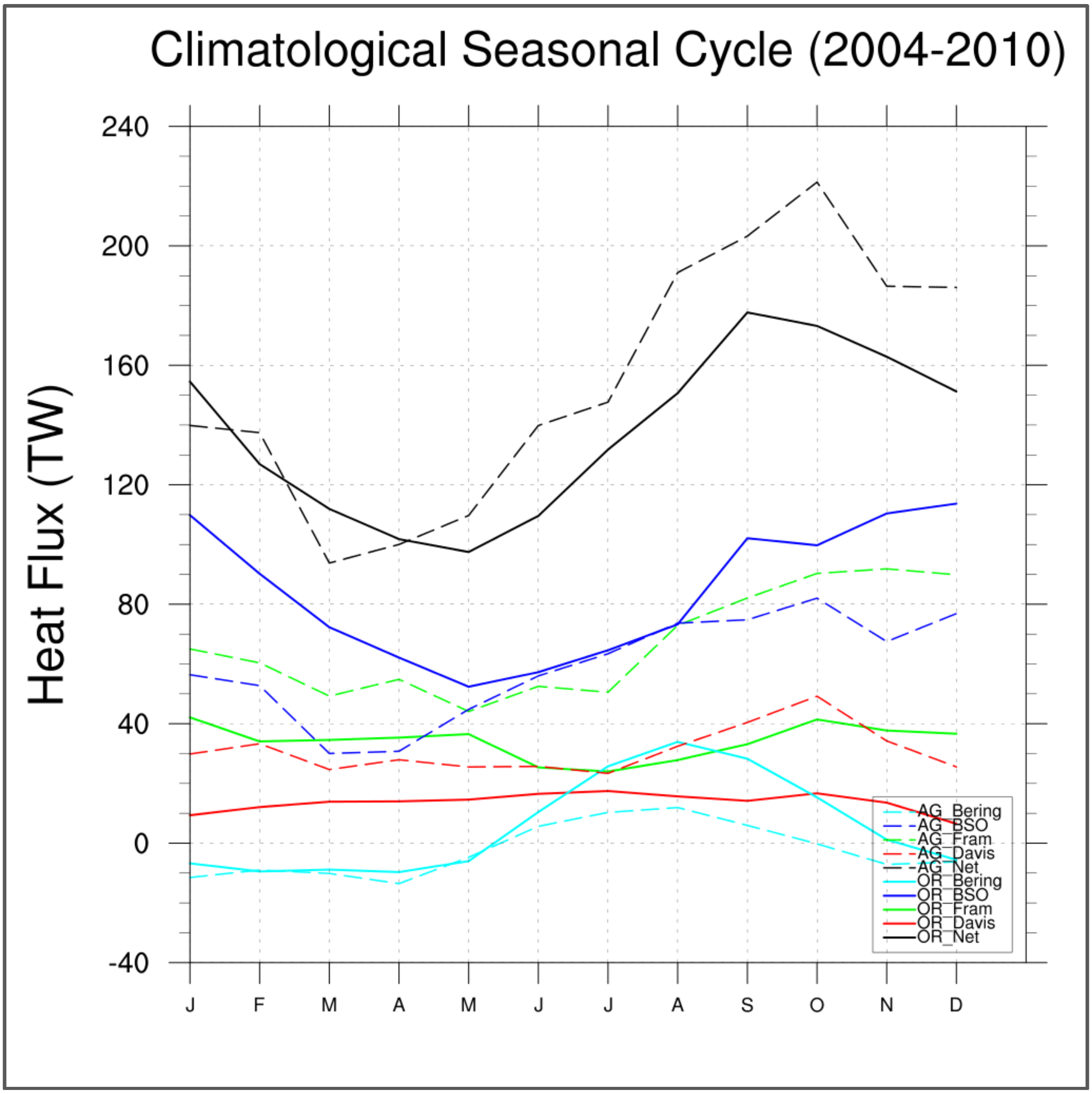

Figure 30: Seasonal cycle of the heat transports obtained from ORAS5 (solid lines) and ARCGATE (dashed lines), calculated for the period 10/2004 – 05/2010. Davis Strait is plotted in red, Fram Strait in green, Bering Strait is coloured in cyan and BSO is shown in blue. Net transports are also plotted in black. All units are Terawatt (*TW*).

Concerning the anomaly time-series, no clear statement about the improvement or disparagement of ORAS5 compared to CGLORSv5 can be made. While some correlations are better (Bering Strait or Davis Strait), also a decline in correlation between reanalysis and observational data can be noticed (BSO and net transport).

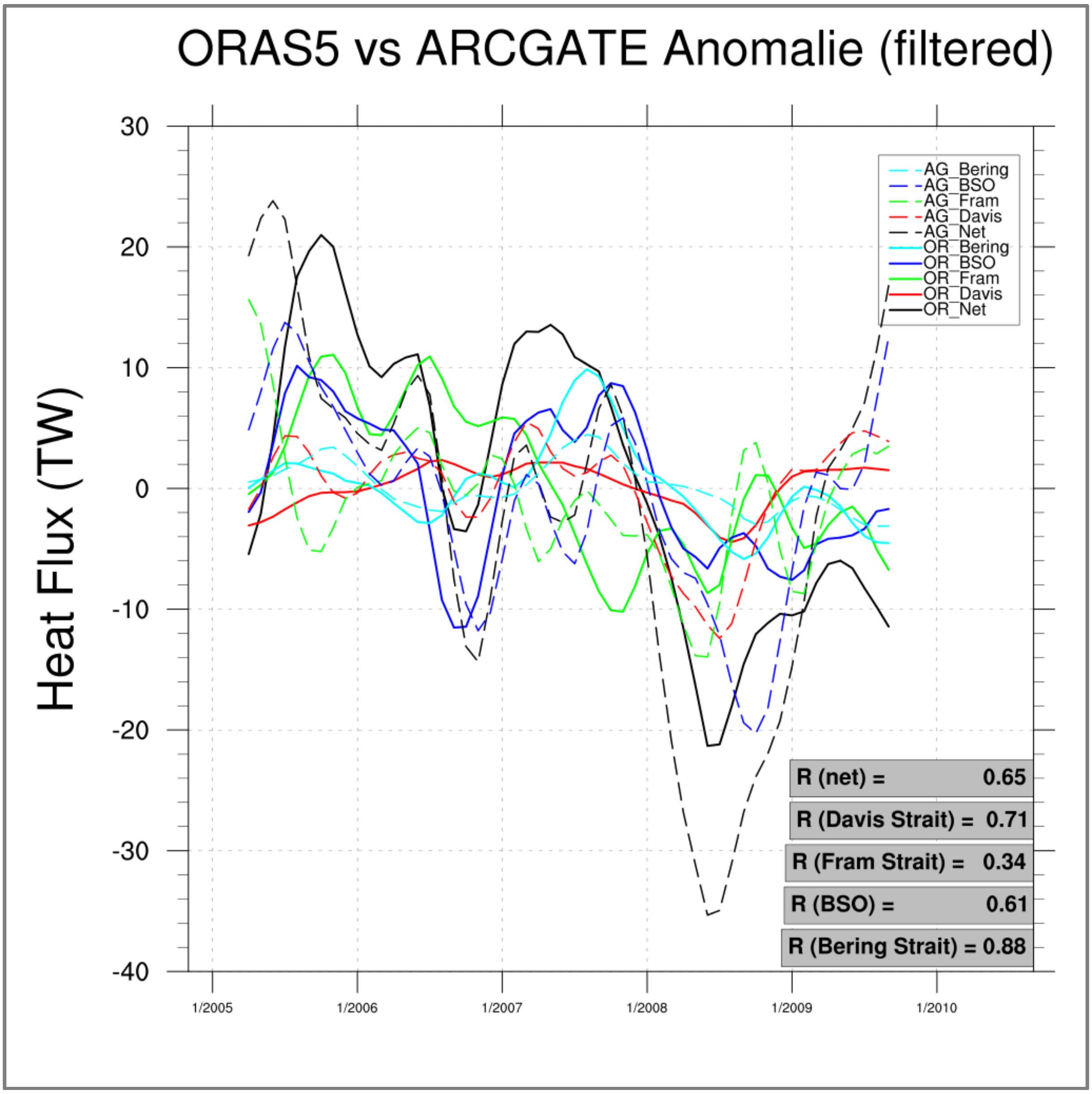

Figure 31: Anomaly time-series of the heat transports from ORAS5 (solid lines) and ARCGATE (dashed lines), calculated for the period 10/2004 – 05/2010. Davis Strait is plotted in red, Fram Strait in green, Bering Strait is coloured in cyan and BSO is shown in blue. Net transports are also plotted in black. All units are Terawatt (*TW*).

3.2.2. Hovmoeller diagrams

In the following section the Hovmoeller-diagrams of heat transports through each of the straits are shown. Again, two different figures are shown for each gateway, one showing a time versus width visualization, the other a time versus depth visualization.

Starting with the depth-integrated rendering for **Bering Strait**, there are some interesting differences between ARCGATE and both reanalysis products. First of all, it is clear to see, that each of the three datasets shows seasonality in heat transports. Since the volume transports through Bering Strait are positive most of the time (see section 3.1), this variation is solely temperature driven. Colder waters transported during winter and spring cause heat loss to the Pacific Ocean, while during the warmer season heat is transported into the Arctic Ocean through Bering Strait. Although both reanalyses capture this variation quite well, heat transports are much larger during summer in those datasets (see also Tables 4 & 5). For C-GLORSv5, larger negative heat transports can be found during the colder season. This behaviour was already expected from the time-series plots; nevertheless this visualization is somewhat more intuitive. Further differences can be found regarding the location of the transports. ARCGATE and C-GLORSv5 indicate most of the heat is transported through the Russian side of Bering Strait. In contrast, minor peaks of heat transport can be seen on the Alaskan side of the Strait in ORAS5. Since this feature is found for volume transports too, it can be explained through the different velocity patterns in the datasets.

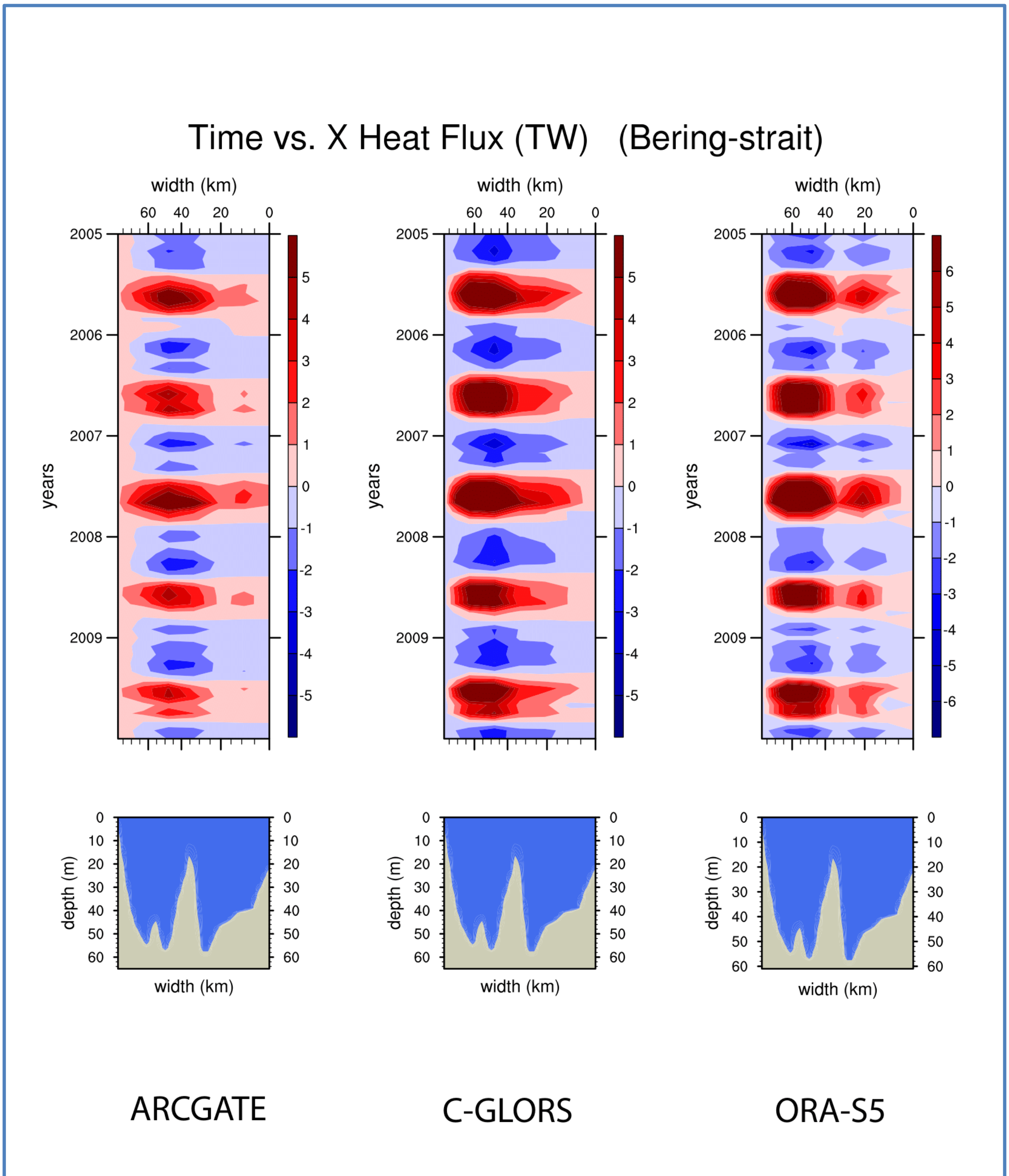

Figure 32: Time versus width Hovmoeller diagram for Bering Strait. ARCGATE is shown to the left; C-GLORSv5 in the middle and ORAS5 is on the right side. In the bottom section the bathymetry of Bering Strait is plotted.

Comparing now the width-integrated Hovmoeller diagrams of the three datasets, only small differences can be seen. The most obvious among them is again the overestimation of the heat transports by both ocean reanalysis. By looking in more detail at Figure 33, some smaller discrepancies between the data can be found. This is especially true for the negative heat transports during winter captured by the ARCGATE observations. From both reanalysis products, only ORAS5 shows comparable fluctuations at that time of the year.

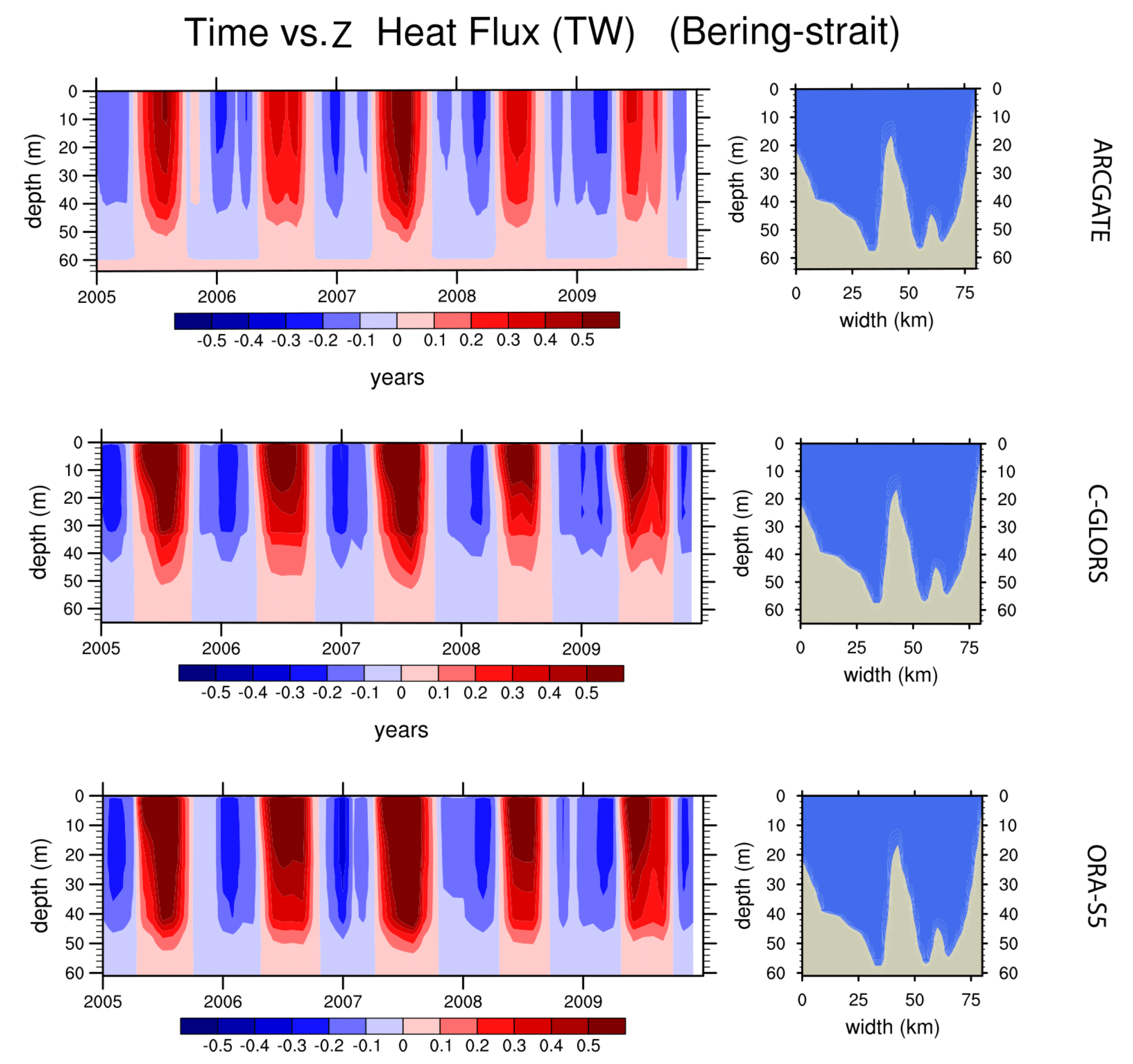

Figure 33: Time versus depth Hovmoeller diagram for Bering Strait. ARCGATE is shown in the top-panel, followed by C-GLORSv5 in the middle and ORAS5 at the bottom. To the right of the plots, again the bathymetry of Bering Strait is plotted.

Turning now towards **Barents Sea Opening**, more differences between the visualizations for observations and reanalyses are expected. This is again true for the Bear Island region (see Fig. 34). While ARCGATE shows predominantly negative heat transports north of Bear Island due to colder waters leaving the Arctic, both ocean reanalyses indicate an additional inflow-branch in this region. Since this pattern and the stationary eddy-circulation in the middle of the graphics are very similar to the ones found for volume transports, the discrepancies between observation and reanalyses might also arise solely due to differences in the velocity fields. Additionally, some minor changes in the assimilated temperature give rise to the discrepancy between all data. The rest of Figure 34 reveals only slight differences between the data. Seasonality and location of the transports are captured again well, by C-GLORSv5 and ORAS5.

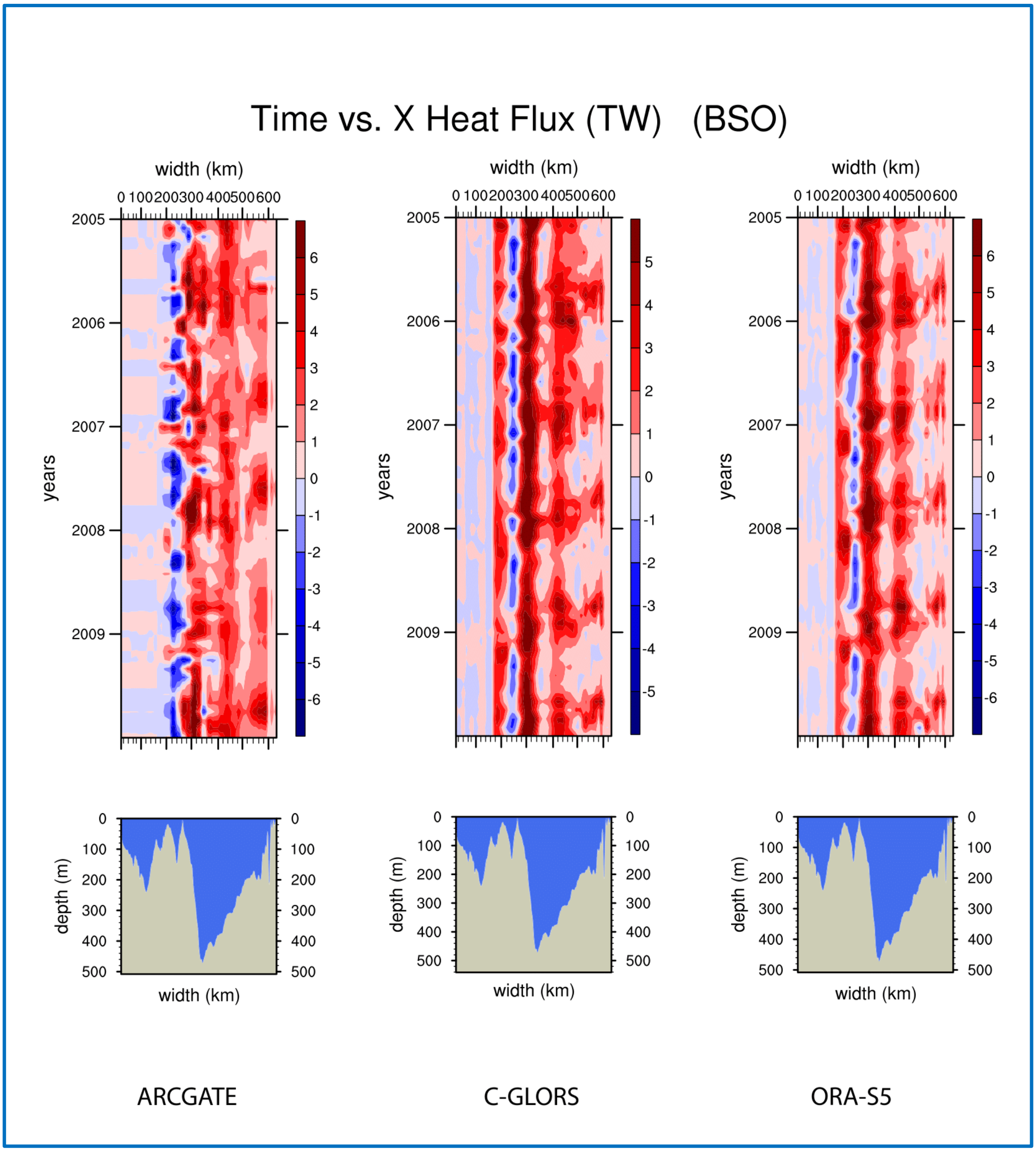

Figure 34: Time versus width Hovmoeller diagram for Barents Sea Opening. ARCGATE is shown to the left, C-GLORSv5 in the middle and ORAS5 is on the right side. In the bottom section the bathymetry of BSO is plotted.

Concerning the vertical structure of the transports, also some differences between the individual datasets can be seen. The most obvious difference is the vertical distribution of the heat transports. While ARCGATE heat transports are concentrated mainly to the surface layers with sharp boundaries to the underlying layers, the distribution is much smoother for both reanalyses. Especially the higher heat transports in depths exceeding 200 metres can again be explained by the velocity structure in these depths. The excessive ARCGATE heat transport in surface layers instead might be an indication for different temperatures used for observations.

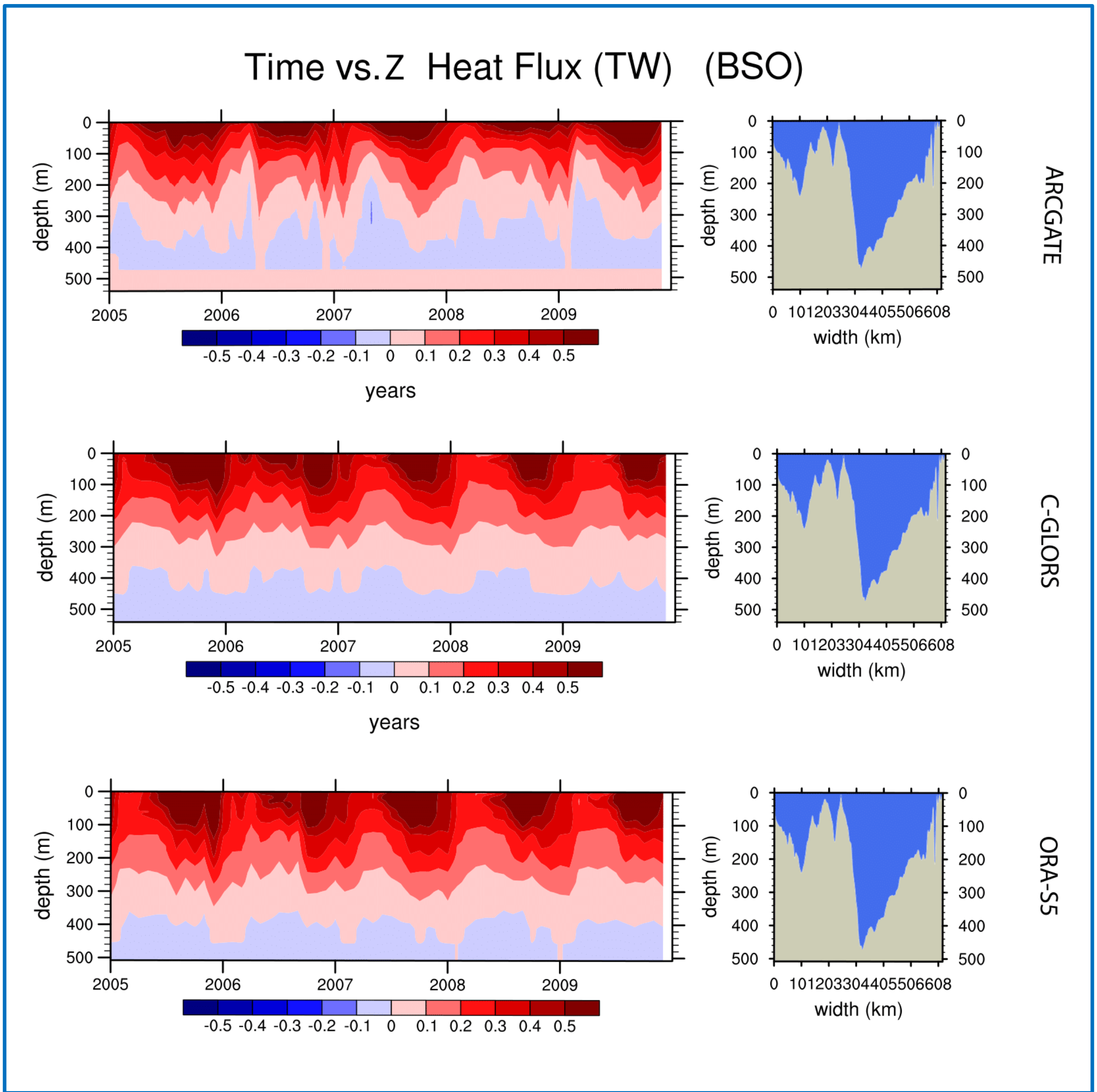

Figure 35: Time versus depth Hovmoeller diagram for Barents Sea Opening. ARCGATE is shown in the top-panel, followed by C-GLORSv5 in the middle and ORAS5 at the bottom. To the right of the plots, again the bathymetry of BSO is plotted.

Hovmoeller diagrams for **Fram Strait** show among the largest differences between the datasets. From Figure 36 it is clear to see, that most of the heat transported through Fram Strait enters the Arctic Ocean via the West Spitsbergen Current. This pattern is the same for all three data-sources; even though there are differences in the magnitudes of the transports. While ARCGATE- and C-GLORSv5 transports indicate eddies in the middle of Fram Strait, these eddies are entirely absent in the ORAS5 reanalysis. It is also remarkable, that the eddies in the observational dataset seem to be more variable in terms of location and time than in C-GLORSv5. This might be explained with the only partly eddy-resolving resolution of the reanalysis, by what only larger scale features are displayed. Another interesting finding of Figure 36 is, that only small amounts of heat are leaving the Arctic Ocean through East Greenland Current. This is especially true for ORAS5. Interestingly, the ECMWF reanalysis shows an Arctic Ocean heat loss due to inflow of colder waters near Belgica Bank, which is not captured by either of the other datasets.

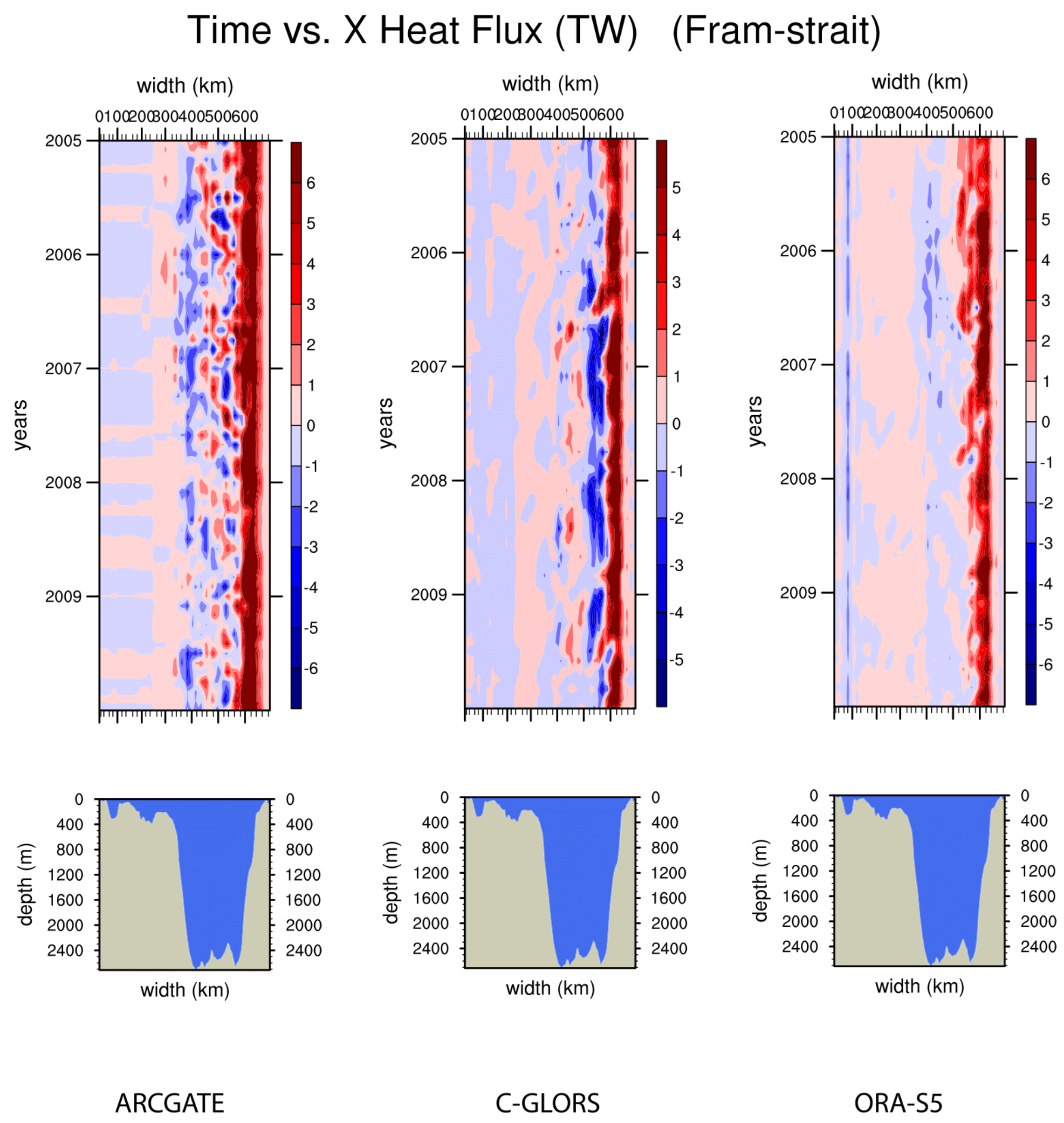

Figure 36: Time versus width Hovmoeller diagram for Fram Strait. ARCGATE is shown to the left, C-GLORSv5 in the middle and ORAS5 is on the right side. In the bottom section the bathymetry of Fram Strait is plotted.

The time versus depth visualization also reveals some interesting differences between the data. The largest positive heat transports can be found in the upper layers in all three datasets. Nevertheless, heat transports are much higher in ARCGATE than in the reanalysis products. Underneath this section of positive transports, also a seasonal fluctuating branch of negative heat transports can be seen (ARCGATE and C-GLORSv5). This negative branch cannot be found in the same extent in ORAS5 although the seasonality is again visible. Further differences concern depths below 1500m. While ARCGATE shows transports of heat into the Arctic at those depths, there is hardly any signal in one of the reanalyses. Since Fram Strait is the only deep-water connection to the Arctic Ocean, this finding is of special interest.

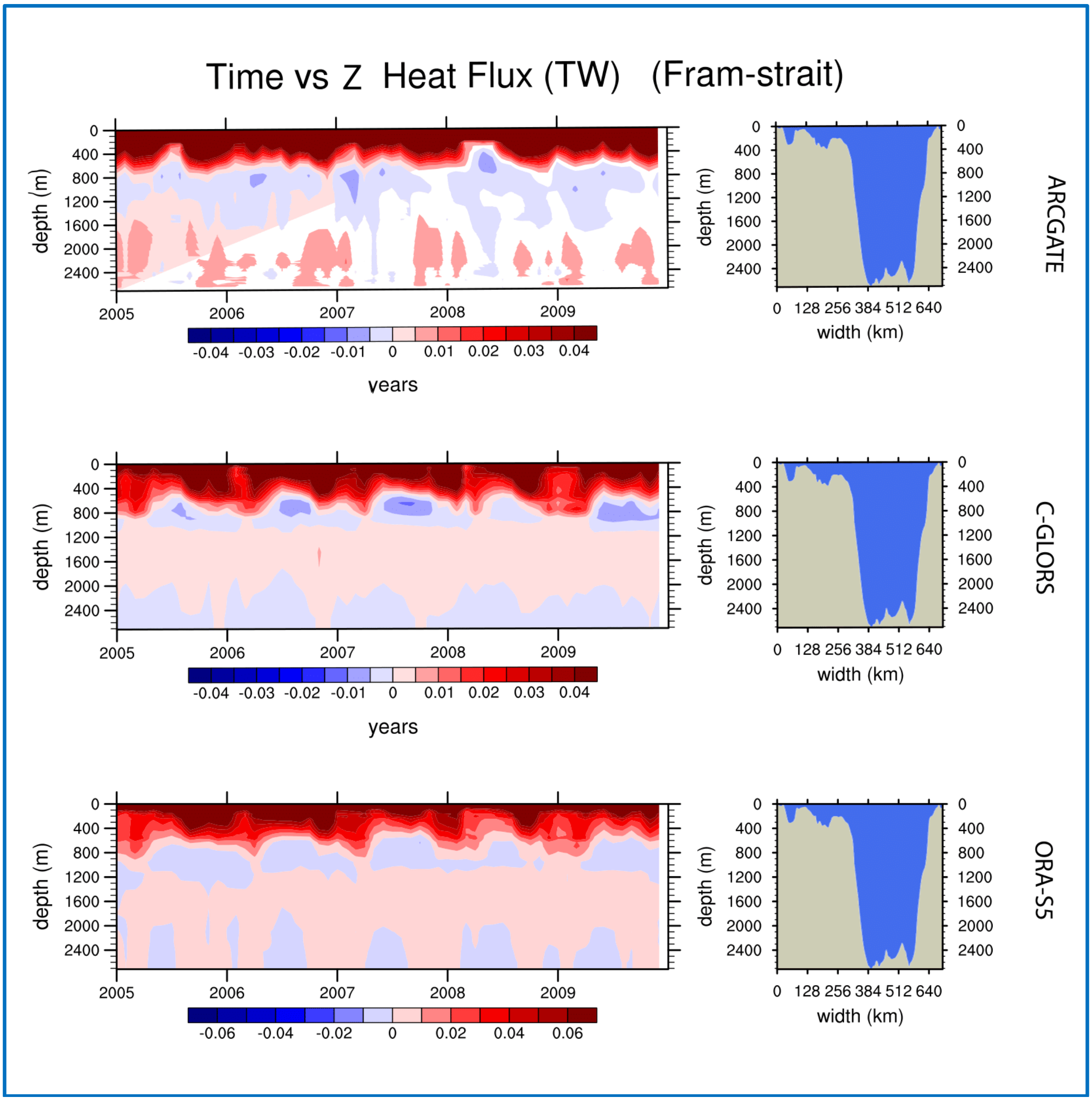

Figure 37: Time versus depth Hovmoeller diagram for Fram Strait. ARCGATE is shown in the top-panel, followed by C-GLORSv5 in the middle and ORAS5 at the bottom. To the right of the plots, again the bathymetry of Fram Strait is plotted.

To complete this section, a comparison of heat transports through **Davis Strait** will be given. Comparing Figure 38 and Figure 39 with those obtained for volume transports, one can see, that the main source of the discrepancies arise from the inflow pattern in WGC and WGS. While positive heat transports are prevailing in the ARCGATE data throughout the year, they are only seasonal in both reanalysis products, with more temporal extent in ORAS5. Additionally, both Ocean reanalyses show eddy-structures in this region, which are completely absent in the observations. Other differences can be found on the East side of Davis Strait. The Outflow through the Baffin Island Current is again steady all year round in the observation-based data, but highly variable in time for C-GLORSv5 and ORAS5. The better coverage of the spatial distribution by ORAS5 may explain the improvement in the time-series plots.

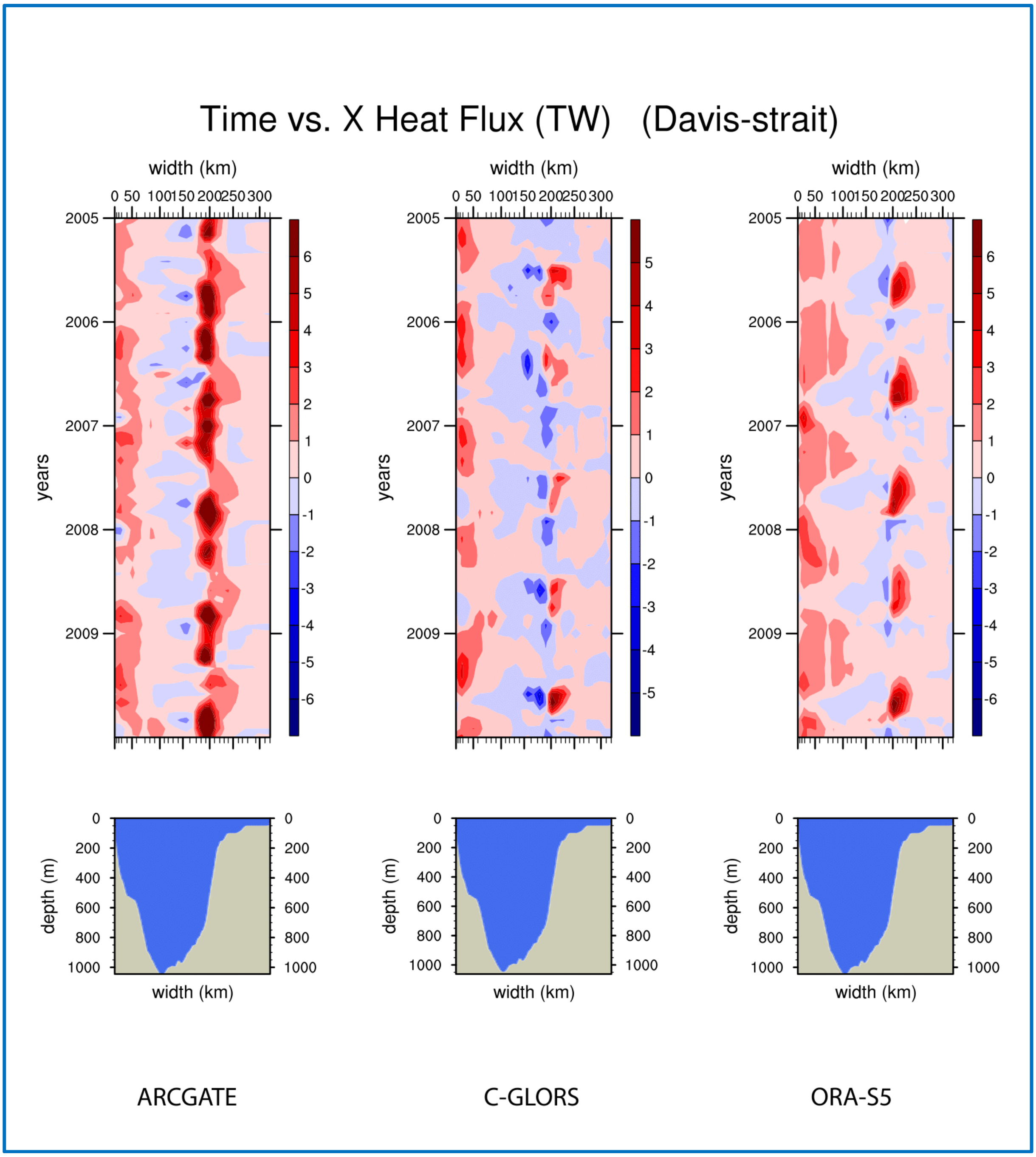

Figure 38: Time versus width Hovmoeller diagram for Davis Strait. ARCGATE is shown to the left, C-GLORSv5 in the middle and ORAS5 is on the right side. In the bottom section the bathymetry of Davis Strait is plotted.

Regarding the vertical structure, the differences are small and concentrated to the upper layers of the column. Since ARCGATE transports are constant all over the year, also the vertical structure predominately shows positive heat transport, albeit with clear seasonality. This is not true for both reanalyses. Instead of this steady pattern, they show a seasonal eddy-structure in the upper layers. Furthermore, the transports are limited to the upper 50 to 100 metres in the reanalyses, while significant ARCGATE transports can be found till depths of 200 metres.

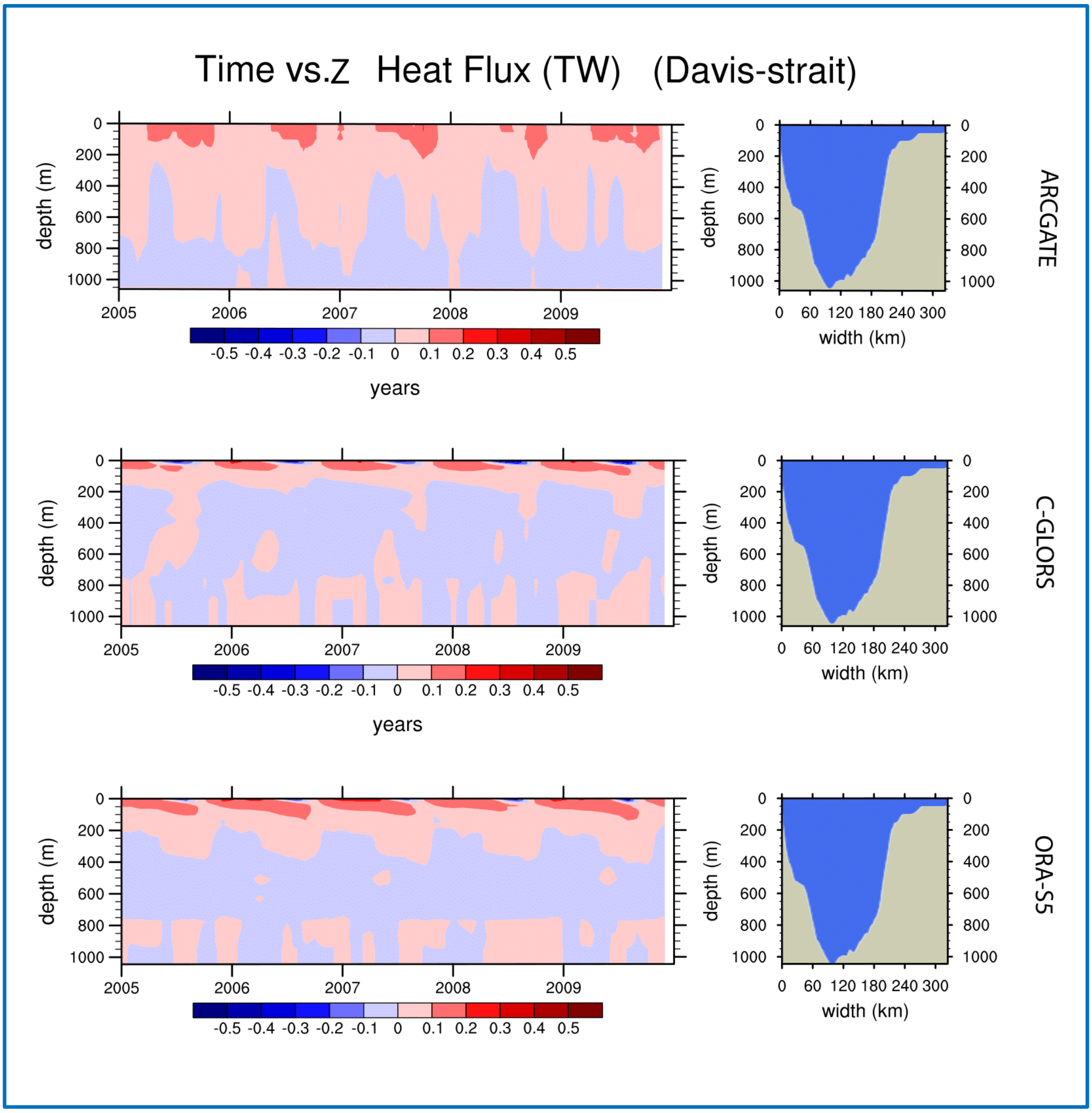

Figure 39: Time versus depth Hovmoeller diagram for Davis Strait. ARCGATE is shown in the top-panel, followed by C-GLORSv5 in the middle and ORAS5 at the bottom. To the right of the plots, again the bathymetry of Davis Strait is plotted.

3.3. Freshwater Transports

The last of the three investigated transports are freshwater transports through the Arctic Gateways. Again, these transports are computed on a tripolar grid for both re-analyses, the ARCGATE freshwater transports are included in the dataset.

3.3.1. Time Series

In the following passage, the time-series plots for freshwater transports through the major Arctic Gateways are discussed.

3.3.1.1. C-GLORSv5

Starting with the comparison of C-GLORSv5 with ARCGATE, Figure 40 shows time-series of freshwater transports. The comparison period is again chosen to be whole ARCGATE-period, from October 2004 to May 2010.

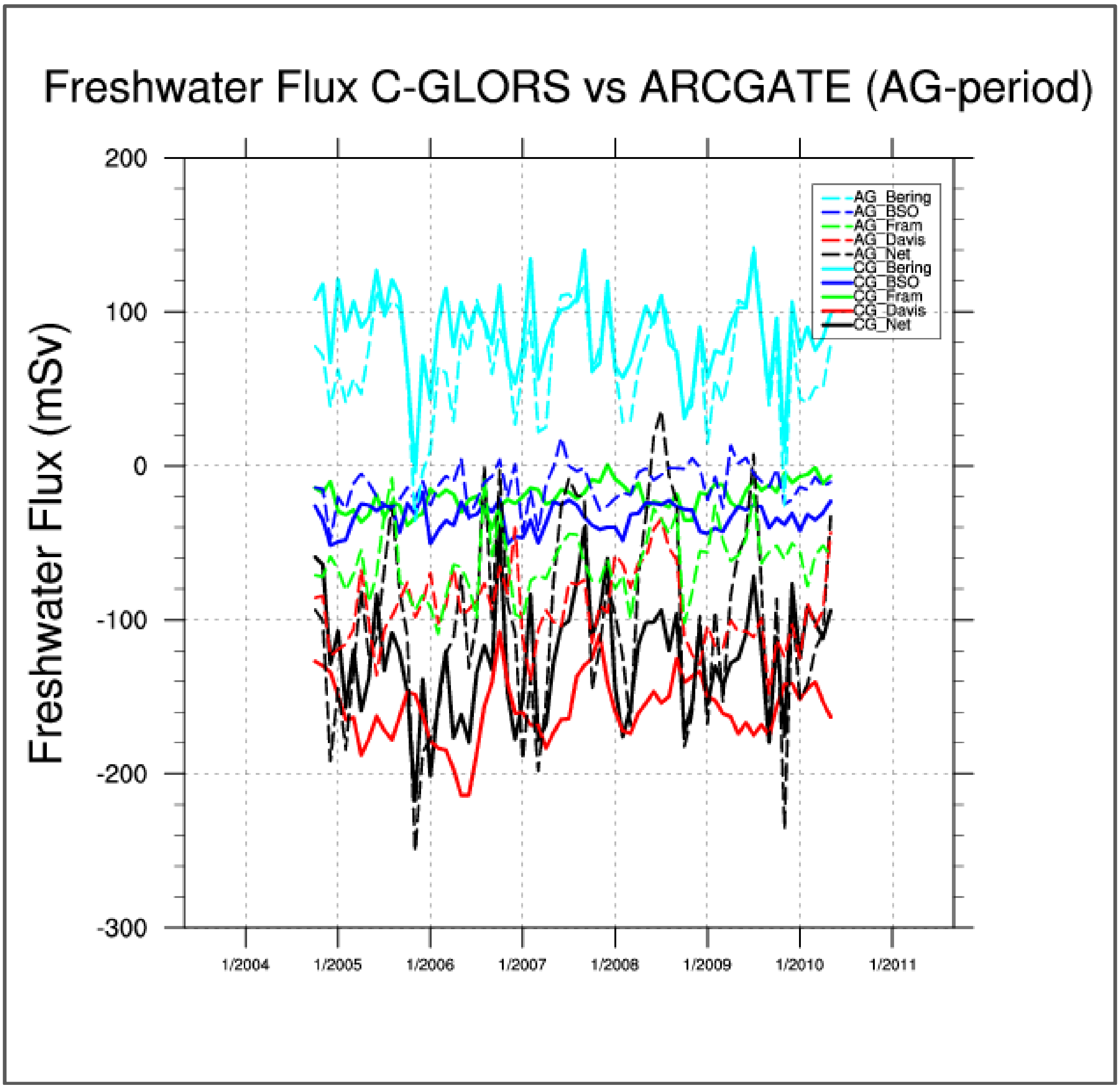

Figure 40: Freshwater transports from C-GLORSv5 (solid lines) and ARCGATE (dashed lines) for the period 10/2004 – 05/2010. Davis Strait is plotted in red, Fram Strait in green, Bering Strait is coloured in cyan and BSO is shown in blue. Net transports are also plotted in black. The units are Millisverdrup (mSv).

The colours of the straits as well as the line style are the same like in the previous sections (Davis Strait in red, Fram Strait in green, BSO in blue and Bering Strait in cyan). Net transports of both data sources are shown in black. Transports of freshwater into the Arctic Ocean have positive values, while freshwater leaving the Arctic is represented by negative values.

By comparing the C-GLORSv5 ocean reanalysis with observation-based data, some interesting information is gained. For some of the Straits the freshwater transports calculated from the reanalysis fits those of the observations very well, while for others this is not the case. A good agreement can be found for Bering Strait and Barents Sea

Opening. The net transports match well for some time, but also major deviations can be found. In average the net transports are -117,77 ± 39,06 *mSv* for C-GLORSv5 and -102,22 ± 44,63 *mSv* for ARCGATE. Substantial disagreements between both datasets can also be found for Davis Strait and Fram Strait.

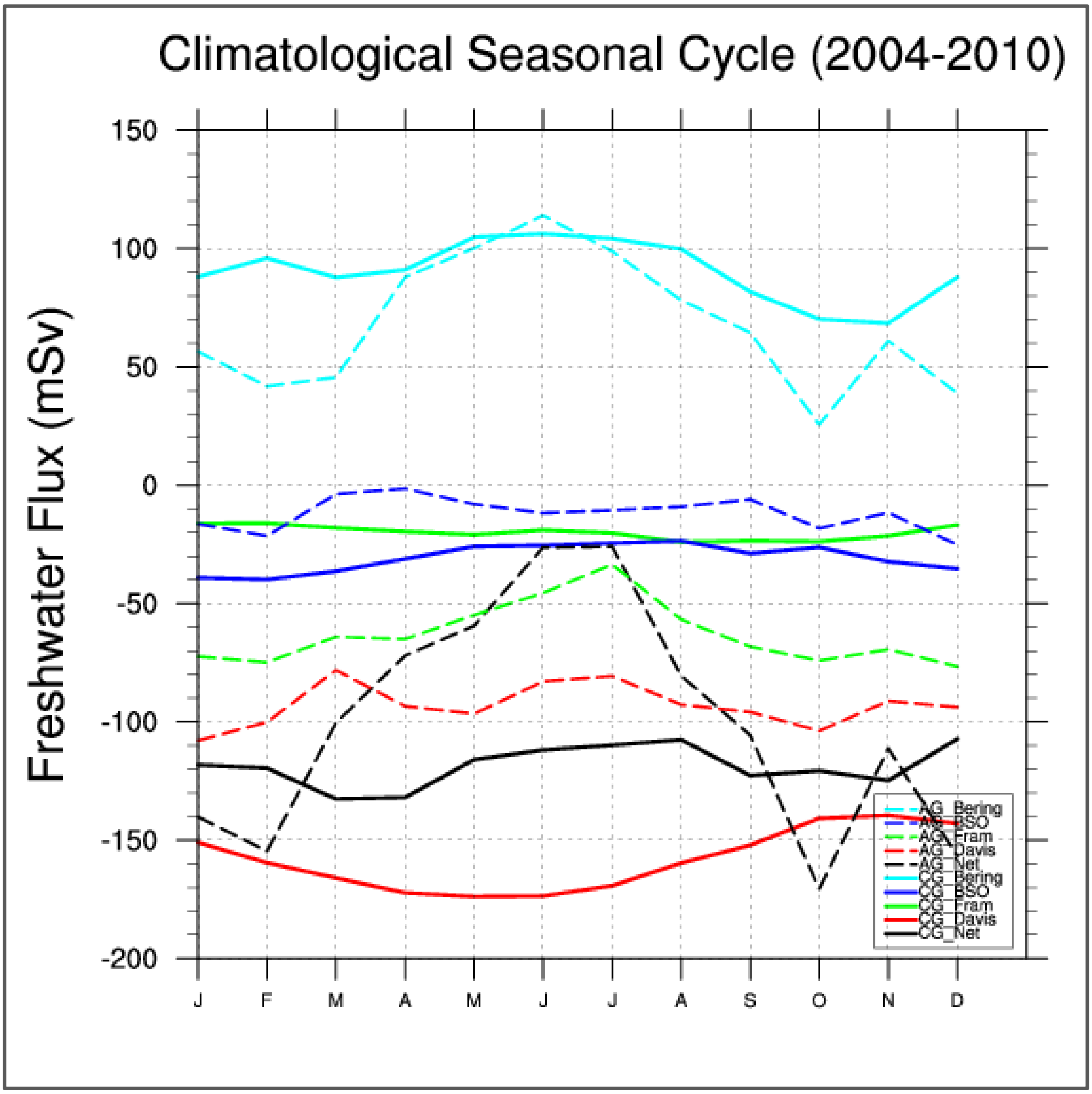

Figure 41: Seasonal cycle of the freshwater transports obtained from C-GLORSv5 (solid lines) and ARCGATE (dashed lines), calculated for the period 10/2004 – 05/2010. Davis Strait is plotted in red, Fram Strait in green, Bering Strait is coloured in cyan and BSO is shown in blue. Net transports are also plotted in black. Units: mSv

Concerning the comparison of the climatologies of C-GLORSv5 and ARCGATE in Figure 41, the situation is a bit different. While BSO match is still good, albeit with little offset, Bering Strait transports only agree very well during summer months. During the colder season, differences up to 50 *mSv* can be found. Better agreement during summer is also present for Fram Strait transports. Generally, the degree of conformity between observation and reanalysis is low for Fram Strait. Hardly any match can be found for Davis Strait freshwater transports. The large differences in the individual straits for some parts of the year also result in a very different shape of the net-transport curve. While ARCGATE shows a high interannual variability, only minor fluctuations can be found in the reanalysis net transports.

For **Bering Strait**, Figure 40 shows good agreement over the whole period. Only minor deviations are visible, especially at the beginning of the time-series and during the colder season of the year. Regarding the average values of freshwater transports, substantial differences are visible (89,44 ± 24,78 *mSv* for C-GLORSv5 and 66,70 ± 24,99 *mSv* for ARCGATE respectively). Nevertheless, both datasets agree within their uncertainty bounds. Comparing these values with literature estimates obtained by Woodgate & Aagaard (2005) one can also find good agreement, especially for the C-GLORSv5 dataset (see Table 6). The differences in average values are also visible in the climatologies of both datasets (Fig. 41). While the ARCGATE data indicates a maximum of freshwater transports during June, C-GLORSv5 transports are constant throughout the first half of the year. The minimum in transports can be found in October for the observation-based data, while the C-GLORSv5 minimum is slightly shifted towards November. However, the ARCGATE climatology shows qualitatively good agreement with the seasonal cycle found by Woodgate (2017), although slightly different reference values were used for the literature estimates.

A good agreement between ocean reanalysis and observation-based data can also be found for **Barents Sea Opening**. It seems like the reanalysis captures the important features of BSO very well. Nevertheless, there is a constant overestimation of the freshwater transports out of the Arctic Ocean by C-GLORSv5 compared to ARCGATE. Because of this overestimation, differences in the means of both datasets can be found as well (see Table 6). Smedsrud et al. (2010) estimated the average transport of freshwater through Barents Sea Opening with -19,7 *mSv;* however, they used a higher reference salinity (35,0 *PSU*). Taking into account the difference in reference salinity, the literature values match those of both datasets very good.

Turning now towards **Fram Strait**, the differences between ARCGATE freshwater transports and the C-GLORSv5 ones are somewhat bigger. From Figure 40 it is clear to see, that there is an underestimation of the freshwater export by the reanalysis throughout the whole period. This finding is exactly the opposite of what is true for BSO. In question of mean values of the transports, C-GLORSv5 values are only one third of the ARCGATE ones for the entire period (C-GLORSv5: -18,17 ± 8,91 *mSv,* ARCGATE: -63,15 ± 19,36 *mSv).* The comparison of these values with literature estimates is hampered due to the use of different reference salinities. Nevertheless, de Steur et al. (2009) found freshwater transports via the EGC and Greenland shelf regions to be approximately -66 *mSv* (S_{ref} = 34,93 *PSU*), which is comparable with the estimates presented in this section. Comparing the seasonal cycles of ARCGATE and C-GLORSv5, hardly any agreement can be found. While the observational data shows a slight seasonality, the reanalysis derived climatology is nearly constant throughout the year.

Regarding freshwater transports through **Davis Strait**, neither qualitative nor quantitative agreements between the two datasets can be found. The freshwater export calculated from C-GLORSv5 exceeds the observation-based data at some parts of the time-series by nearly 100%. This overestimation is also present in the comparison of the average values. While ARGATE data shows a freshwater transport of -93,10 ± 23,41 *mSv*, the ocean reanalysis average transports are nearly twice as high (-157,73 ± 18,31 *mSv*). Comparing these values with literature estimates from Curry et al. (2011) one finds good agreement for the ARCGATE data. This is also true for the comparison of the seasonal cycles. There is a good qualitative and quantitative match between the literature values and ARCGATE, while the C-GLORSv5 climatology shows far higher export rates during the whole year.

Table 6: Average values for C-GLORSv5, ARCGATE and literature for the different straits. Additionally, correlation coefficient (R) and STDDEV are computed. All average values (AVG) and STDDEV are in *mSv*.

	C-GLORSV5 (AVG)	ARCGATE (AVG)	R	STDDEV (DIFF)	LITERATURE (AVG)
Davis Strait	-157,73 ± 18,31	-93,10 ± 23,41	-0,00	33,54	-116 ± 41
Fram Strait	-18,17 ± 8,91	-63,15 ± 19,36	0,07	23,48	-66
BSO	-31,31 ± 7,44	-12,69 ± 10,59	0,61	10,30	-19,7
Bering Strait	89,44 ± 24,78	66,70 ± 24,99	0,82	20,13	80 ± 10

3.3.1.2. ORAS5

In this section the differences and similarities in question of freshwater transports between ORAS5 and ARCGATE will be highlighted. Like it is true for C-GLORSv5, no general degree of agreement can be detected. Instead, every gateway has to be treated separately (Fig. 42). Regarding the net freshwater transports slight improvements, compared to C-GLORSv5, can be found (-111,63 ± 44,46 *mSv* (ORAS5) and -102,22 ± 39,06 *mSv* (ARCGATE)). Generally, Figure 42 shows good agreement for Bering Strait and BSO and still poor agreement for Fram and Davis Strait. This is also true for the climatologies of the different straits. Compared to C-GLORSv5, improvements can be found especially for Bering Strait and Davis Strait, although the match for Davis Strait is still very low. Improvements are also visible for the net freshwater transports, nevertheless, the agreement with observations remains low.

Table 7: Average values for ORAS5, ARCGATE and literature for the different straits. Additionally, correlation coefficient (R) and STDDEV are computed. All average values (AVG) and STDDEV are in *mSv*.

	ORAS5 (AVG)	ARCGATE (AVG)	R	STDDEV (DIFF)	LITERATURE (AVG)
Davis Strait	-142,24 ± 15,09	-93,10 ± 23,41	0,12	31,87	-116 ± 41
Fram Strait	-17,51 ± 9,58	-63,15 ± 19,36	0,30	21,17	-66
BSO	-37,18 ± 8,34	-12,69 ± 10,59	0,64	10,36	-19,7
Bering Strait	85,30 ± 29,92	66,70 ± 24,99	0,91	15,23	80 ± 10

Comparing ORAS5 freshwater transports through **Bering Strait** with the other data sources, some differences can be found compared to ARCGATE and C-GLORSv5 as well. Although the average values of ORAS5 transports match those of ARCGATE better, there is still a difference of 20 *mSv*. This difference arises mainly during late summer and fall, when ARCGATE transports decrease much faster than the simulated ones of ORAS5 (Fig. 43). Nevertheless, the calculated transports agree within their uncertainty range. Regarding the temporal patterns, ORAS5 shows very good agreement with ARCGATE (r = 0,91). The comparison with literature values reveals a better match for ORAS5 than for ARCGATE; however, all transports are in accordance with literature values.

Hardly any change compared to the C-GLORSv5 time-series can be seen for **Barents Sea Opening**. While the temporal variations within the time-series are captured well by the ocean reanalysis (r = 0,64), there is continuous overestimation of the freshwater export through BSO. Compared to the C-GLORSv5 derived mean values, ORAS5 simulates slightly more freshwater transport out of the Arctic Ocean (-31,31 ± 7,44 *mSv* (C-GLORSv5) compared to -37,18 ± 8,34 *mSv* (ORAS5)). Despite these differences, all datasets still agree with the literature values obtained by Smedsrud et al. (2010) within their uncertainty range. However, taking into account the higher reference salinity used in their work, better agreement with ARCGATE data is expected when using the same reference value.

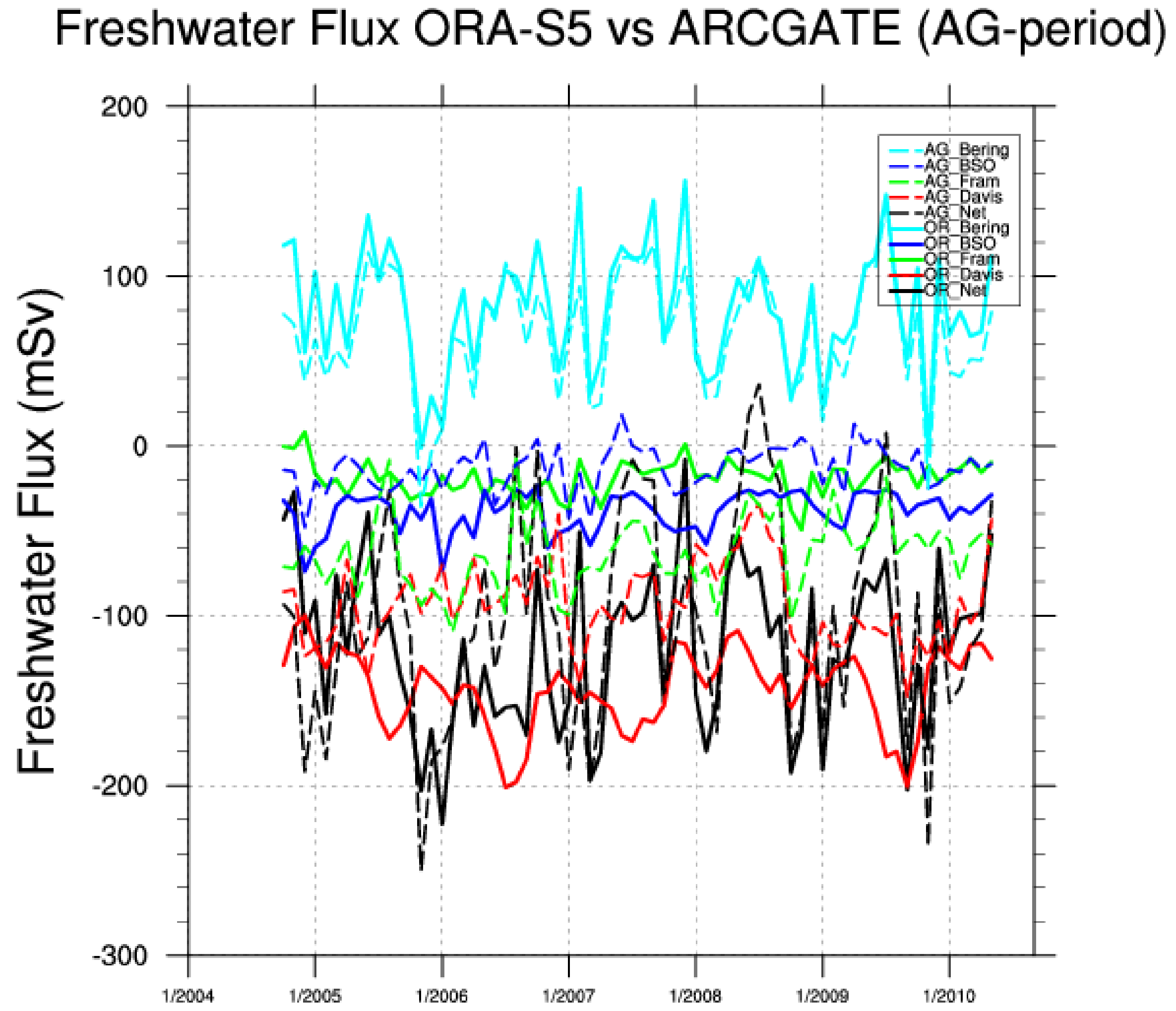

Figure 42: Freshwater transports (FW) from ORAS5 (solid lines) and ARCGATE (dashed lines) for the period 10/2004 – 05/2010. Davis Strait is plotted in red, Fram Strait in green, Bering Strait is coloured in cyan and BSO is shown in blue. Net transports are plotted in black. Units: Millisverdrup (mSv).

Freshwater transports through **Fram Strait** obtained from ORAS5 are also very similar the ones obtained from C-GLORSv5. Nevertheless, there are some improvements regarding the temporal variations. Looking at the correlation coefficient in Table 7, one can see this amendment at first sight. Concerning the 2004-2010 mean values, there is still underestimation of freshwater exports. Interestingly, the transports calculated by ORAS5 and C-GLORSv5 match within 0,5 *mSv*. The comparison with literature values is again hampered, since only values for the eastern Fram Strait are available and because of the difference in reference salinity used in the work of de Steur et al. (2009).

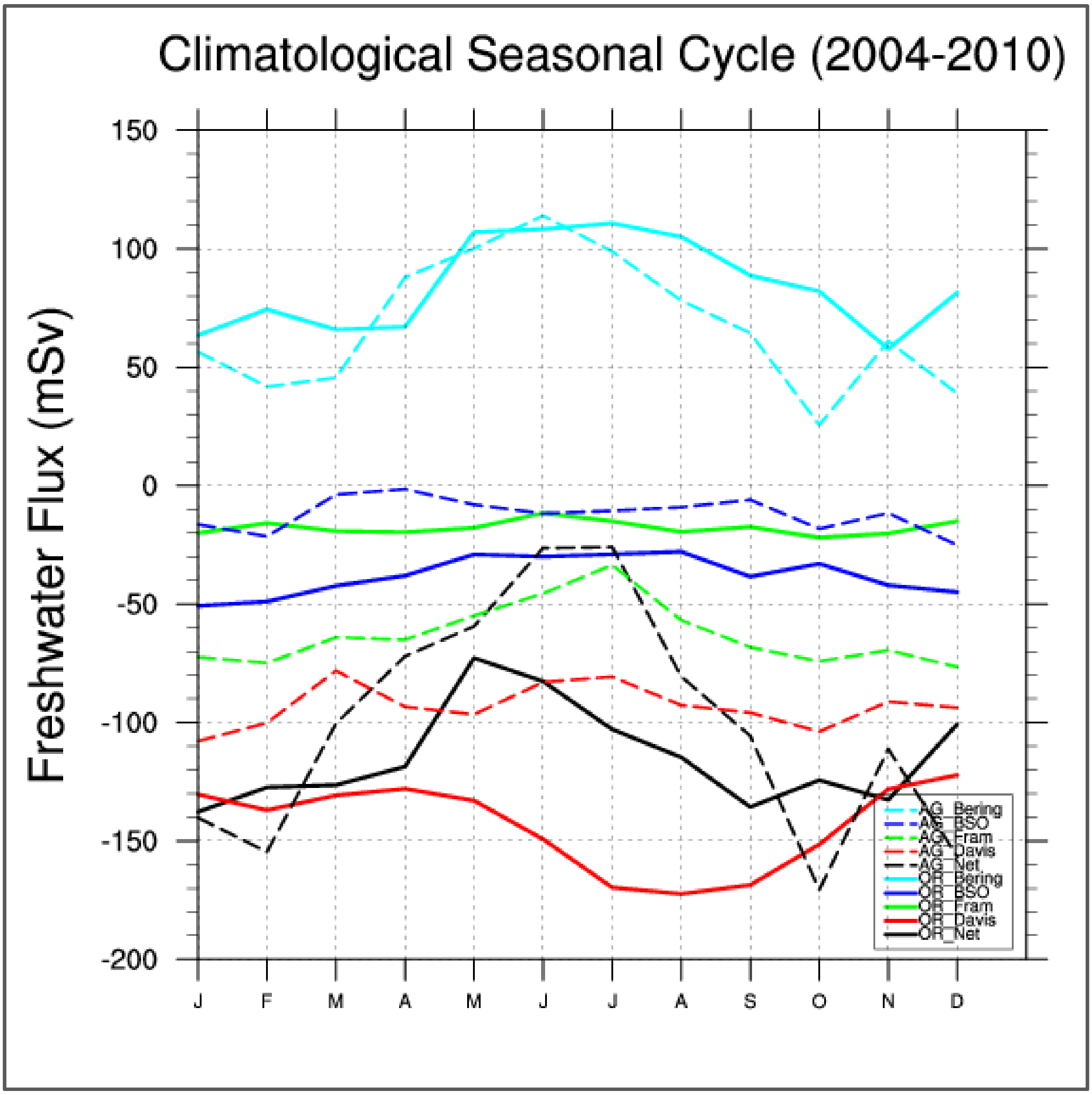

Figure 43: Seasonal cycle of the freshwater transports from ORAS5 (solid lines) and ARCGATE (dashed lines), calculated for the period 10/2004 – 05/2010. Davis Strait is plotted in red, Fram Strait in green, Bering Strait is coloured in cyan and BSO is shown in blue. Net transports are also plotted in black. Units: mSv

To complete this section, the differences in freshwater transports through **Davis Strait** are discussed in this paragraph. Although there are large differences between ORAS5 and ARCGATE in the time-series (Fig. 42) as well in the climatologies (Fig. 43), compared to C-GLORSv5 some improvements can be found. Looking at Table 7, these improvements can be seen in a better, but still very low, agreement of the mean values and slight amendments in the correlation coefficient. The literature estimates for Davis Strait obtained from Curry et al. (2011) are somewhat in the middle of both, hence matching both datasets within their uncertainty range. Again, taking into account the higher reference salinity used in this work, better agreement can be found for the ARCGATE data. Concerning the seasonal cycle, Figure 43 shows clear inter-annual variations in the ORAS5 data, while the ARCGATE transports are nearly constant throughout the year. The seasonality of the freshwater transports in ORAS5 might be caused by a wrong simulation of the velocity field in the area of WGC and the shelf regions (see section 3.1 for comparison).

3.3.2. Hovmoeller diagrams

In the following section the Hovmoeller-diagrams for freshwater transports through each of the straits are shown. In contrast to volume transport plots, the interpretation is somewhat more difficult. Positive freshwater transports can be obtained not only by transporting fresher water into the Arctic, but also by transporting salty water out of the Arctic. The same is true for negative freshwater transports through the straits.

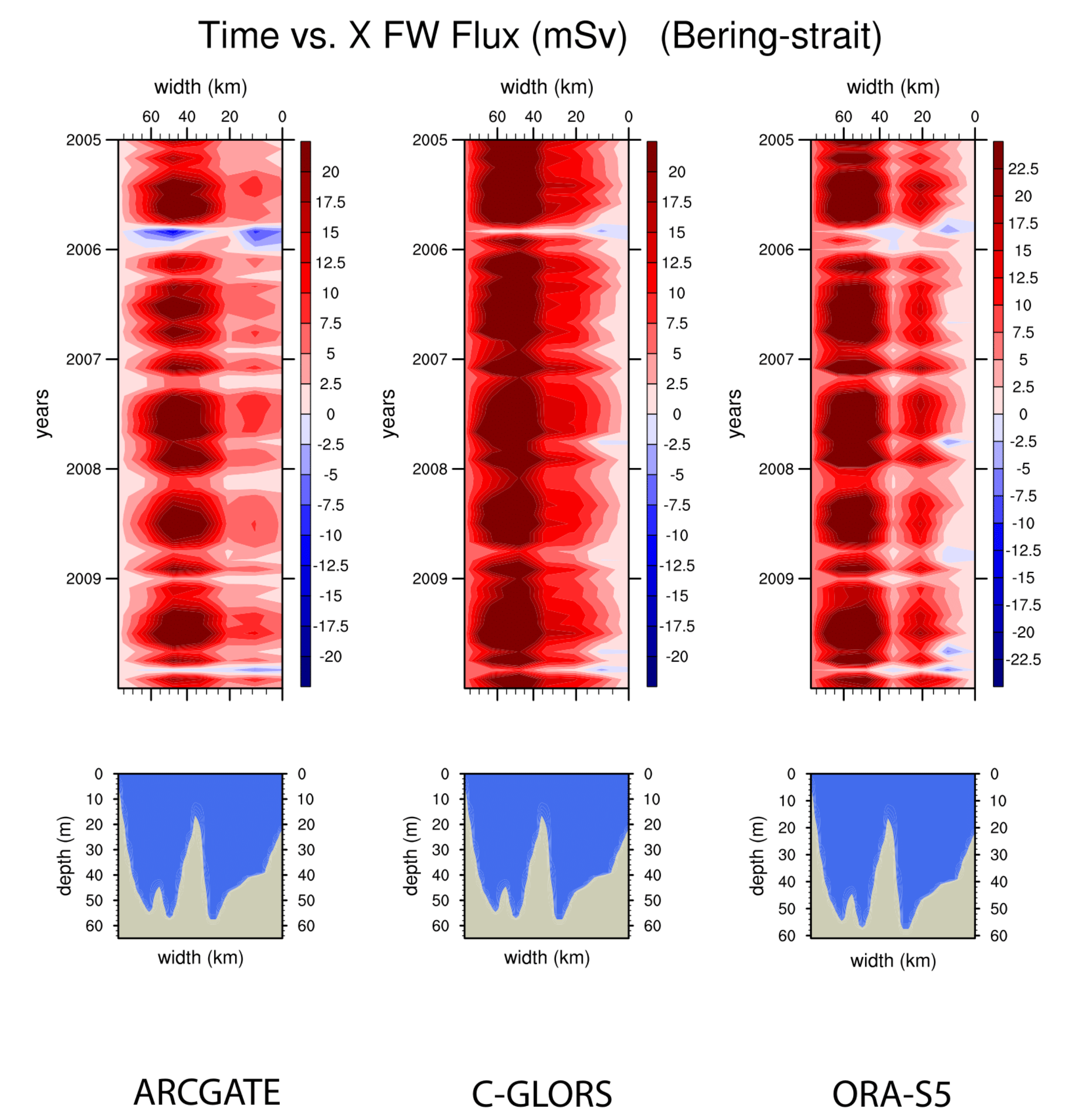

Figure 44: Time versus width Hovmoeller diagram for freshwater transports through Bering Strait. ARCGATE is shown to the left; C-GLORSv5 in the middle and ORAS5 is on the right side. In the bottom section the bathymetry of Bering Strait is plotted.

Starting with **Bering Strait**, there are only small differences between ARCGATE and both reanalysis products. The direction of the currents through Bering Strait is predominantly northward; hence, less salty waters of pacific origin are transported into the Arctic through this gateway (see Figure 44). However, there are some cases, where the transport is negative. These negative transports are caused by relative fresh water being recirculated and subsequently transported out of the Arctic Ocean. These patterns are captured by the reanalysis reasonably well.

Slight overestimations of freshwater transports can be found for C-GLORSv5 in the colder season and for ORAS5 in late summer and fall (compare seasonal cycle plots in previous section). Since this figure is very similar to the one obtained for volume transports, most of the differences between the data is due to differences in the velocity field. This is also true for the vertical distribution of the transports in Figure 45.

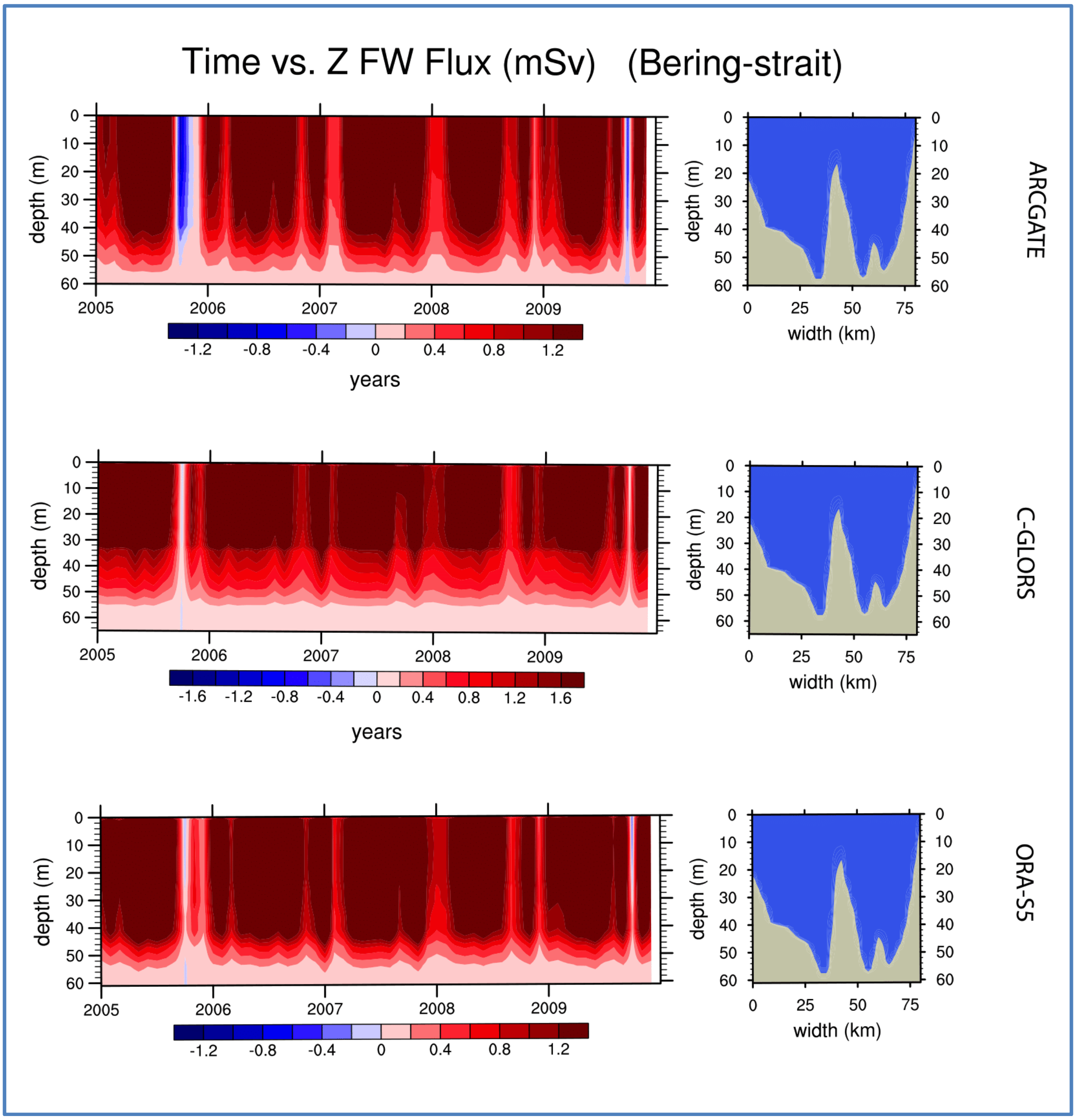

Figure 45: Time versus depth Hovmoeller diagram of freshwater transports through Bering Strait. ARCGATE is shown in the top-panel, followed by C-GLORSv5 in the middle and ORAS5 at the bottom. To the right of the plots, again the bathymetry of Bering Strait is plotted.

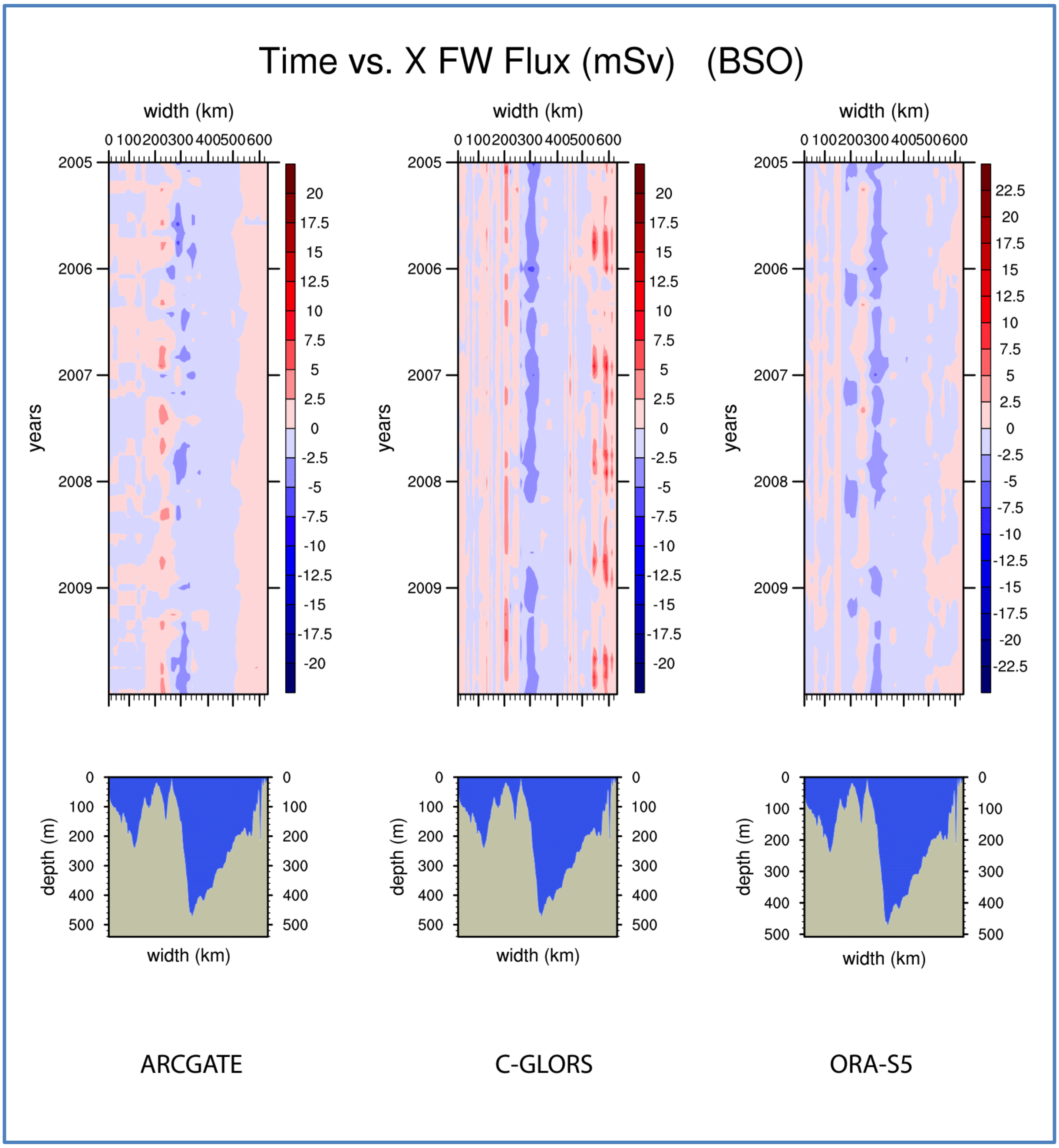

Figure 46: Time versus width Hovmoeller diagram for freshwater transports through Barents Sea Opening. ARCGATE is shown to the left; C-GLORSv5 in the middle and ORAS5 is on the right side. In the bottom section the bathymetry of BSO is plotted.

Next, the freshwater transports through **Barents Sea Opening** are examined. As already discussed in section 3.3.1, both ocean reanalyses capture freshwater transports through BSO reasonably well. Nevertheless, the overestimation of negative freshwater transport is also visible in Figure 46, showing the horizontal distribution with time. The large extent of bluish colours indicates negative freshwater transports. These transports are caused by salty Atlantic water flowing through BSO into the Arctic Ocean. The ARCGATE data as well as the C-GLORSv5 data show an additional positive branch in the area of Bear Island. Since velocities are negative in this region (compare section 3.1), the positive values arise from recirculation of salty Atlantic waters. This recirculation-pattern is missing in the ORAS5 rendering entirely, what might be an explanation for the slightly lower average values in Table 7 compared to Table 6. Further differences can be found for the Norwegian Coastal region. The red colour in the C-GLORSv5 reanalysis indicates fresh water being transported into the

Arctic. Taking into account the northward (eastward) current in this region, this feature might be explained with meltwater flowing into the Sea during spring.
A similar feature can also be observed in ORAS5 data, however, less clear. The observation-based data indicates this source of fresher water near the Norwegian Coast all year round. The plot of the vertical structure of freshwater transports through BSO also reveals some interesting differences. While ARCGATE shows positive transports in the upper layers (due to fresh coastal waters entering and salty waters near Bear Island leaving the Arctic), both reanalyses show negative transports. This is especially true for ORAS5.

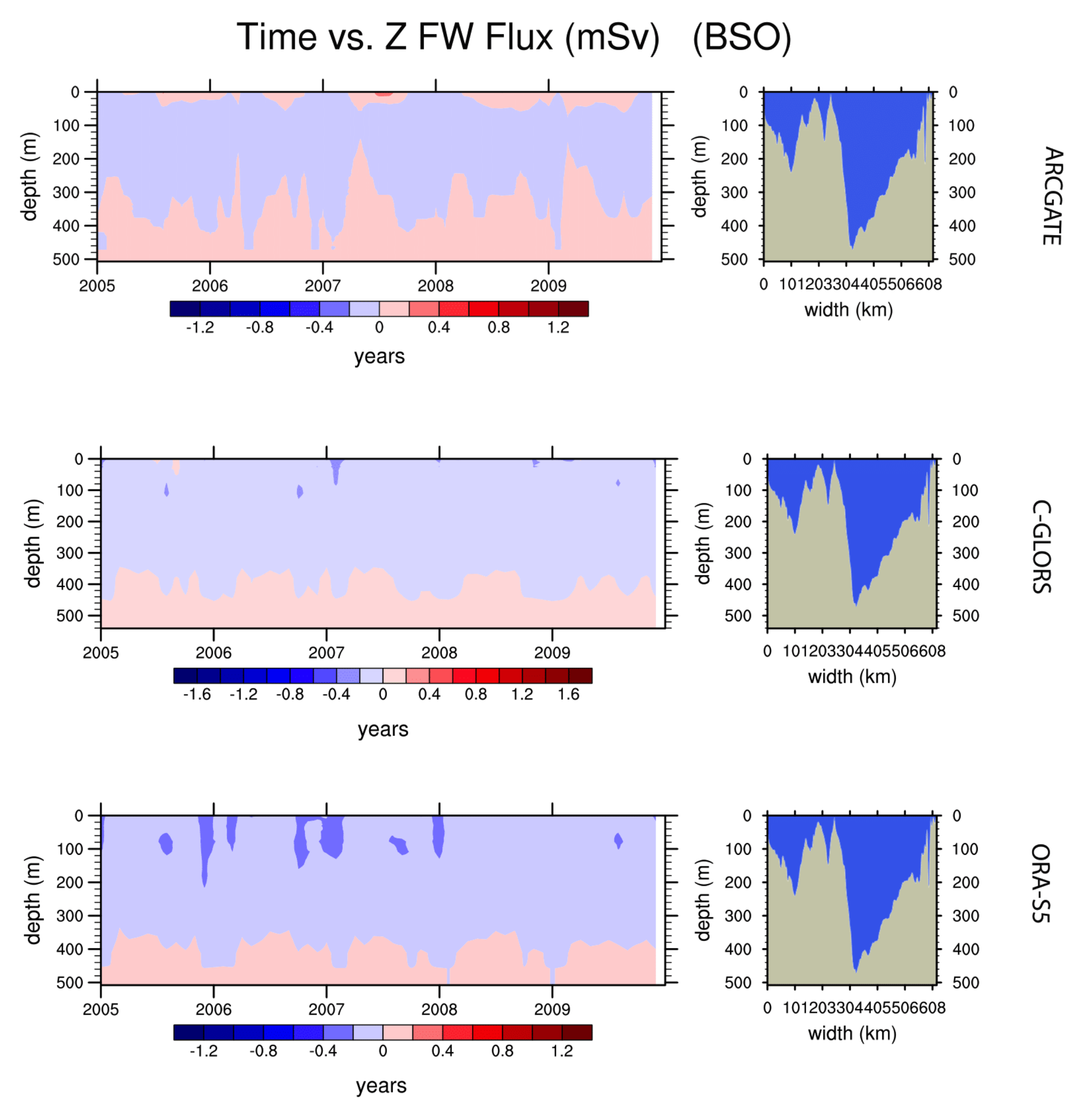

Figure 47: Time versus depth Hovmoeller diagram of freshwater transports through BSO. ARCGATE is shown in the top-panel, followed by C-GLORSv5 in the middle and ORAS5 at the bottom. To the right of the plots, again the bathymetry of BSO is plotted.

Hovmoeller diagrams for **Fram Strait** are amongst the most difficult for interpretation. Strong and at least partly opposing currents in the centre of Fram Strait make it hard to determine the correct reason for the transports in this area. Nevertheless, the coastal regions of both sides of Fram Strait show some interesting differences. Beginning on the eastern side of the channel, the transports through West Spitsbergen Current are simulated quite differently by the reanalyses. While ORAS5 shows predominant inflow of salty water near the coast, a small band of positive freshwater transports can be found in C-GLORSv5. Again, coastal waters entering the Arctic Ocean in this area may explain this positive branch.

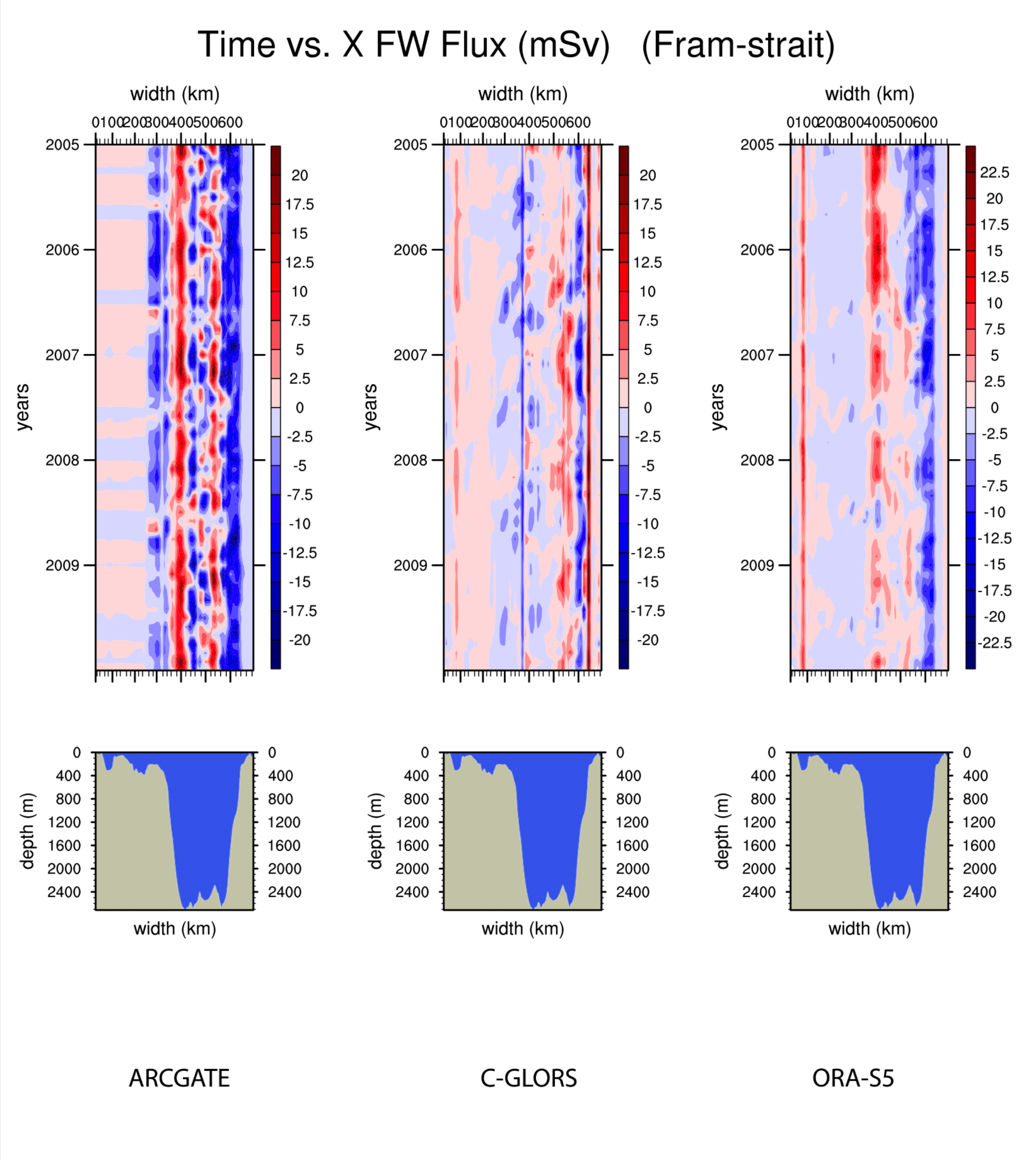

Figure 48: Time versus width Hovmoeller diagram for freshwater transports through Fram Strait. ARCGATE is shown to the left; C-GLORSv5 in the middle and ORAS5 is on the right side. In the bottom section the bathymetry of Fram Strait is plotted.

Note that there is no such signal in the observation-based dataset. Turning now towards the northern part of Fram Strait, also some differences are visible in Figure 48. Both reanalysis products, but especially the ORAS5 data, show freshwater input near Belgica Bank. Since the volume transports are positive in this area, this may be explained by meltwater or river runoff in this area, which is then transported northward. The time vs. depth visualization for Fram Strait shows also some differences and gives an insight, why both reanalyses may underestimate the freshwater export. Besides differences in magnitude of near-surface transports, there is also a positive branch in both reanalysis products, which is missing in the observations. These differences can be explained by different velocity fields (compare section 3.1), but also by differences in salinity.

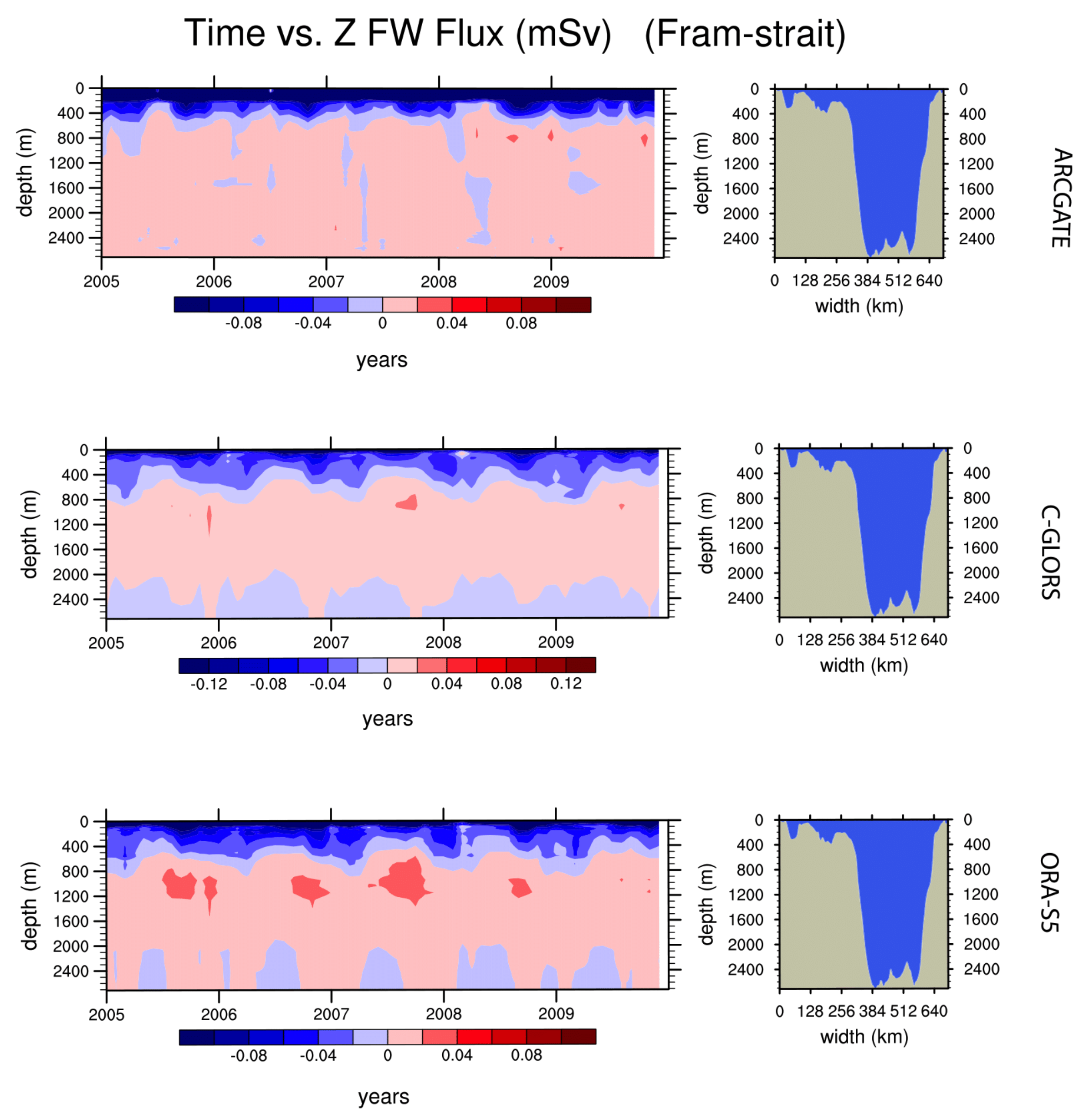

Figure 49: Time versus depth Hovmoeller diagram of freshwater transports through Fram Strait. ARCGATE is shown in the top-panel, followed by C-GLORSv5 in the middle and ORAS5 at the bottom. To the right of the plots, again the bathymetry of Fram Strait is plotted.

The last strait is again **Davis Strait**. Since the differences in the time-series plots were among the largest, the depth-integrated Hovmoeller diagrams show the probable cause of these differences. While ARCGATE data shows an inflow of salty Atlantic water in the West Greenland shelf regions and through WGC, there is no such transport in both reanalysis products. This is especially true for C-GLORSv5, which simulates large amount of freshwater leaving the Arctic in this area. ORAS5 freshwater transports are somewhat better, but have also deficits in simulating the correct freshwater transport.

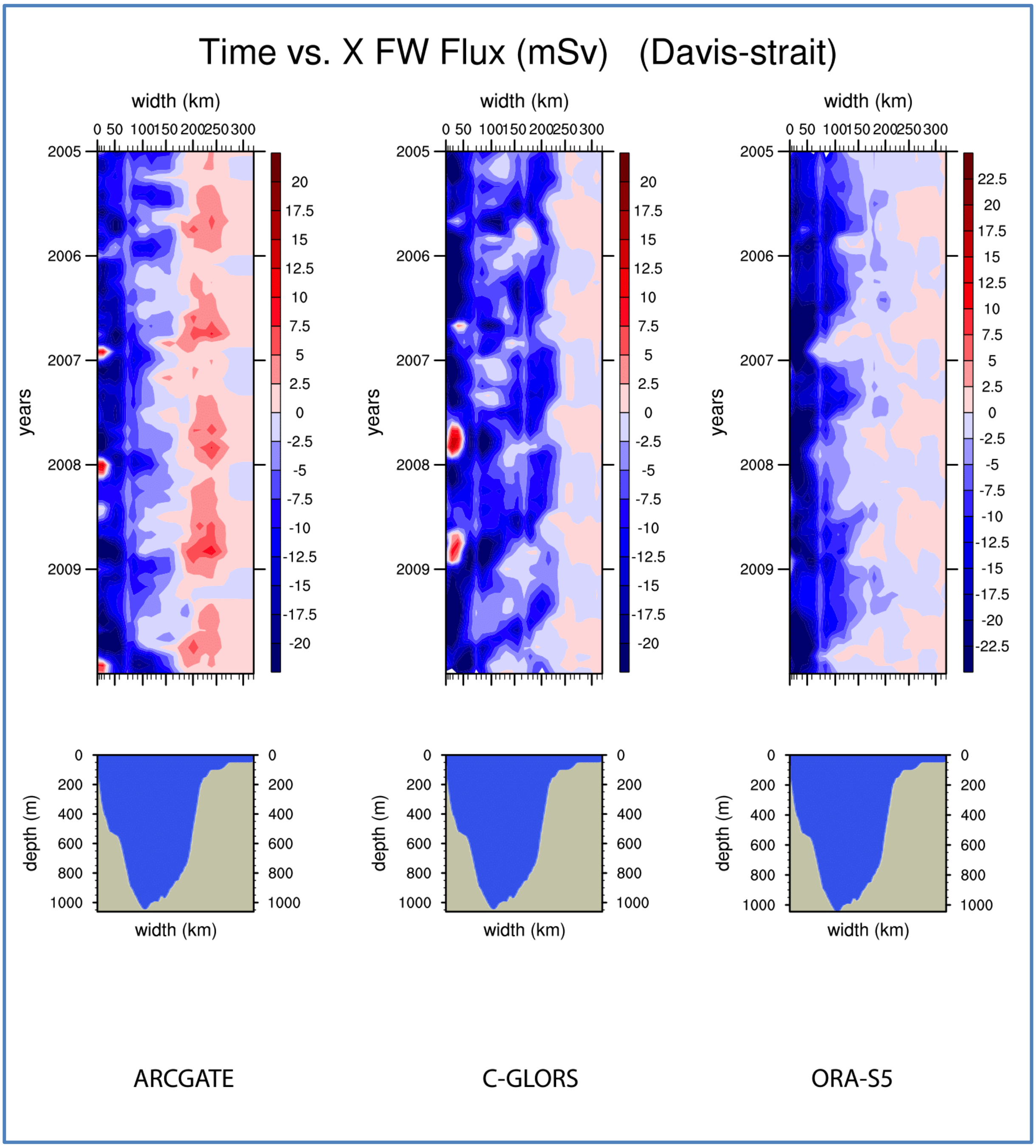

Figure 50: Time versus width Hovmoeller diagram for freshwater transports through Davis Strait. ARCGATE is shown to the left; C-GLORSv5 in the middle and ORAS5 is on the right side. In the bottom section the bathymetry of Davis Strait is plotted.

Only small differences can be seen from the vertical visualization. The negative transports are much more prominent in the reanalyses, what can be explained with the non-existing northward transport of freshwater on the eastern side of Davis Strait.

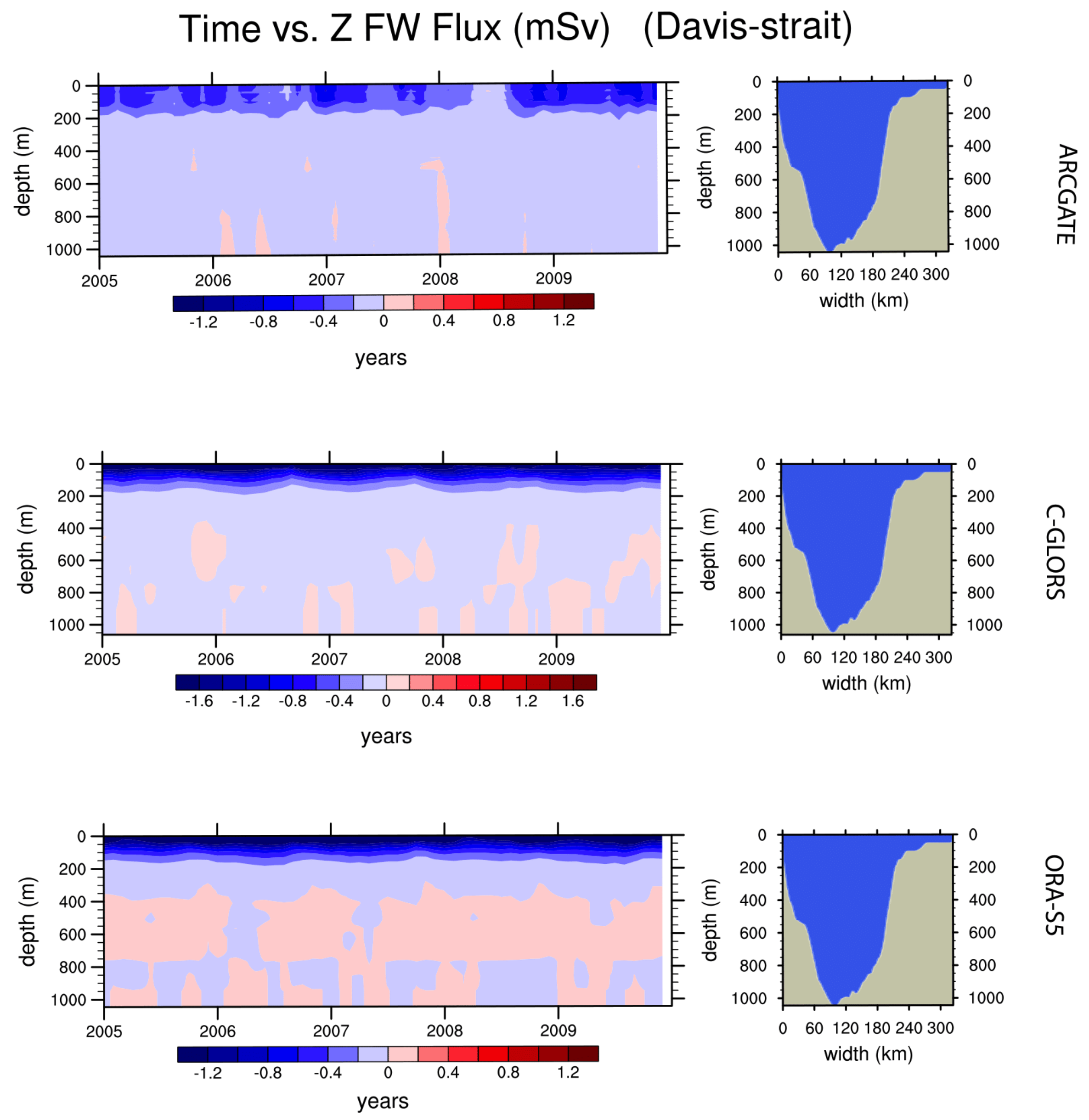

Figure 51: Time versus depth Hovmoeller diagram of freshwater transports through Davis Strait. ARCGATE is shown in the top-panel, followed by C-GLORSv5 in the middle and ORAS5 at the bottom. To the right of the plots, again the bathymetry of Davis Strait is plotted.

3.4. Diagnostics

This section is meant to give some additional information about the characteristics of the different data-sources.
By looking at the different time-series plots for the straits, it becomes obvious, that the values have a high variability between the single months. This is not only true for the ARCGATE data, but also, in alleviated form, for both reanalyses. To investigate this problem, periodograms of each of the data´s volume transports were created. These plots reveal some interesting facts. From Figure 52 one can see, that there are two peaks in the ARGATE time-series. While the first peak can be explained with the seasonality of the transports, the second one is due to high frequency noise in the dataset. This phenomenon is much more present in the ARCGATE data because of its method of compensation for the conservation of volume within the Arctic domain. This method is applied for each month separately, which is believed to cause these fluctuations. Figure 52 shows the compensation of Davis Strait inflow by the other straits for each month.

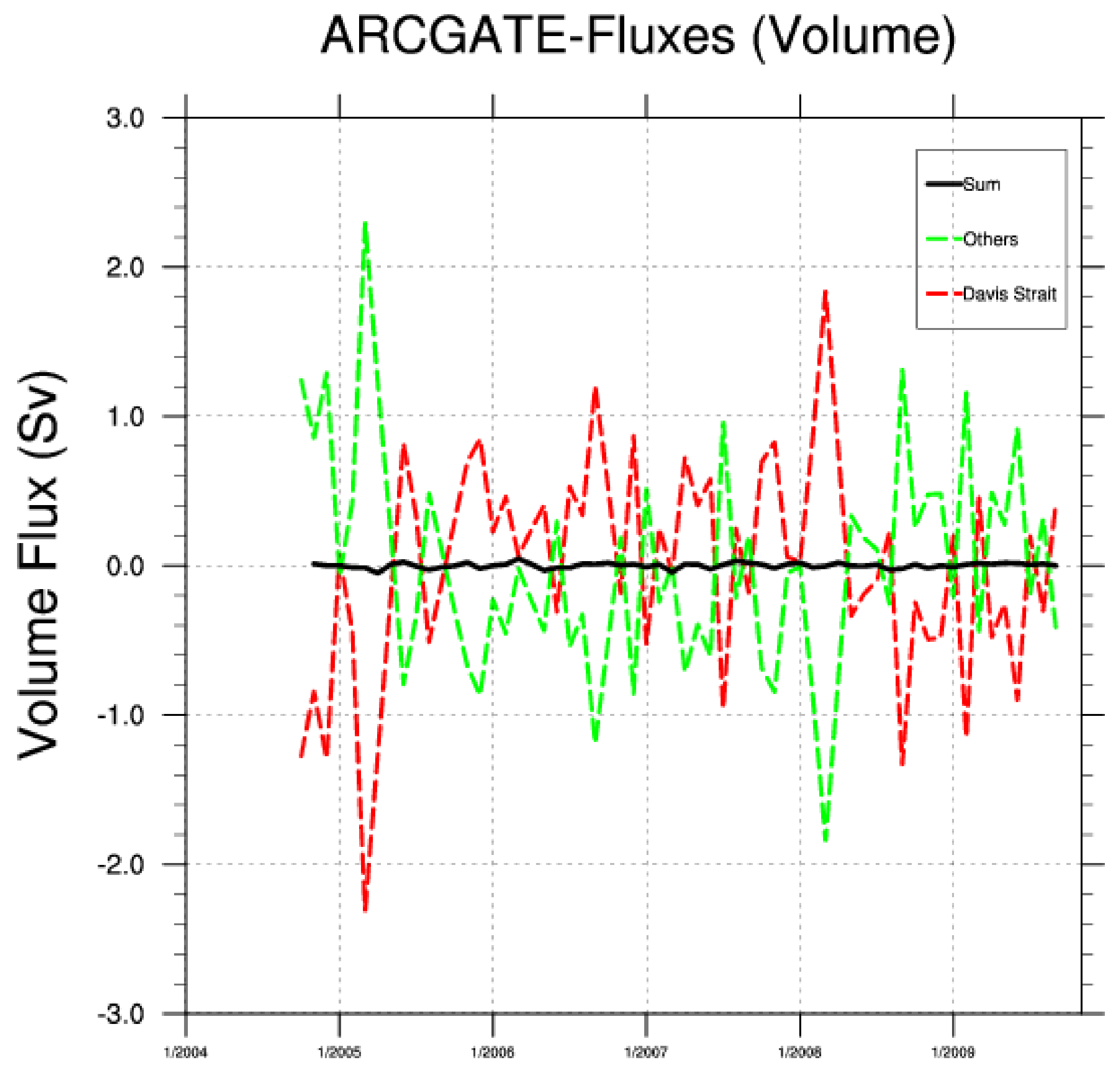

Figure 52: Conservation of Volume by the ARCGATE model.

The high frequency noise is also present for both reanalyses, although it is only relevant for BSO. Figure 53 shows Periodograms for all three datasets.

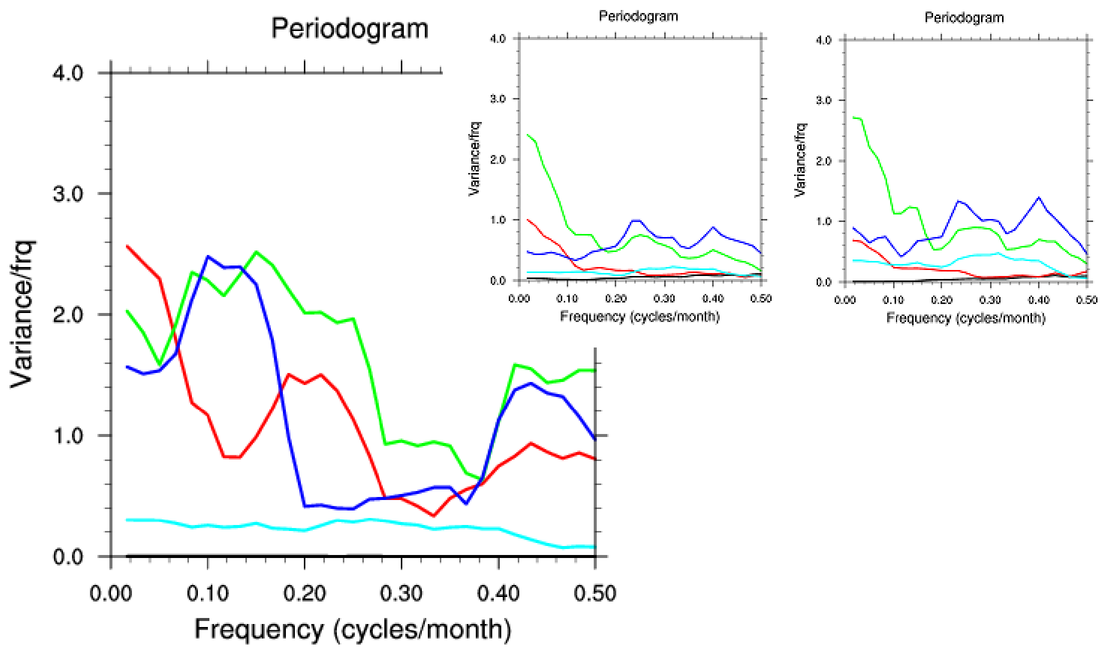

Figure 53: Periodograms for ARCGATE (left) and both reanalysis (C-GLORSv5 in the middle, ORAS5 to the right). The colours of the straits are the same like in the time-series plots – Davis Strait red, BSO blue, Fram Strait green and Bering Strait cyan.

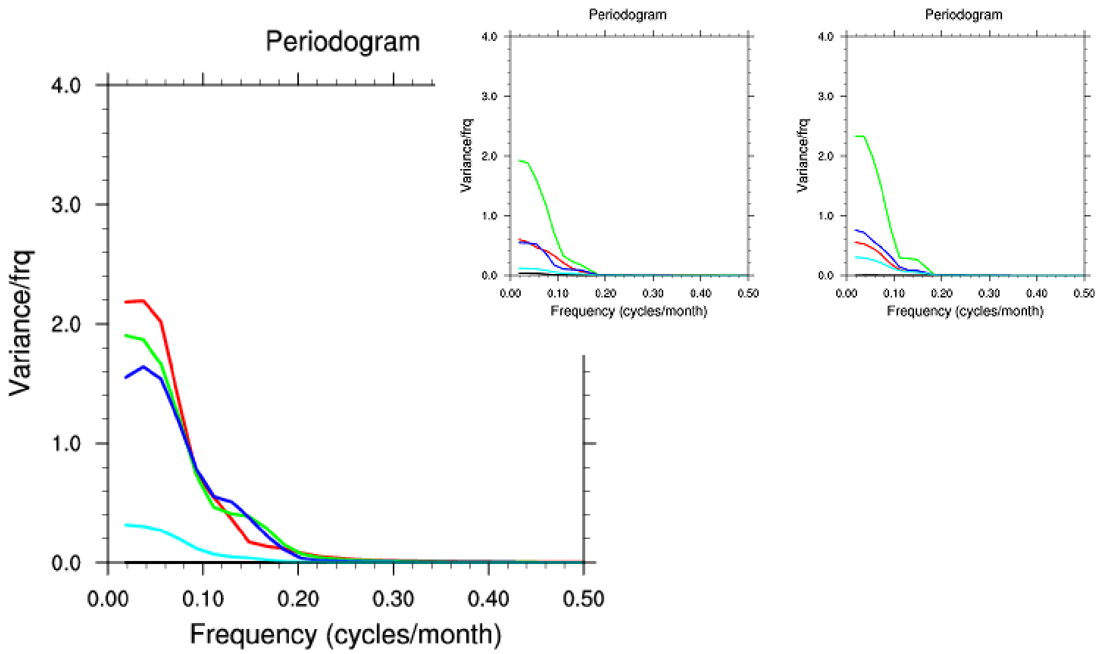

Figure 54: Periodograms for ARCGATE (left) and both reanalysis (C-GLORSv5 in the middle, ORAS5 to the right) after removing the high frequency noise. The colours of the straits are the same like in the time-series plots – Davis Strait red, BSO blue, Fram Strait green and Bering Strait cyan.

Since the noise in the time-series may deteriorate the correlation coefficient between the ARCGATE data and the reanalyses (see Tables in sections 3.1 to 3.3), it was tried to remove these traces by applying a filter on the time series. The Periodograms of all three datasets after the filtering can be seen in Figure 54.
Unfortunately, although the removal of the unwanted frequencies was successful, hardly any improvement in the correlations between the datasets could be found. In some cases, the correlation coefficient even decreased a bit.

The next diagnostic applied on the data deals with the processes within the models. This was investigated by correlating the transports through each of the straits with each other. The idea behind this approach is, to research what happens in the Arctic Ocean with water masses entering through one of the straits. Such a situation is for example realistic for a stationary high- (or low) pressure system south of Greenland. In the case of a high-pressure system, large amounts of water are forced through Davis Strait and the CAA into the Arctic Ocean (This is only one of the possibilities, the inflow can be through each of the straits).

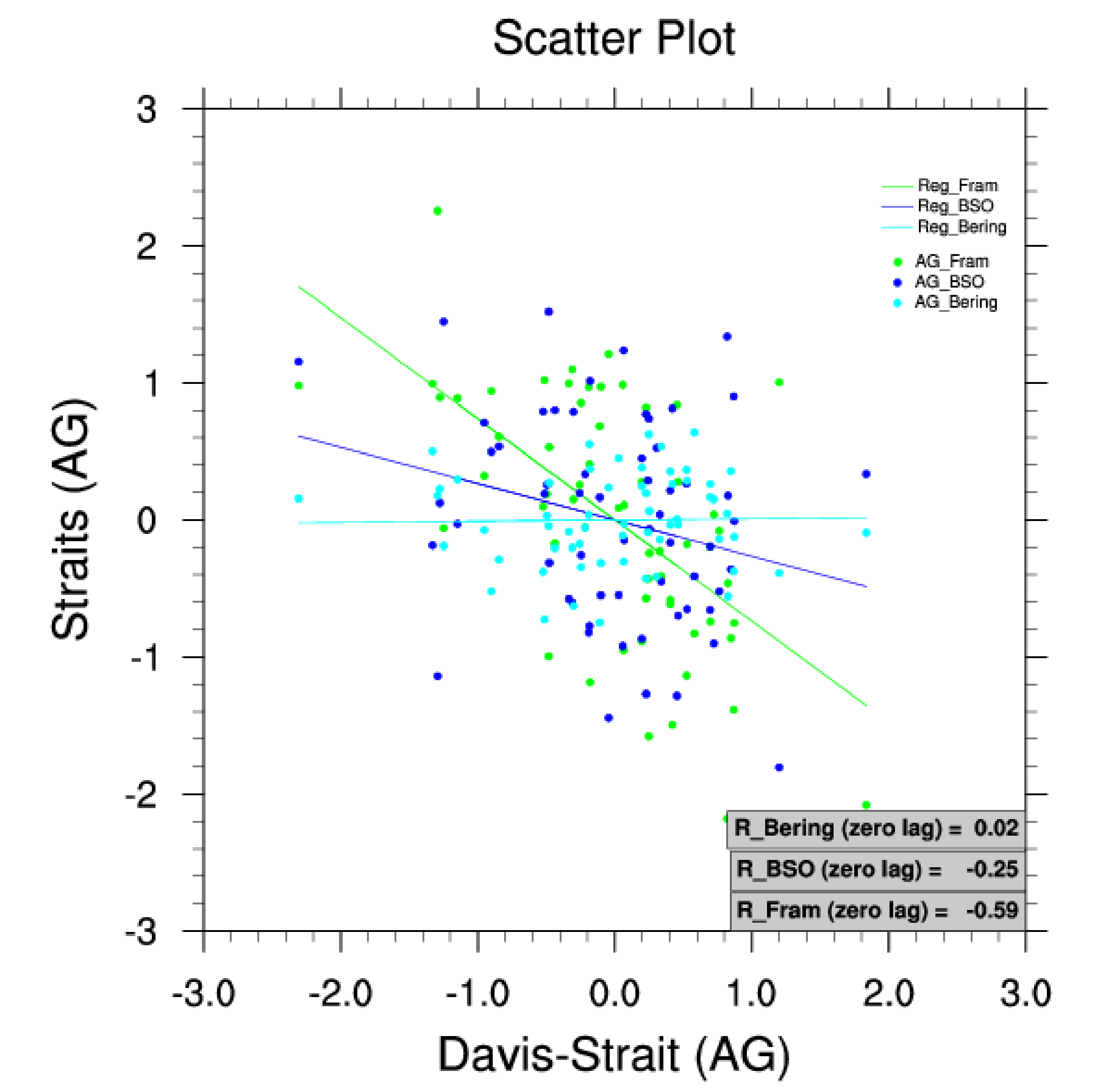

Figure 55: Scatterplot of the correlation between the individual straits for ARCGATE. The colours of the straits are the same like in the time-series plots – BSO blue, Fram Strait green and Bering Strait cyan.

Starting with the **ARCGATE** data, one can see, that inflow through Davis Strait is highly negative correlated with Fram Strait transports. This is not surprising and what is expected from literature. The inflowing waters are transported via the Beaufort Gyre and the Transpolar Drift to Fram Strait, where they leave again the Arctic domain. Since not all water leave through Fram Strait, additional signals can be found for BSO (outflow near Bear Island, see section 3.1 for comparison). Hardly any correlation is present between Davis Strait and Bering Strait. That means, that Bering Strait is not affected by Davis Strait inflow. As already mentioned the same procedure was done for the other Straits as well, but the results are not shown here.

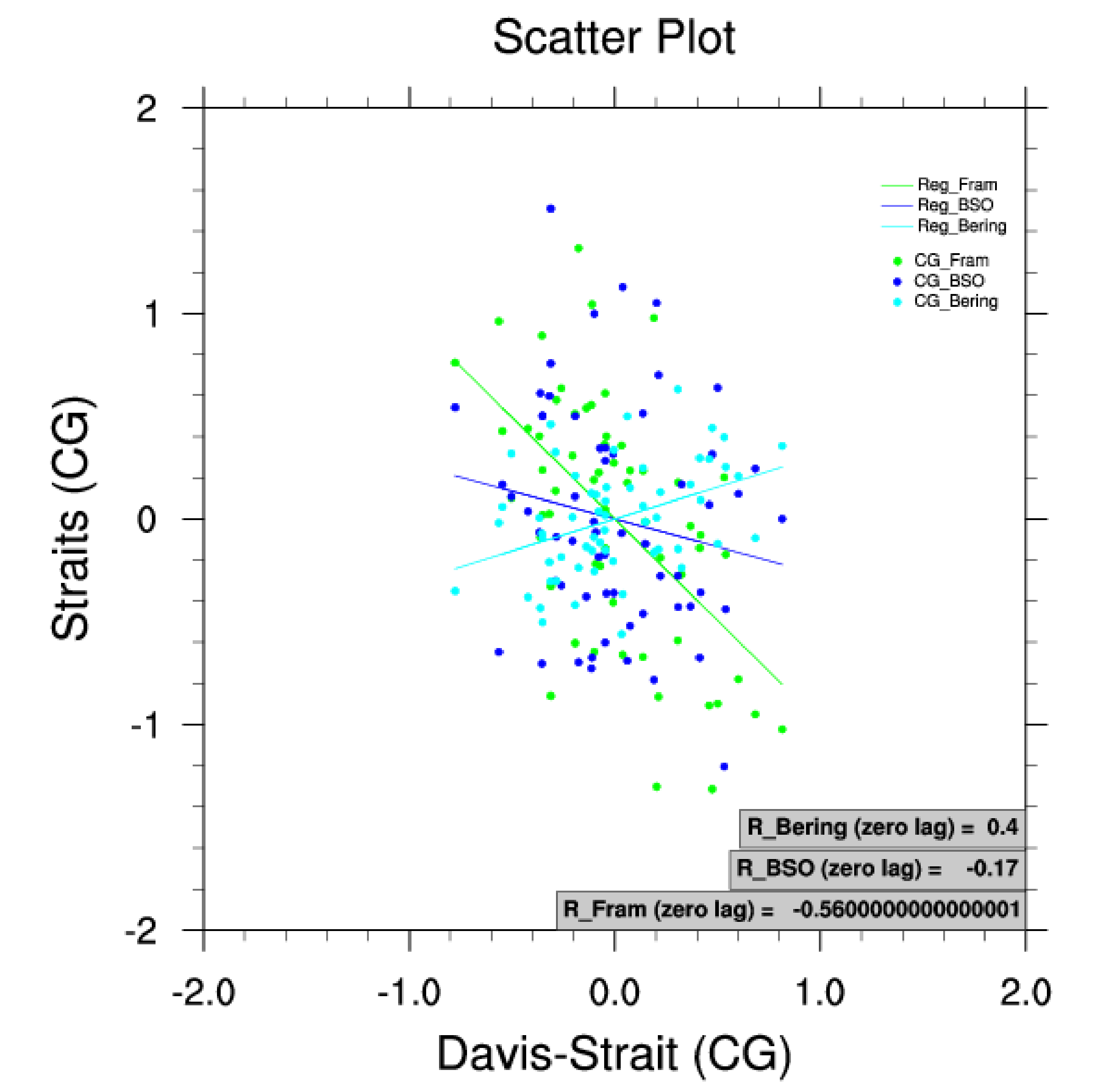

Figure 56: Scatterplot of the correlation between the individual straits for C-GLORSv5. The colours of the straits are the same like in the time-series plots – BSO blue, Fram Strait green and Bering Strait cyan.

Turning now towards the ocean reanalyses used in this thesis, one can find slightly different results, especially regarding Bering Strait. Beginning with the CMCC ocean reanalysis **C-GLORSv5**, the anticorrelation between Davis Strait and Fram Strait is nearly the same as for ARCGATE. A difference is visible for BSO, which shows a weaker anticorrelation with Davis Strait inflow in C-GLORSv5. This lower correlation reflects the patterns seen for BSO in the Hovmoeller diagrams in section 3.1. One interesting aspect of Figure 56 is the relatively high correlation with Bering Strait, which was entirely absent in the observation-based dataset. This correlation indicates, that inflow through Davis Strait is coupled with an inflow through Bering Strait. This finding is a bit surprising; nevertheless, a correlation of volume transports with the surface pressure field supports this finding (M. Mayer (2017), Personal communication).

Creating these plots for **ORAS5**, again different results can be seen (Fig. 57). Compared to the other two datasets, the negative correlation with Fram Strait is lower. At the same time the anticorrelation with Barents Sea Opening is very similar to the ARCGATE one. Comparing the outflows into the Atlantic Ocean through these two Straits from ARCGATE and ORAS5, one can see that there is weaker anticorrelation for the reanalysis product. Concerning Bering Strait, the ORAS5 data shows some correlation between Davis Strait and Bering Strait too. Although the value is lower than for C-GLORSv5, there seems to be a coupling between Davis Strait and Bering Strait as well.

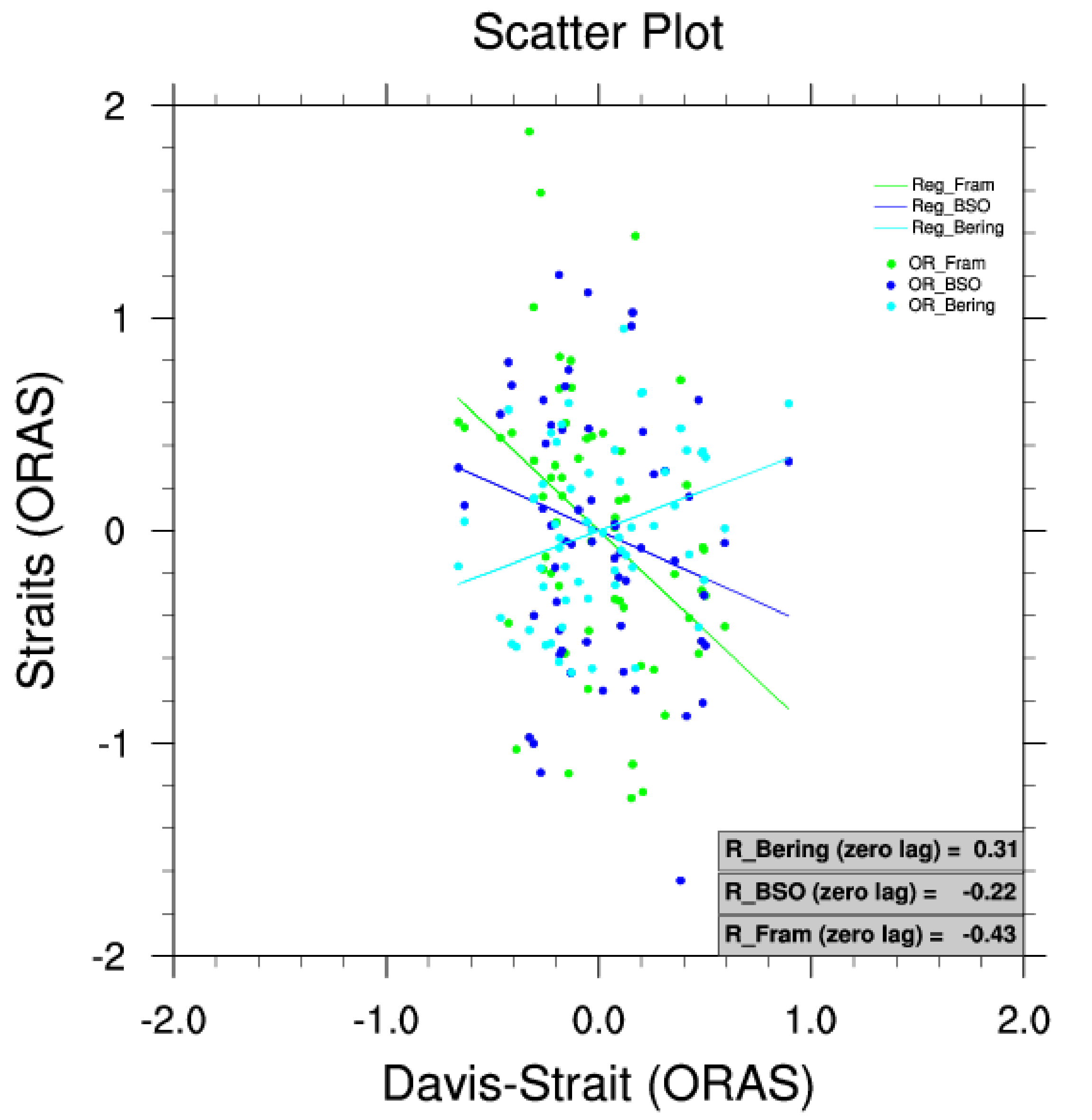

Figure 57: Scatterplot of the correlation between the individual straits for ORAS5. The colours of the straits are the same like in the time-series plots – BSO blue, Fram Strait green and Bering Strait cyan.

3.5. Reanalysis inter- Comparison

The last section in this chapter deals with a comparison of different model versions of the CMCC ocean reanalysis. As already mentioned in the chapter 2, for a limited period of time a newer version of the C-GLORS reanalysis was available. This period extend over one year, from September 2005 till August 2006. One of the major improvements compared to Version 5 is the increased vertical resolution in the newer Version 7. Since most of the other model settings are the same, these two versions are perfectly suited to investigate the influence of this higher resolution. Additionally, a control run of the Version 7 with disabled data assimilation was available for this comparison. To compare the different versions, time-series plots for volume and heat transports were created with the ARCGATE data as reference.

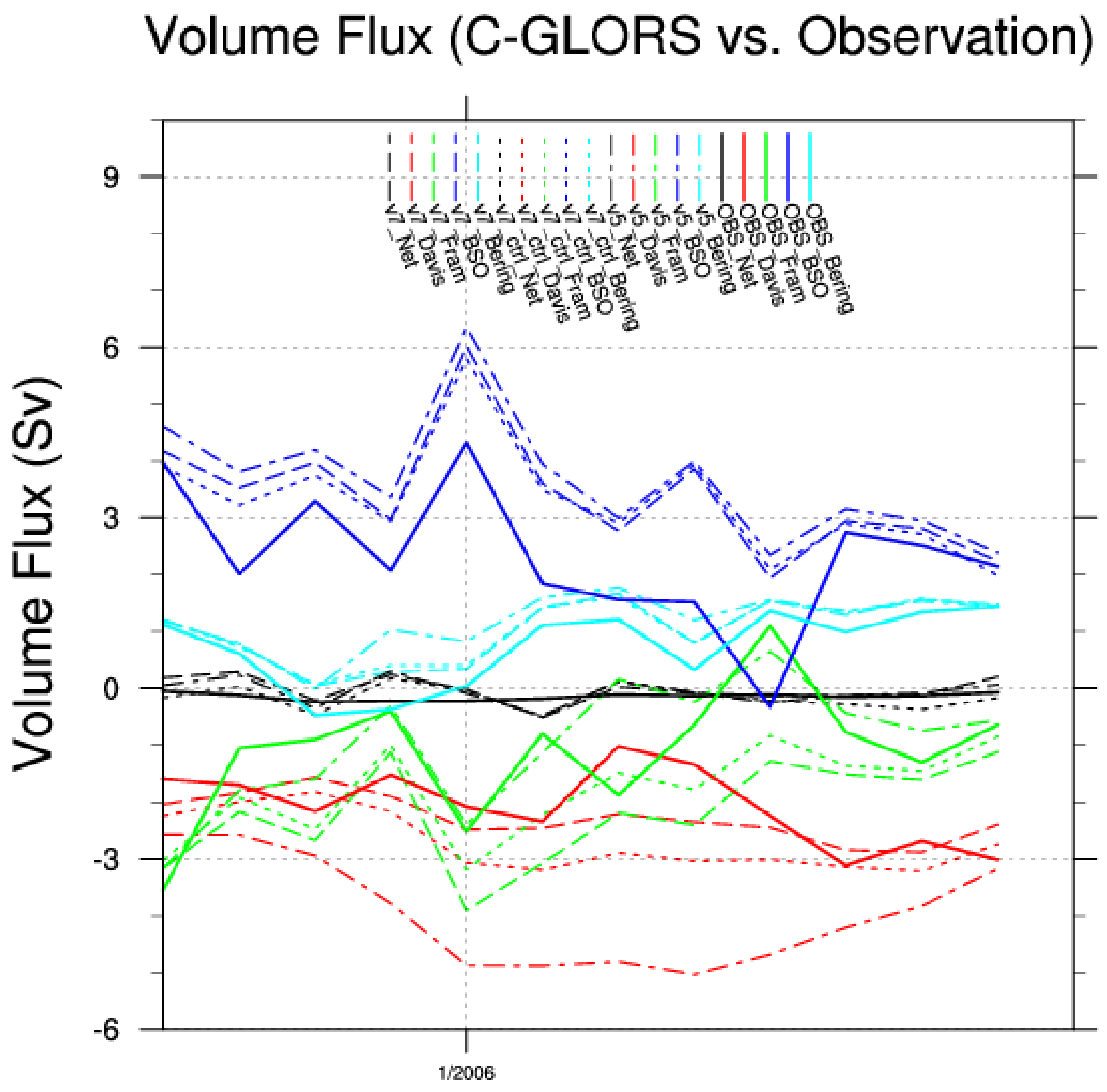

Figure 58: Comparison of the different model version of C-GLORS for a 09/2005 – 08/2006 period (Volume transports). Davis Strait is shown in red, BSO blue, Fram Strait green and Bering Strait cyan. (M Pietschnig, et al., 2017)

Starting with volume transport time-series, no clear conclusion can be drawn for the impact of higher resolution and data assimilation (Fig. 58). Although clear improvements are visible for Davis Strait, deterioration can be found for Fram Strait. For the other straits, the deviations among the models are very small and negligible. The improvement of Davis Strait volume transport might be explained with more vertical levels in the upper part of the ocean. With this increased resolution, it is possible to capture the flows over the West Greenland shelf region and through the WGC much better than in the previous version 5. The worsening in Fram Strait transports compared to ARCGATE is somewhat puzzling, since this strait is characterised by its huge depth (a higher vertical resolution in the upper layers should not have large influence on the total transport).

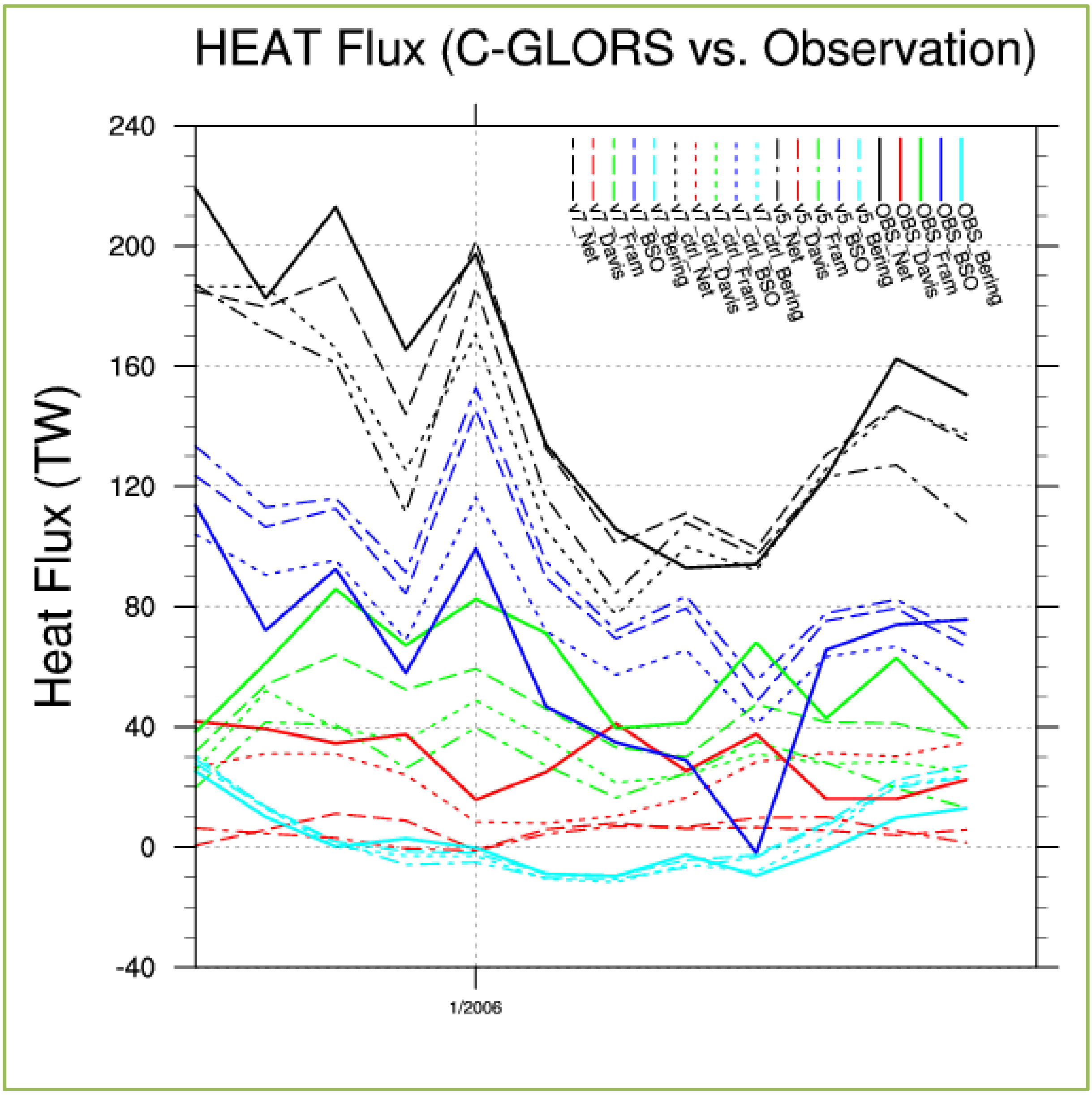

Figure 59: Comparison of the different model version of C-GLORS for a 09/2005 – 08/2006 period (Heat transports). Davis Strait is shown in red, BSO blue, Fram Strait green and Bering Strait cyan. (M Pietschnig et al., 2017)

Regarding heat transports through the straits, this comparison reveals also some interesting information (Fig. 59). Starting with Bering Strait, hardly any differences can be seen. This is not true for the other straits. For Davis Strait for example, a slight improvement of heat transports can be seen for the version 7 of C-GLORS. Interestingly, the best match with the ARCGATE-derived heat transports is obtained from C-GLORSv7-ctrl, which has no data assimilation. The pattern can be found for Barents Sea Opening, but with very good match of C-GLORSv7-ctrl with ARCGATE for large parts of the time-series. Fram Strait transports also show some improvements in the newer version. In fact, the transports through this strait are as one would them expect to be. Version 7 shows the best match, followed by C-GLORSv7-ctrl and C-GLORSv5. The comparison for the models regarding freshwater transport is also very interesting. Starting with Bering Strait, one can see, that the control run of C-GLORSv7 matches best with the observations. This is somehow surprising, since this run does not assimilate salinity measurements and was therefore expected to perform worst. The largest disagreements can be found for C-GLORSv5, but with only small offset to C-GLORSv7 (Fig. 60). A similar pattern can be seen for BSO and Davis Strait too, only for Fram Strait freshwater transports the high resolution and assimilating C-GLORSv7 yields the best results compared to ARCGATE. Furthermore, it is interesting to see, that a higher vertical resolution accounts for only small improvements (e.g. in shallow water). The biggest improvements are due to the absence of data assimilation in the C-GLORSv7 control run.

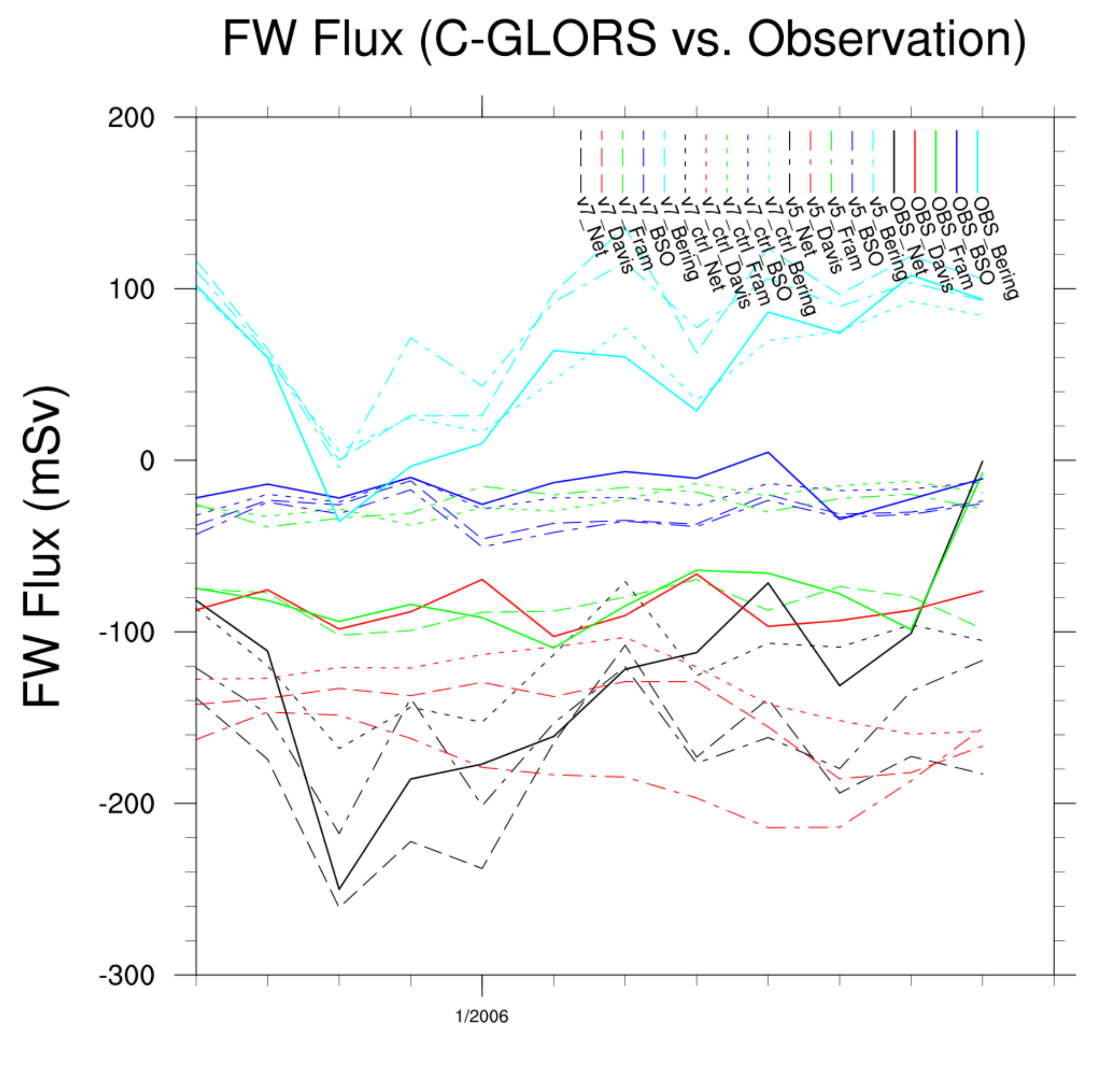

Figure 60: Comparison of the different model version of C-GLORS for a 09/2005 – 08/2006 period (FW transports). Davis Strait is shown in red, BSO blue, Fram Strait green and Bering Strait cyan.

4. Conclusion

In this last chapter of this thesis, the results obtained and discussed in chapter 3 are summarized and a conclusion on the reliability of ocean reanalysis for the Arctic domain will be given. A high reliability is desirable, especially for evaluating coupled volume, heat and freshwater budgets for the Arctic domain.

The transports obtained by both ocean reanalysis (C-GLORSv5 and ORAS5) match those of ARCGATE reasonably well. Nevertheless, it should be pointed out again, that also the observation-based data should not be viewed as truth, since there are large uncertainties in this data set as well. This blurring arises from uncertainties and spatial gaps in the measurements and from possible errors due to spatial and temporal interpolation. However, the net transports of volume, heat and freshwater of both reanalysis agree reasonably well with the observation-based estimates (Table 8).

Table 8: Average values of volume, heat and freshwater transport for ARCGATE, C-GLORSv5, C-GLORSv7 and ORAS5. Values for C-GLORSv7 cover only a one-year period (09/2005-08-2006)! Average values for volume transport are in *Sv*, those for heat transports are in *TW* and freshwater transports are in *mSv*.

	ARCGATE (AVG)	C-GLORSV5 (AVG)	C-GLORSV7 (AVG)	ORAS5 (AVG)
Vol transport (*Sv*)	-0,14 ± 0,02	-0,10 ± 0,16	-0,02±0,24	-0,14 ± 0,14
HT transport (*TW*)	154,31 ± 24,05	114,81 ± 20,74	139,57±32,77	133,76 ± 21,74
FW transport (*mSv*)	-102,22 ± 44,63	-117,77 ± 39,06	-166,40±50,35	-111,63 ± 44,46

Despite this overall good agreement between reanalysis and observation-based data, differences in the individual straits may hamper an effective closure of the budget terms in the Arctic. A method to deal with these discrepancies would be the incorporation of the differences as uncertainties in the transports. The largest mismatch between observations and reanalysis output can be found in Davis Strait and Fram Strait. Due to differences in the velocity fields, these discrepancies arise not only in the volume transports, but also in heat and freshwater transport time-series. With the use of Hovmoeller diagrams it was possible to detect the source of the mismatch. For example for Davis Strait, both reanalysis struggle to capture the flow through the WGC and the adjacent shelf regions. Since this flow is observed to be northward, an important inflow is missing or only partly present in the ocean reanalysis. An increased vertical resolution (ORAS5) improved the patterns for all three transports, but still major differences between the datasets exist. For Fram Strait also differences in the velocity structure may explain most of the discrepancies between the used datasets. An example is Belgica Bank. While reanalysis currents are northward on the northern end of the shelf, ARCGATE shows no indication of such currents. Since both reanalysis are only partly eddy resolving, also in the middle of Fram Strait bigger differences in the flow pattern can be observed.
Regarding the discrepancies in Barents Sea Opening similar reasons can be found. Both transports - heat and freshwater – are overestimated by the reanalysis compared to the observation-based data. The main sources of this mismatch are again different velocity patterns in the area of Bear Island. Especially for the freshwater transport an additional source of error may be the coastal meltwater, which are transported with the currents.

For Bering Strait, the differences are relatively small, particularly for volume and heat transports. Most of the differences arise from the velocity structures through the straits but also minor differences in the temperature field give rise to slightly different heat transport time-series. For freshwater transport the discrepancies are somewhat bigger, at least for C-GLORSv5. The ORAS5 freshwater transports match those of ARCGATE reasonably well.

The largest differences across all straits can be seen for heat transports. Especially for coupled arctic energy budget evaluations, discrepancies of 40 *TW* (C-GLORSv5 vs. ARCGATE) can cause significant errors (40 TW ~ $3 W/m^2$).

To conclude, the CMCC as well as the ECMWF ocean reanalysis yield good overall agreement with the observation-based data. The main source of discrepancies seems to be the velocity field, which is not assimilated into the reanalysis. Nonetheless, the results presented in this thesis are not always straightforward to interpret. Going deeper into the model physics and assimilation schemes could possibly yield further insights, but this clearly is beyond the scope of this thesis.

Acknowledgements

This Master`s thesis has been developed at the Institute for Meteorology and Geophysics Vienna (IMGW) - University of Vienna. At the end of this work, I would like to thank all those who contributed to the success of the work.

My special thanks go to Prof. Leopold Haimberger and Dr. Michael Mayer for the expert supervision of this work. They always guided me with scientific expertise and interesting questions through this thesis.

On a personal level, I would like to thank all my friends and especially Clemens for his helpful advice and for the competition through the studies.
Further I would like to thank my family, who always gives me the courage and strength to carry on or to start with new duties. Last but not least, I would like to thank my girlfriend Angela who supported me very much and always manages to cheer me up when I encounter a problem. She always makes me smile when I am down and enriches my life in so many different ways.

References

Aguilar, E., Auer, I., Brunet, M., Peterson, T. C., & Wieringa, J. (2003). *Guidelines on climate metadata and homogenization*.
AWI. (2017). Maximizing the potential of Arctic Ocean Gateway array. Retrieved June 8, 2017, from https://www.awi.de/en/science/climate-sciences/physical-oceanography/projects/arcgate.html
Beszczynska-Möller, A., Woodgate, R. A., Lee, C. M., Melling, H., & Karcher, M. (2011). A synthesis of exchanges through the main oceanic gateways to the Arctic Ocean. *Oceanography*, *24*(3), 82–99. https://doi.org/10.5670/oceanog.2011.65
Blindheim, J. (1989). Cascading of Barents Sea bottom water into the Norwegian Sea. *Rapp. P.-v. Réun. Cons. Int. Explor. Mer*, *188*, 49–58.
Collins, S. N., James, R. S., Ray, P., Chen, K., Lassman, A., & Brownlee, J. (2013). Climate Change and Regional/Local Responses. In *Grids in Numerical Weather and Climate Models* (pp. 111–127). Melbourne: InTech. https://doi.org/10.5772/55922
Curry, B., Lee, C. M., & Petrie, B. (2011). Volume, Freshwater, and Heat Fluxes through Davis Strait. *Journal of Physical Oceanography*, *41*(3), 429–436. https://doi.org/10.1175/2010JPO4536.1
Dawson, C., & Gerritsen, M. (2013). *Computational Challenges in the Geosciences*. (M. Gerritsen, Ed.). New York: Springer.
de Steur, L., Hansen, E., Mauritzen, C., Beszczynska-Möller, A., & Fahrbach, E. (2014). Impact of recirculation on the East Greenland Current in Fram Strait: Results from moored current meter measurements between 1997 and 2009. *Deep Sea Research Part I: Oceanographic Research Papers*, *92*, 26–40. https://doi.org/10.1016/j.dsr.2014.05.018
Dee, D. P., Uppala, S. M., Simmons, A. J., Berrisford, P., Poli, P., Kobayashi, S., … Dee, D. P. (2011). The ERA-Interim reanalysis : configuration and performance of the data assimilation system, (April), 553–597. https://doi.org/10.1002/qj.828
Eakins, B. W., & Sharman, G. F. (2010). *Volumes of the World's Oceans from ETOPO1*. Boulder. Retrieved from https://ngdc.noaa.gov/mgg/global/etopo1_ocean_volumes.html
Fieg, K., Fahrbach, E., Gerdes, R., Beszczynska-Möller, A., & Schauer, U. (2010). Simulation of oceanic volume transports through Fram Strait 1995-2005. *Ocean Dynamics*, *60*(3), 491–502. https://doi.org/10.1007/s10236-010-0263-9
Finlayson, D. (2006). Davis Strait. Retrieved June 17, 2017, from http://www.thecanadianencyclopedia.ca/en/article/davis-strait/
GDAC. (2000). ARGO. Retrieved June 8, 2017, from http://www.argo.ucsd.edu/
Gouretski, V. (2017). Expendable bathythermograph (XBT). Retrieved July 5, 2017, from http://icdc.cen.uni-hamburg.de/1/daten/ocean/xbt.html
Haimberger, L. (2015). *Variability and change of arctic energy and freshwater budgets*. University of Vienna.
International Hydrgraphic Organization. (1953). Limits of Ocean and Seas, *28*(3), 38. Retrieved from http://www.iho-ohi.net/iho_pubs/standard/S-23/S23_1953.pdf
Kongsberg. (2017). Seaglider. Retrieved July 5, 2017, from https://www.km.kongsberg.com/ks/web/nokbg0240.nsf/AllWeb/EC2FF8B58CA491A4C1257B870048C78C?OpenDocument
Large, W. G., & Yeager, S. G. (2009). *Climate Dynamics*. Springer. https://doi.org/10.1007/s00382-008-0441-3
Lee, C., Curry, B., Gobat, J., Petrie, B., & Azetsu-Scott, K. (n.d.). *Davis Strait Transport and Freshwater Fluxes*. Washington.
Madec, G. (2016). NEMO Ocean Engine Handbook. Retrieved July 4, 2017, from https://www.nemo-ocean.eu/doc/

Madec, G. (2017). ORCA family: global ocean with tripolar grid. Retrieved July 4, 2017, from https://www.nemo-ocean.eu/doc/node108.html
Masina, S., Di Pietro, P., Storto, A., & Navarra, A. (2011). Global ocean re-analyses for climate applications. *Dynamics of Atmospheres and Oceans*, *52*(1–2), 341–366. https://doi.org/10.1016/j.dynatmoce.2011.03.006
Mayer, M., & Haimberger, L. (2011). Poleward Atmospheric Energy Transports and Their Variability as Evaluated from ECMWF Reanalysis Data. *JOURNAL OF CLIMATE*, *25*(1991), 734–752. https://doi.org/10.1175/JCLI-D-11-00202.1
Mayer, M., Haimberger, L., Edwards, J., & Hyder, P. (2017). Towards consistent diagnostics of the coupled atmosphere and ocean energy budgets. *JOURNAL OF CLIMATE (AMERICAN METEOROLOGICAL SOCIETY)*. https://doi.org/10.1175/JCLI-D-17-0137.1
Mayer, M., Haimberger, L., Pietschnig, M., & Storto, A. (2016). Facets of Arctic energy accumulation based on observations and reanalyses 2000–2015, (2), 420–429. https://doi.org/10.1002/2016GL070557.Received
Melling, H., Agnew, T. A., Falkner, K. K., Greenberg, D. A., Lee, C. M., Münchow, A., … Woodgate, R. A. (2008). Fresh-Water Fluxes via Pacific and Arctic Outflows Across the Canadian Polar Shelf. In R. R. Dickson, J. Meincke, & P. Rhines (Eds.), *Arctic--Subarctic Ocean Fluxes: Defining the Role of the Northern Seas in Climate* (pp. 193–247). Dordrecht: Springer Netherlands. https://doi.org/10.1007/978-1-4020-6774-7_10
NAS. (2005). National Academy of Science: The International Geophysical Year. Retrieved June 22, 2017, from http://www.nas.edu/history/igy/
NCAR. (2017). NCAR Command Language. Boulder: NCAR. https://doi.org/http://dx.doi.org/10.5065/D6WD3XH5
NOAA. (2008). ADCP, Acoustic Doppler Current Profiler. Retrieved July 5, 2017, from http://oceanservice.noaa.gov/education/kits/currents/07measure5.html
NOAA. (2015). Expendable bathythermograph (XBT). Retrieved July 5, 2017, from http://oceanexplorer.noaa.gov/facts/xbt.html
NSIDC. (2017). National Snow & Ice Data Center: All about Sea Ice. Retrieved June 10, 2017, from https://nsidc.org/cryosphere/seaice/index.html
Pietschnig, M. (2017). *Volume and Energy fluxes in the Arctic Ocean- A comparison between an ocean reanalysis and in-situ observations*. University of Vienna.
Pietschnig, M., Mayer, M., Tsubouchi, T., Storto, A., & Stichelberger, S. (2017). Comparing reanalysis-based volume and temperature transports through Arctic Gateways with mooring-derived estimates. *JGR-Ocean*.
RGS. (n.d.). The Arctic. Retrieved June 30, 2017, from http://arctic.ru/resources/
Rodgers, J. L., & Nicewander, W. A. (1988). Thirteen Ways to Look at the Correlation Coefficient. *The American Statistician*, *42*(1), 59–66.
Schauer, U., & Beszczynska-Möller, A. (2009). Problems with estimation and interpretation of oceanic heat transport - Conceptual remarks for the case of Fram Strait in the Arctic Ocean. *Ocean Science*, *5*(4), 487–494. https://doi.org/10.5194/os-5-487-2009
Schauer, U., Fahrbach, E., Osterhus, S., & Rohardt, G. (2004). Arctic warming through the Fram Strait : Oceanic heat transport from 3 years of measurements. *JOURNAL OF GEOPHYSICAL RESEARCH*, *109*, 1–14. https://doi.org/10.1029/2003JC001823
Schönwiese, C. D. (2006). *Praktische Statistik für Meteorologen und Geowissenschaftler* (4th ed.). Berlin: Bornträger.
SeaBird Scientific. (2017). Moored Instruments. Retrieved July 5, 2017, from http://www.seabird.com/products/moored-time-series-instruments
Serreze, M. C., Barrett, A. P., Slater, A. G., Woodgate, R. A., Aagaard, K., Lammers, R. B., … Lee, C. M. (2006). The large-scale freshwater cycle of the Arctic. *Journal of Geophysical Research*, *111*(11), 1–19. https://doi.org/10.1029/2005JC003424
Serreze, M. C., & Barry, R. G. (2014). *The Arctic Climate System* (Second ed.). Cambridge: Cambridge University Press.

Serreze, M. C., & Barry, R. G. (2014). *The Arctic Climate System* (Second edi). Cambridge: Cambridge University Press. https://doi.org/10.1017/CBO9781139583817
Skagseth, Ø. (2008). Recirculation of Atlantic Water in the western Barents Sea. *Geophysical Research Letters*, *35*(11), 1–5. https://doi.org/10.1029/2008GL033785
Smedsrud, L. H., Esau, I., Ingvaldsen, R. B., Eldevik, T., Haugan, P. M., Li, C., … Sorokina, S. A. (2013). The role of the Barents Sea in the Arctic climate system. *Reviews of Geophysics*, *51*(3), 415–449. https://doi.org/10.1002/rog.20017
Smedsrud, L. H., Ingvaldsen, R., Nilsen, J. E. Ø., & Skagseth, Ø. (2010). Heat in the Barents Sea: transport, storage, and surface fluxes. *Ocean Science*, *6*(1), 219–234. https://doi.org/10.5194/os-6-219-2010
Smith, E. H., Soule, F. M., & Mosby, O. (1937). *The Marion and General Green expeditions to Davis Strait and the Labrador Sea*. Bull: U.S. Coast Guard.
Steur, L. De, Hansen, E., Gerdes, R., Karcher, M., Fahrbach, E., & Holfort, J. (2009). Freshwater fluxes in the East Greenland Current : A decade of observations. *Geophysical Research Letters*, *36*, 2–6. https://doi.org/10.1029/2009GL041278
Storto, A., Masina, S., & A, and N. (2016). Evaluation of the CMCC eddy-permitting global ocean physical reanalysis system (C-GLORS, 1982_2012) and its assimilation components. *Quarterly Journal of the Royal Meteorological Society*, *142*, 738_758. https://doi.org/10.1002/qj.2673
Tang, C. C. L., Ross, C. K., Yao, T., Petrie, B., DeTracey, B. M., & Dunlap, E. (2004). The circulation, water masses and sea-ice of Baffin Bay. *Progress in Oceanography*, *63*(4), 183–228. https://doi.org/10.1016/j.pocean.2004.09.005
Tomczak, M., & Godfrey, J. S. (2003). Arctic Oceanography. In *Regional Oceanography: An Introduction* (second edi, p. 390). Dehli: Daya Publishing House.
Trenberth, K. E. (1997). Using Atmospheric Budgets as a Constraint on Surface Fluxes. *JOURNAL OF CLIMATE*, *10*, 2796–2809.
Trenberth, K. E., & Caron, J. M. (2001). Estimates of Meridional Atmosphere and Ocean Heat Transports. *JOURNAL OF CLIMATE*, *14*, 3433–3443.
Tsubouchi, T. (2016). *Davis UW mooring data in 200410*. Bremerhaven.
Tsubouchi, T., Bacon, S., Garabato, A. C. N., Aksenov, Y., Ingvaldsen, R., Schauer, U., … Curry, B. (2017). The Arctic Ocean seasonal cycle : an observation-based inverse estimate. *JGR-Ocean*, 59.
Tsubouchi, T., Bacon, S., Naveira Garabato, C., Aksenov, Y., Laxon, S. W., Fahrbach, E., … Ingvaldsen, R. B. (2012). The Arctic Ocean in summer: A quasi-synoptic inverse estimate of boundary fluxes an water mass transformation. *Journal of Geophysical Research*, *117*. https://doi.org/10.1029/2011JC007174
UN. (2016). UN ATLAS OF THE OCEANS. Retrieved June 10, 2017, from http://www.oceansatlas.org/
von Appen, W. J., Schauer, U., Somavilla, R., Bauerfeind, E., & Beszczynska-Möller, A. (2015). Exchange of warming deep waters across Fram Strait. *Deep-Sea Research Part I: Oceanographic Research Papers*, *103*, 86–100. https://doi.org/10.1016/j.dsr.2015.06.003
von der Lippe, P. (1993). Einführung in die Zeitreihenanalyse. In *Deskriptive Statistik* (4th ed., pp. 393–436). Stuttgart: Gustav Fischer Verlag.
Wood, K. R., & Overland, J. E. (n.d.). The first International Polar Year. Retrieved June 22, 2017, from https://www.pmel.noaa.gov/arctic-zone/ipy-1/
Woodgate, R. (2008). Cruise Report for Bering Strait Mooring Project 2008 , Rusalca 2008, (October), 1–28.
Woodgate, R. A. (2017). Increases in the Pacific inflow to the Arctic from 1990 to 2015, and insights into seasonal trends and driving mechanisms from year-round Bering Strait mooring data. *Progress in Oceanography*, 56.
Woodgate, R. A., & Aagaard, K. (2005). Revising the Bering Strait freshwater flux into the Arctic Ocean. *Geophysical Research Letters*, *32*, 3–6.

https://doi.org/10.1029/2004GL021747
Woodgate, R. A., Aagaard, K., & Weingartner, T. J. (2004). A Year in the Physical Oceanography of the Chukchi Sea: Moored measurements from Autumn 1990-1991. *Deep-Sea Research*.
Woodgate, R. A., Aagaard, K., & Weingartner, T. J. (2006). Interannual changes in the Bering Strait fluxes of volume, heat and freshwater between 1991 and 2004. *Geophysical Research Letters*, *33*(15), 2–6. https://doi.org/10.1029/2006GL026931
Woodgate, R. A., Weingartner, T., & Lindsay, R. (2010). The 2007 Bering Strait oceanic heat flux and anomalous Arctic sea-ice retreat. *Geophysical Research Letters*, *37*(1), 1–5. https://doi.org/10.1029/2009GL041621
Worldatlas. (2017). Retrieved June 10, 2017, from http://www.worldatlas.com/aatlas/infopage/bering.htm
Zuo, H., & Mogensen, K. (2014). Arctic sea ice in the ECMWF MyOcean2 ocean reanalysis ORAP5, (October).

Declaration of Authorship

I hereby declare that the master thesis submitted is my own unaided work. All direct or indirect sources used are acknowledged as references. Whenever a source is cited after the last full stop in a paragraph, the citation concerns the whole paragraph.

Vienna, 2017